Double-Stranded DNA as a Model Polymer: Validation through Rheological Characterization

Submitted in partial fulfillment of the requirements
for the degree of

Doctor of Philosophy

of the

Indian Institute of Technology Bombay, India

and

Monash University, Australia

by

Sharadwata Pan

Supervisors:

Prof. P. Sunthar (IIT Bombay)
Prof. Ravi Prakash Jagadeeshan (Monash University)
Prof. Tamarapu Sridhar (Monash University)

The course of study for this award was developed jointly by
the Indian Institute of Technology Bombay, India and Monash University, Australia
and given academic recognition by each of them.
The programme was administrated by the IITB-Monash Research Academy

Year 2014

Declaration

I declare that this written submission represents my ideas in my own words and where others' ideas or words have been included, I have adequately cited and referenced the original sources. I also declare that I have adhered to all principles of academic honesty and integrity and have not misrepresented or fabricated or falsified any idea / data / fact / source in my submission. I understand that any violation of the above will be cause for disciplinary action by the Institute/the Academy and can also evoke penal action from the sources which have thus not been properly cited or from whom proper permission has not been taken when needed.

Place: IIT Bombay

Signature

Date: June 30, 2014

Name: Sharadwata Pan

Acknowledgements

My sincere gratitude and respect to my advisors Prof. Ravi Prakash Jagadeeshan, Dept. of Chemical Engineering, Monash University, Prof. P. Sunthar, Dept. of Chemical Engineering, IIT Bombay and Prof. Tamarapu Sridhar, Ex-Dean (Faculty of Engineering), Monash University, for their constant supervision and encouragement. This project would not have materialized without their patience, assistance in data analysis and rational and insightful suggestions.

I am grateful to Prof. Douglas E. Smith and his group in University of California (San Diego, USA) for preparing the majority of the special DNA fragments and to Dr. Brad Olsen (then at Caltech, USA) at MIT (Cambridge, USA) and Dr. Rae Anderson at University of California (San Diego, USA) for sending the bacterial cultures containing them. I thank Prof. Santosh Noronha and his group (IIT Bombay, India) for helpful discussions, laboratory support, and the two special DNA fragments (pBSKS and pHCMC05) used in this work; and Prof. Sarika Mehra (IIT Bombay, India) for brief laboratory support during the initial phase of the work. I acknowledge the funding received from DST, DBT, and MHRD and IITB-Monash Research Academy for general support. The Sophisticated Analytical Instrument Facility (SAIF) at IIT Bombay is thanked for access to the static light scattering facility.

I thank Dr. Duc At Nguyen, Dept. of Chemical Engineering, Monash University for his kind help with the shear and extensional viscosity measurements. This work would not have been possible without his assistance. The efforts of Ms. Li Xin Ong and Ms. Yi Lan Elaine Fun (Monash University) are highly acknowledged and lauded in preparing DNA samples and some shear viscosity measurements.

I would like to extend my thanks to Dr. Suresh Bhat and Dr. G. Kumaraswamy at National Chemical Laboratory (NCL), Pune, India for offering the light scattering facilities (both static and dynamic), and careful assistance with data analysis.

I have also benefitted from many fruitful discussions with A/Prof. Michael K. Danquah (adjunct faculty), Dept. of Chemical Engineering, Monash University (currently at Department of Chemical and Petroleum Engineering, Curtin University of Technology, Sarawak, Malaysia) in improving the DNA yield. I would also like to thank my Research Progress Committee (RPC) members: Dr. R. Prabhakar, Dept. of Mechanical and Aerospace Engineering, Monash University; Prof. Anirban Sain, Dept. of Physics and Prof. Ajay S. Panwar, Dept. of Metallurgical Engineering and Materials Sciences at IIT Bombay for their technical advice and suggestions. In addition, I must acknowledge the insightful suggestions by Prof. Burkhard Dünweg, visiting faculty from Max Planck Institute for Polymer Research, Mainz, Germany, specially in the context of understanding the 'blob' concept.

To the aforementioned: without your kind help and timely assistance, this work would not have materialized. Heartfelt thanks to all of you.

Sharadwata Pan

Abstract

Solutions of double-stranded DNA (ds-DNA) have been investigated in the presence of excess salt to represent a model neutral polymer system. However, very recently, there have also been some contrary discussions regarding the suitability of using ds-DNA as a model polymer, based on scaling arguments and simulations. Here, we report systematic experimental investigations of dilute and semidilute unentangled ds-DNA solutions, to test the hypothesis that ds-DNA is a model polymer. In addition, we have meticulously characterized the behaviour of ds-DNA solutions far from equilibrium, in shear and extensional flows.

In order to study the behaviour of ds-DNA to compare with well known results from neutral polymers, we first characterize its solutions **close to equilibrium**. We use the solvent quality parameter z and the dimensionless concentration c/c^* (where c^* is the overlap concentration), as the scaling variables. We have determined the θ-temperature of DNA in Tris-EDTA buffer under excess salt conditions to be $T_\theta = 14.7 \pm 0.5$°C, and provide the formula to determine z for DNA of any molecular weight at any temperature above T_θ. We also show that the temperature crossover for *dilute DNA solutions* of various molecular weights (from 2.9 to 289 kilobasepairs) for the second virial coefficient, the hydrodynamic radius and the viscosity radius agree with the scaling behaviour of neutral synthetic polymers.

The scaling behavior of the zero shear rate viscosity of **semidilute DNA solutions**, in the double crossover regime driven by temperature and concentration, is shown to have a power law dependence on the scaled concentration c/c^*, with an effective exponent that depends on z, in agreement with reported Brownian Dynamics Simulations of flexible polymer chains.

Away from equilibrium, in shear flow, the shear rate dependence of viscosity for semidilute and dilute DNA solutions, at various temperatures and concentrations, can be collapsed onto master curves when interpreted in terms of a different relaxation time based Weissenberg number. In extensional flow, the concentration dependence of the steady state uniaxial extensional viscosities of semidilute DNA solutions has been studied and compared with theoretical predictions.

The material functions obtained in this work will also provide benchmark data that are useful for the characterization of industrially important semidilute systems. Equilibrium rheological characterization carried out on dilute and semidilute DNA solutions, investigated under excess salt conditions, show a remarkable agreement with other neutral synthetic polymers, asserting that DNA can be used as a model polymer for rheological studies.

Key Words: Double-stranded DNA, model polymer, dilute polymer solution, semidilute solutions, solvent quality, zero shear rate viscosity, Weissenberg number, relaxation time, shear flow, extensional flow, steady state uniaxial extensional viscosity.

Contents

List of Tables

List of Figures

List of Notations

English

A_2	Second virial coefficient	25
b	Monomer length	107
b_k	Kuhn-step length	31
c	Absolute concentration (in mg/ml)	4
c_blob	Concentration within a correlation blob	76
c^*	Overlap concentration, Equation 1.8	4
$\tilde{c}$	Number of monomers per unit volume	106
$\mathcal{D}$	Diffusion Coefficient	3
D	Mid-filament diameter	131
$\mathcal{D}_\mathrm{c}$	Diffusion Coefficient of a correlation blob	107
$\mathcal{D}^\theta$	Diffusion Coefficient at T_θ	3
$G(\tau)$	Correlation coefficient (DLS)	36
I_0	Intensity of scattered light at $q \to 0$	26
I_ex	Excess scattered intensity	25
I_i	Incident intensity	25
$I(q)$	Intensity of scattered light at q	17
I_s	Intensity of light scattered by the solvent	26
K	Optical constant (light scattering)	25
k	Chemistry dependent constant (for z), Equation 1.1	3
k_H	Huggins constant	54
k_K	Kraemer's constant	54
k_SC	Solomon-Ciută constant	55
k_B	Boltzmann constant	6
L	Filament length	131

L_o	Contour length of the polymer (DNA)	11
M	Molecular weight (in g/mol)	2
M_{blob}	M of a chain segment within a thermal blob	146
m	Number of correlation blobs within a Pincus blob	109
m_{k}	Molar mass per Kuhn-step	31
N	Number of monomers	106
n	number density of polymers	134
N_{A}	Avogadro's number	5
N_{blob}	Number of Kuhn-steps in a thermal blob	144
N_{c}	Number of correlation blobs	106
N_{k}	Number of Kuhn-steps	11
N_{p}	Total number of polymers in the system	106
P	Persistence length	11
p	Number of modes	110
$P(q)$	Form factor	25
q	Magnitude of scattering vector	17
R	End to end distance	144
R_0	Cross section of polymer (rods)	134
R_{blob}	Mean size of a thermal blob	144
R_{eq}	Mean chain size at equilibrium	106
R_{g}	Radius of gyration	3
R_{g}^{θ}	Radius of gyration at T_θ	3
R_{H}	Hydrodynamic radius, Equation 2.1	3
R_{H}^{θ}	Hydrodynamic radius at T_θ	3
R_η	Viscosity radius, Equation 5.1	3
R_η^{θ}	Viscosity radius at T_θ	3
R_θ	Rayleigh excess ratio	25
r	Distance of sample from the detector (light scattering)	25
T	Temperature	3
T_θ	θ-temperature	3

Tr	Trouton ratio, Equation 8.2 131
Tr^+	Transient Trouton ratio, Equation 8.1 131
t	time 36
$U_{\eta\lambda}$	Universal ratio of relaxation times, Equation (6.6) 80
$U_{\eta\mathrm{R}}$	Universal viscosity ratio, Equation 5.2 48
$U^{\theta}_{\eta\mathrm{R}}$	Universal viscosity ratio at T_θ 48
U_{R}	Universal amplitude ratio 146
U_{RD}	Universal size ratio 146
U^{θ}_{RD}	U_{RD} at T_θ 41
V	System volume 106
v_0	Chemistry dependent constant (for EV parameter) 145
$v(T)$	Excluded volume parameter at T 145
Wi	Weissenberg number 5
z	Solvent quality parameter, Equation 1.1 2

Greek

α_{g}	Swelling of R_{g}, Equation 1.2 3
α_η	Swelling of R_η, Equation 1.6 3
α_{H}	Swelling of R_{H}, Equation 1.4 3
$\dot{\varepsilon}$	Extension rate or strain rate 5
ε	Strain 130
Φ	Flory-Fox constant 48
ϕ	Volume fraction of polymers (rods) in a suspension 134
Φ_0	Flory-Fox constant at T_θ 48
$\dot{\gamma}$	Shear rate 5
η	Shear viscosity 19
η_0	Zero shear rate viscosity 54
$[\eta]$	Intrinsic viscosity (in ml/mg), Equation 5.3 3
η_{E}	Steady-state extensional viscosity 130

η_{E}^{+}	Transient extensional viscosity 131
η_{p0}	Polymer contribution to zero shear rate viscosity 5
η_{p0}^{*}	η_{p0} at $c = c^{*}$ 72
η_{p}	Polymer contribution to solution shear viscosity 5
η_{s}	Solvent viscosity 18
η_{sp}	Specific viscosity, Equation 5.3 54
$[\eta]_{\theta}$	Intrinsic viscosity at T_{θ} 3
ξ_{c}	Size of a correlation blob 106
ξ_{S}	Size of a Pincus blob 108
λ	Any large scale relaxation time 5
λ_{1}	Longest relaxation time 79
$\lambda_{1,\mathrm{z}}$	λ_{1} in the dilute limit 80
$\lambda_{\mathrm{D}}^{\theta}$	Relaxation time based on $\mathcal{D}^{\theta}$ 11
λ_{η}	Large scale relaxation time based on η_{0}, Equation 1.9 5
λ_{η}^{*}	λ_{η} at $c = c^{*}$ 105
λ_{η}^{θ}	λ_{η} at T_{θ} 11
$\lambda_{\eta,\mathrm{z}}$	λ_{η} in the dilute limit 80
λ_{Z}	Large scale relaxation time based on $[\eta]$, Equation 6.5 117
ν	Flory exponent 23
ν_{eff}	Effective exponent 69
Π_{H}	Dimensionless scaling variable based on R_{H}, Equation A.2 144
τ	Delay time (DLS) 36
τ_{0}	Monomer relaxation time 108
τ_{c}	Relaxation time of a correlation blob 108
τ_{chain}	Relaxation time of a chain 108
χ	Flory-Huggins parameter 150
ζ_{c}	Friction coefficient of a correlation blob 107

1

Introduction

Double-stranded Deoxyribonucleic acid (DNA) has been used in several experimental studies in recent years as a model polymer (Sorlie and Pecora, 1990; Robertson et al., 2006; Smith et al., 1996; Sunthar and Prakash, 2005; Smith and Chu, 1998; Sunthar et al., 2005; Laib et al., 2006; Valle et al., 2005; Nayvelt et al., 2007; Ostrander and Gray Jr, 1973; Ross and Scruggs, 1968; Hodnett et al., 1976; Sibileva et al., 1987; Marathias et al., 2000; Nicolai and Mandel, 1989; Fujimoto et al., 1994; Leighton and Rubenstein, 1969; Doty et al., 1958). This is largely because the most significant advantage of using DNA molecules lies in their monodispersity (Pecora, 1991). Even though DNA is a polyelectrolyte, it is widely accepted that in the presence of excess salt, the charges on the backbone are screened, leading to behaviour identical to that of neutral synthetic polymers (Barrat and Joanny, 1996; Smith et al., 1996; Sorlie and Pecora, 1990; Robertson et al., 2006; Marko and Siggia, 1995). Recently, however, there has been some discussion in the literature based on scaling arguments and simulations, regarding the appropriateness of using double-stranded DNA to represent linear flexible chains due to the essentially semiflexible character of DNA which arises from the structural rigidity of the double helix (Latinwo and Schroeder, 2011; Tree et al., 2013). Earlier studies have justified their use of DNA

by noting that the diffusivity of single molecules scales with molecular weight M as $M^{0.6}$, which is the expected power law scaling for linear polymers under good solvent conditions (Robertson et al., 2006; Smith et al., 1996). However, it is clearly important to resolve the question of whether DNA is a model polymer or not by carrying out a thorough and systematic investigation not only in the limit of good solvent conditions, but also across a range of other conditions in which the behaviour of linear synthetic polymers is well understood.

The most outstanding feature of polymer solutions at equilibrium is their universal behaviour, which is exhibited not only in the power law scaling of large scale properties, but also by the existence of universal crossover scaling functions, independent of the details of polymer and solvent chemistry. A convincing establishment of the appropriateness of using DNA as a model polymer requires a satisfactory demonstration that solutions of double-stranded DNA also exhibit universal behaviour at equilibrium, for sufficiently long chains.

One of the two central goals of this thesis is to carry out a systematic investigation of **equilibrium properties** in dilute and semidilute DNA solutions, to test the hypothesis that *double-stranded DNA is a model polymer*. The second goal of this thesis is to meticulously characterize the behaviour of double-stranded DNA solutions **away from equilibrium**, in shear and extensional flows. In characterizing the DNA solutions we use three independent scaling variables discussed in the following sections.

1.1 Scaling variable z

As is well known, large scale properties of linear polymers in dilute solutions obey power laws under θ-conditions and under very good solvent conditions. For instance, the radius of gyration $R_g \sim M^{\nu}$, where M is the molecular weight, while the diffusivity $\mathcal{D} \sim M^{-\nu}$, where the Flory exponent ν has a value 0.5 in θ-solvents and $\nu \approx 0.6$ in very good solvents (de Gennes, 1979; Rubinstein and Colby, 2003). In the intermediate region between θ and very good solvents, the behaviour of dilute polymer solutions can be described in terms of a single scaling variable z , which

combines the dependence on temperature T and M, i.e.,

$$z \equiv k\left(1 - \frac{T_\theta}{T}\right)\sqrt{M}, \tag{1.1}$$

where, T_θ is the θ-temperature and k is a chemistry dependent parameter (Schäfer, 1999; Rubinstein and Colby, 2003). For instance, the 'swelling' α_{g} , of the radius of gyration R_{g} at any temperature T relative to that at the θ-temperature, defined as

$$\alpha_{\mathrm{g}} \equiv \frac{R_{\mathrm{g}}\,(T)}{R_{\mathrm{g}}^{\theta}}, \tag{1.2}$$

is found to exhibit universal scaling behaviour such that (Miyaki and Fujita, 1981; Schäfer, 1999; Kumar and Prakash, 2003),

$$\alpha_{\mathrm{g}} = f_{\mathrm{g}}(z) \tag{1.3}$$

is independent of polymer-solvent chemistry. Here R_{g}^{θ} is the radius of gyration under θ-conditions . Similarly, the swelling α_{H} of the hydrodynamic radius R_{H} , is defined by

$$\alpha_{\mathrm{H}} \equiv \frac{R_{\mathrm{H}}}{R_{\mathrm{H}}^{\theta}} = \frac{\mathcal{D}^{\theta}}{\mathcal{D}(T)}, \tag{1.4}$$

where R_{H}^{θ} and $\mathcal{D}^{\theta}$, the hydrodynamic radius and diffusivity under θ-conditions respectively, obeys the universal scaling expression (Tominaga et al., 2002; Sunthar and Prakash, 2006),

$$\alpha_{\mathrm{H}} = f_{\mathrm{H}}(z). \tag{1.5}$$

Here $\mathcal{D}(T)$ is the diffusivity coefficient in good solvents. Another dynamic property that is often used to characterize dilute polymer solutions is the swelling of the viscosity radius R_η ,

$$\alpha_\eta \equiv \frac{R_\eta}{R_\eta^{\theta}} = \left(\frac{[\eta]}{[\eta]_\theta}\right)^{\frac{1}{3}}, \tag{1.6}$$

where R_η^{θ} is the same under θ-conditions. Here, $[\eta]$ and $[\eta]_\theta$ are the intrinsic viscosities of a polymer solution in good and θ-solvents, respectively. Experimental observations of several polymer-solvent systems have demonstrated (Tominaga

et al., 2002; Miyaki and Fujita, 1981) that,

$$\alpha_\eta = f_\eta(z), \tag{1.7}$$

such that, provided a suitable choice is made of the chemistry dependent parameter k, data across the different polymer-solvent systems collapses on to a master curve.

The functions f_g, f_H, and f_η are well known for linear synthetic polymer solutions (Kumar and Prakash, 2003; Sunthar and Prakash, 2006; Pan et al., 2014). If data for dilute solutions of double-stranded DNA, in the presence of excess salt, can be shown to satisfy these functions, then we would have succeeded in showing that in dilute solutions at least, DNA is a model linear polymer.

In order to characterize the behaviour of DNA solutions in the temperature crossover regime between θ and very good solvents, both in dilute and semidilute solutions, it is necessary to determine the solvent quality z of DNA solutions in the particular solvent that has been used in the current experiments. For determining z, the knowledge of the θ-temperature is essential. In spite of the extensive utilization of DNA solutions in a variety of experimental contexts, to date there is no reported measurement of the θ-temperature of any DNA solution.

1.2 Scaling variable c/c^*

Recently, Jain et al. (2012a) have developed detailed scaling predictions for the behaviour of linear polymers in semidilute solutions, in the phase space of temperature and concentration c . They show that in addition to the scaling variable z, the scaled concentration, $\frac{c}{c^*}$ is necessary to obtain chemistry independent predictions. Here, c^* is the 'overlap' concentration, which is the threshold concentration at which polymer coils just begin to touch each other. Note that, the c^* is given by (Rubinstein and Colby, 2003; Doi and Edwards, 1986)

$$c^* = \frac{3M}{4\pi N_A R_g^3}, \tag{1.8}$$

where, N_A is Avogadro's number and is calculated based on the estimated values of R_g. Using the 'blob' concept (de Gennes, 1979; Colby and Rubinstein, 1990), they have derived explicit scaling relations for the mean size, diffusivity and viscosity of semidilute solutions of linear polymers. Further, by carrying out Brownian dynamics simulations, they have verified the validity of their scaling relationships for the mean size and the diffusivity. However, the scaling predictions of Jain et al. (2012a) have not been verified by experimental observations. This provides us with an opportunity to demonstrate that double-stranded DNA solutions satisfy the universal scaling predictions for flexible, linear and neutral chains, under semidilute as well as under dilute solution conditions.

1.3 Scaling variable Wi

For polymer solutions subject to a flow velocity gradient, typically, the strength of the flow is characterized by the non-dimensional Weissenberg number $\mathrm{Wi} = \lambda\dot{\gamma}$ (in shear flow) or $\mathrm{Wi} = \lambda\dot{\varepsilon}$ (in extensional flow, where $\dot{\varepsilon}$ is the extension rate). The quantity λ is some measure of the large scale relaxation time for the solution. The use of λ to scale the strength of flow often leads to the revelation of universal behaviour in polymer solutions (Bird et al., 1987; Doi and Edwards, 1986). For instance, when the scaled viscosity $\frac{\eta_p}{\eta_{p0}}$ is plotted versus $\lambda\dot{\gamma}$, master curves independent of T, molecular weight and polymer-solvent system have been obtained for dilute polymer solutions (Bird et al., 1987; Doi and Edwards, 1986). Here η_p and η_{p0} are the polymer contributions to the solution shear viscosity and zero shear rate viscosity , respectively. In recent simulations of semidilute polymer solutions, Huang et al. (2010) have suggested that the use of a relaxation time that follows the known equilibrium scaling dependence on (c/c^*), would lead to universal observations for the dependence of $\frac{\eta_p}{\eta_{p0}}$ on $\lambda\dot{\gamma}$, far from equilibrium. The validity to this suggestion has not been examined by experiments so far.

The extensive data that we have accumulated on η_{p0} as a function of z and c/c^* enables us to calculate the large scale relaxation time λ_η , defined as (Öttinger,

1996),

$$\lambda_\eta = \frac{M\eta_{p0}}{cN_A\, k_B\, T}, \tag{1.9}$$

as a function of these scaling variables. Here k_B is the Boltzmann constant . This definition is often used to represent flow data, with the product $\lambda_\eta\dot{\gamma}$ referred to as the characteristic shear rate. The scaling of λ_η with c/c^* in the semidilute regime is identical to any other large scale relaxation time, such as the longest relaxation time λ_1 used in the simulations of Huang et al. (2010). As a result, we can carefully examine if the use of λ_η to scale the shear rate $\dot{\gamma}$, reveals the universal behaviour of $\frac{\eta_p}{\eta_{p0}}$, independent of the scaled concentration c/c^*, T and M.

The majority of experimental studies of DNA solutions far from equilibrium have been carried out mainly for dilute solutions, both in shear flow (Hur et al., 2001; Lee et al., 2007; Lueth and Shaqfeh, 2009; Schroeder et al., 2005) and in extensional flow (Schroeder et al., 2003; Babcock et al., 2003; Smith and Chu, 1998; Schroeder et al., 2004; Sunthar et al., 2005). To our knowledge, there is only one study of DNA solutions in shear flow in the semidilute regime (Hur et al., 2001). These experiments were confined to a single temperature and three concentrations $c = c^*, 3c^*$ and $6c^*$. Also, in a previous study from our group, we measured uniaxial extensional viscosities of dilute DNA solutions and predicted the extensional flow properties in terms of solvent quality (Sunthar et al., 2005). It is important to study the extensional rheological behaviour of semidilute polymer solutions, which play a critical role in a number of industrial contexts. However, there is not a single, systematic experimental study to understand the extensional properties of semidilute polymer-solvent systems in terms of the effects of concentration and molecular weight. Clearly, there is a pressing need for developing a more comprehensive set of experimental data both in shear and extensional flows.

1.4 Methodology

In order to study the scaling behaviour of DNA in the chief parameters described, we need highly mono-dispersed population of DNA molecules over a wide range

of molecular weights. We have been guided by the recombinant DNA technology protocol to obtain DNA in a range of molecular weights ranging from ∼3 to 300 kilobasepairs (or kbp) (Laib et al., 2006), and prepared solutions ranging in concentration from a dilute to the semidilute regime. Details of this procedure are given in Chapter 2.

We have characterized these DNA solutions by traditional methods used for neutral polymers, namely static and dynamic light scattering and rheology. We have carried out systematic measurements of second virial coefficients, hydrodynamic and viscosity radii and shear and extensional viscosities of DNA solutions across a range of temperatures, concentrations, molecular weights and flow strengths. These experiments not only help in answering the central question of this thesis (of DNA as a model polymer), but also provides a wealth of data previously unavailable for semidilute polymer solutions.

We also employ scaling arguments based on the blob theory to explain universal scaling in semidilute solutions in strong flows.

1.5 Organization of the Thesis

The schematic 3D phase-space diagram displayed in Figure 1.1 serves as a simple illustration of the parameter space explored in this study. In Part I, Chapter 3 we determine the θ-temperature of DNA. In Chapters 4 and 5, we examine the equilibrium and close to equilibrium behaviour of dilute DNA solutions along the z-axis of the phase diagram, describing the temperature crossover behaviour of polymer solutions. We study the behaviour of double-stranded DNA in dilute solutions for its universal scaling behaviour, in line with earlier observations for synthetic polymer solutions, by measuring the swelling of the hydrodynamic and viscosity radius, α_{H} and α_{η}, respectively, as functions of solvent quality z. In Chapter 6, we extend our studies to the (z—c/c^*) plane of the phase diagram by investigating the close to equilibrium behaviour of semidilute DNA solutions, that describes the double crossover of temperature and concentration. We compare the results with the recent scaling predictions and the predictions of BD simulations by Jain et al. (2012a).

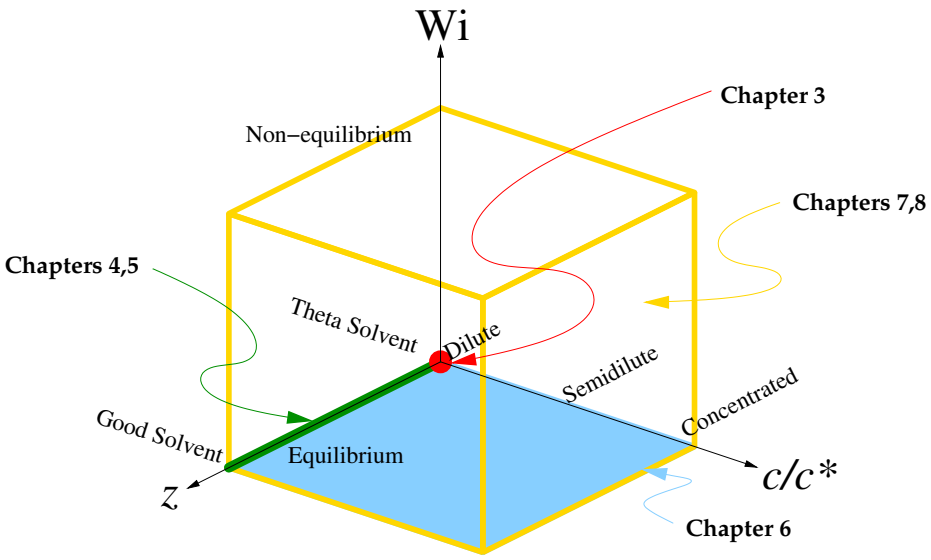

Figure 1.1: A 3-D schematic representation of the parameters that affect the rheological behaviour of a polymer solution. Here c/c^* represents scaled polymer concentration; z represents the excluded volume parameter (defined in Equation 1.1) that combines the dependence of both molecular weight M and temperature T; and Wi represents Weissenberg number, a parameter that characterizes the flow strength. Also indicated are the Chapters numbers of this report which cover the parameter space marked against them.

In Part II of this report, we soar away from equilibrium, into the 3rd dimension of the phase diagram, characterized by the Weissenberg number Wi. In Chapter 7, we examine the proper definition of a relaxation time that reveals the universal scaling of semidilute and dilute DNA solutions in shear flow. In Chapter 8, we study the concentration dependence of extensional properties of semidilute DNA solutions. Finally, in Chapter 9, we summarize our conclusions, and make suggestions for future work.

2

Materials and Methods

The core workhorses of this thesis are the range of monodisperse DNA molecules obtained by recombinant DNA technology, which broadly involves genetic manipulation of bacterial strains, as shown in Figure 2.1. The gene of interest or foreign (donor) DNA is first attached (ligated) to a standard vector (plasmid / fosmid / BAC) through an enzyme (ligase) to produce a recombinant target construct. This recombinant construct is then introduced to a host cell (bacteria). Multiple copies of the desired DNA are produced when the bacterial cell (here *Escherichia coli* or *E. coli*) reproduces and the recombinant DNA replicates. The various DNA fragments are described in detail in the next section which includes details of working conditions and procedures for preparation and quantification of linear DNA fragments.

2.1 Bacterial strains, working conditions and preparation of linear DNA fragments

For the purposes of the experiments proposed here, a range of large molecular weight DNA, each with a monodisperse population, is desirable. This requirement has been met thanks to the work by Smith's group (Laib et al., 2006), who genetically engineered special double-stranded DNA fragments in the range of 2.9

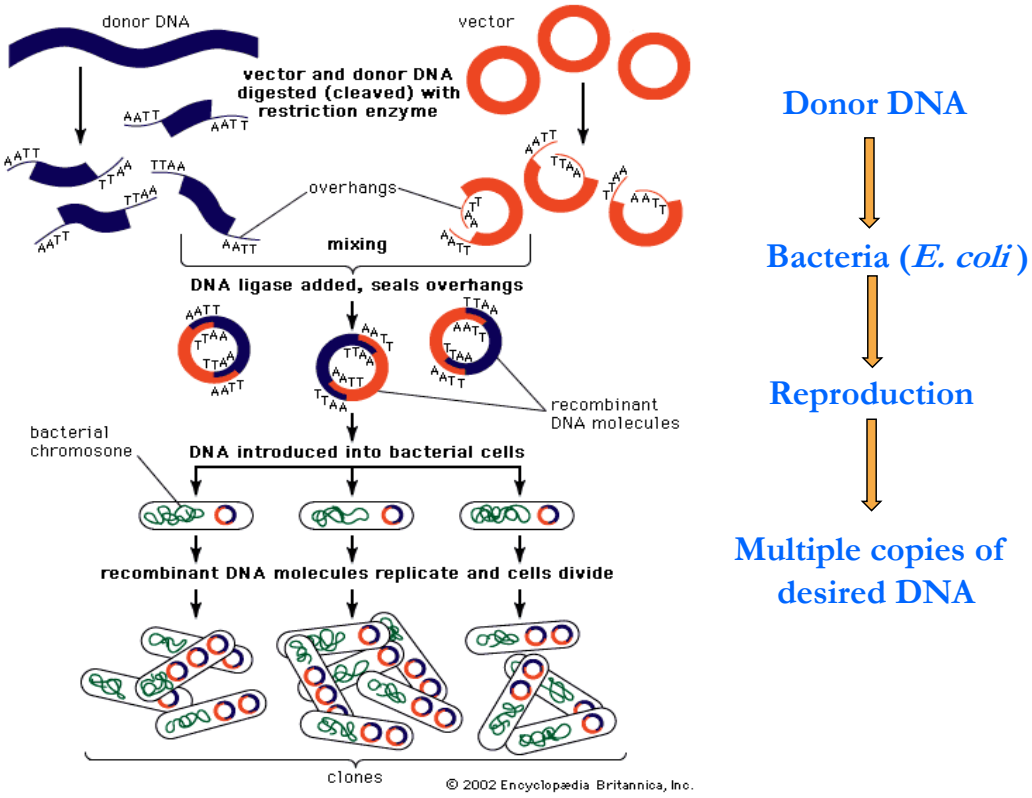

Figure 2.1: DNA from recombinant DNA technology. For explanation, see text. Reprinted (adapted) from Encyclopaedia Britannica (2012) under fair usage policy.

to 289 kbp and incorporated them inside commonly used *E. coli* bacterial strains, which can be selectively extracted for rheological studies. The procedure adopted by Laib et al. (2006) to originally synthesize the circular DNA fragments is related to Figure 2.1. These strains can be cultured to produce sufficient replicas of its DNA, which can be cut precisely at desired locations to extract the special linear DNA fragments. The *E. coli* stab cultures were procured from Smith's laboratory and the DNA fragments were extracted, linearized and purified according to standard molecular biology protocols (Laib et al., 2006; Sambrook and Russell, 2001). Typical properties of all the DNA molecules used in this work for both equilibrium and non-equilibrium characterization are tabulated in Table 2.1.

Primarily, the DNA samples synthesized by Laib et al. (2006) fall into three categories: plasmids, fosmids and Bacterial Artificial Chromosomes (BAC). Altogether six samples (two plasmids, two fosmids and two BACs), which were originally synthesized by Laib et al. (2006), were procured from Dr. Brad Olsen, Caltech, USA. In addition, two special bacterial strains containing the plasmids: pBSKS (2.9 kbp) and pHCMC05 (8.3 kbp) were provided by Prof. Santosh Noronha at IIT Bombay. The details about size, growth conditions of bacteria and single cutters of the DNA samples are mentioned in Table 2.2. After procurement of samples (in the form of agar stab cultures of *E. coli*), glycerol freeze stocks were made using 50% glycerol and stored at -80°C. The cultures can be stored in this way for several years and can be used at any time to produce the DNA samples (Laib et al., 2006).

Standard procedures (Laib et al., 2006; Sambrook and Russell, 2001) involving alkaline lysis (mediated by NaOH) were adopted for extraction, linearization and purification of plasmids, fosmids and BAC from the cultures. The major procedural steps are shown in Figure 2.2. For high copy number plasmids, no inducer was added. For low (fosmids) and very low (BACs) copy number samples, L-arabinose was added as inducer. From each freeze stock, 15 μL of ice was scrapped and transferred to 40 mL LB medium with proper antibiotic (as mentioned in Table 2.2) and incubated overnight (16 to 18 hours) at 37°C with vigorous shaking (200 to 250 rpm). The overnight grown culture was poured into microcentrifuge tubes and

Table 2.1: Representative properties of all DNA samples used in this work. The contour length is estimated using the expression L_o = number of base-pairs $\times$ 0.34 nm; the molecular weight is calculated from M = number of base-pairs $\times$ 662 g/mol, where the base-pair molecular weight has been calculated for a sodium-salt of a typical DNA base-pair segment[†]; the number of Kuhn steps from $N_k = L_0/(2P)$ (where P is the persistence length, which is taken to be 50 nm), and the radius of gyration at the θ temperature is estimated from $R_g^\theta = L_0/\sqrt{6N_k}$. The two relaxation times at the θ-temperature are defined by $\lambda_D^\theta = \left(R_g^\theta\right)^2/\mathcal{D}^\theta$, where $\mathcal{D}^\theta$ is the measured diffusion coefficient under θ conditions, and $\lambda_\eta^\theta = \lambda_\eta$ (defined in Equation 1.9 under θ-conditions. While λ_D^θ is evaluated at $c/c^* = 0.1$, λ_η^θ is calculated at $c/c^* = 1$. The estimation of θ-temperature and subsequently $\mathcal{D}^\theta$ are discussed in Chapters 3 and 4, respectively. The estimation of the overlap concentration c^* is discussed in Chapter 6 and polymer contribution to the zero shear rate viscosity η_{p0}, for dilute and semidilute solutions are discussed in Chapters 5 and 6, respectively.

Size (kbp)	M ($\times 10^6$ g/mol)	L_0 (μ)	N_k	R_g^θ (nm)	λ_D^θ ($\times 10^{-3}$ s)	λ_η^θ ($\times 10^{-1}$ s)
2.96	1.96	1	10	130	7.70	–
5.86	3.88	2	20	182	21.7	–
8.32	5.51	3	28	217	36.9	–
11.1	7.35	4	38	251	56.7	–
25	16.6	9	85	376	197	1.19
45	29.8	15	153	505	480	–
48.5	32.1	16	165	524	–	4.97
114.8	76.0	39	390	807	1970	–
165.6	110	56	563	969	–	51.9
289	191	98	983	1280	7930	–

[†]The molecular weight of DNA has been estimated by calculating the average molecular weight of a nucleotide monomer pair (AT or GC). The molecular weights (in g/mol) of the bases are easily calculated: A = 135.15, T = 126.1, G = 151.15, C = 111.12. Each deoxyribose sugar (M = 134.15 g/mol) looses a water molecule (at the 1′ carbon) on condensation with a nucleotide base and one hydroxyl group on condensation (at 3′) with the phosphate group, and an additional hydroxyl group is lost (at 5′) upon polymerisation (Berg et al., 2002). This loss needs to be doubled for a pair of nucleotide bases. Since the solution contains excess salt (NaCl), it is the sodium ions that are localised around the phosphate group (M = 117.97 g/mol), instead of Hydrogen. DNA used here is therefore a sodium salt. Assuming equal fractions of AT and GC pairs in a DNA, we can therefore calculate the base pair molecular weight to be 662 g/mol.

cells were harvested by centrifugation. The bacterial pellet (obtained above) was resuspended in 100 μL of ice-cold Solution I (4°C) (Sambrook and Russell, 2001) followed by 200 μL of freshly prepared Solution II (Sambrook and Russell, 2001) and 150 μL of ice-cold Solution III (Sambrook and Russell, 2001). The tubes were stored on ice for 3–5 minutes and centrifuged. The supernatant was transferred to a fresh

Table 2.2: DNA Fragments. Here 'LB' stands for Luria Bertini broth, 'Ant^R' refers to Antibiotic resistance, 'Amp' refers to Ampicillin, 'CAM' refers to Chloramphenicol and 'Kan' refers to Kanamycin. All the cultures were incubated overnight at 37°C with vigorous shaking (200–250 rpm). L-arabinose (inducer) was used at a concentration of 0.01 g per 100 mL (stock concentration: 5 g in 100 mL). Stock concentrations for Ampicillin, Chloramphenicol and Kanamycin were 100 mg/mL, 25 mg/mL and 100 mg/mL respectively. The working concentrations for Amp, CAM and Kan are 100 μg/mL, 12.5 μg/mL and 100 μg/mL respectively. Growth conditions for all the plasmids are same (LB + Amp) except pHCMC05 (LB + Amp + CAM). For both the fosmids, growth conditions are identical (LB + CAM + L-arabinose). For both the BACs, growth conditions are the same (LB + CAM + Kan + L-arabinose).

Type	Name	Size (kb) /(Notation)	Ant^R	1 Cutter
Plasmid	pBSKS(+)	2.9 / F2.9	Amp.	BamHI
	pYES2	5.9 / F5.9	Amp.	BamHI
	pHCMC05	8.3 / F8.3	Amp. + CAM	BamHI
	pPIC9K<TRL5>	11.1 / F11.1	Amp.	BamHI
Fosmid	pCC1FOS-25	25 / F25	CAM	ApaI
	pCC1FOS-45	45 / F45	CAM	ApaI
BAC	CTD-2342K16	114.8 / F114.8	CAM + Kan	MluI
	CTD-2657L24	289 / F289	CAM + Kan	MluI

tube. The precipitate (containing mainly the cell debris and genomic DNA) was discarded. RNase was added (at 10 μg/mL) to the tube and incubated at 37°C for 20 minutes. Equal volume of Phenol-Chloroform-Isoamyl Alcohol (25:24:1) mixture was added and mixed well by vortexing. After centrifugation, supernatant was transferred to a fresh tube. Equal volume of Chloroform was added and centrifuged. The supernatant was transferred to a fresh tube. Two volumes of chilled 100% ethanol (at 4°C) was added at room temperature kept for 7 to 8 hours at -20°C. The tube was then centrifuged and the supernatant removed by gentle aspiration. The tube was kept in an inverted position in a paper towel to allow all of the fluid to drain away. Following this, 1 mL of 70% ethanol was added to the tube and centrifuged. When all of the ethanol was evaporated, the resulting DNA pellet was dissolved in 50 μL of Milli-Q grade water and stored at -20°C.

To linearize the extracted DNA fragments, 39 μL of water was added to a 1.7 mL microcentrifuge tube, followed by 10 μL of corresponding 10X Assay Buffer (working concentration is 1X) and 50 μL of DNA solution (purified DNA stored at 4°C). 1 μL of appropriate enzyme was added. A thumb rule is 0.5–1 U enzyme

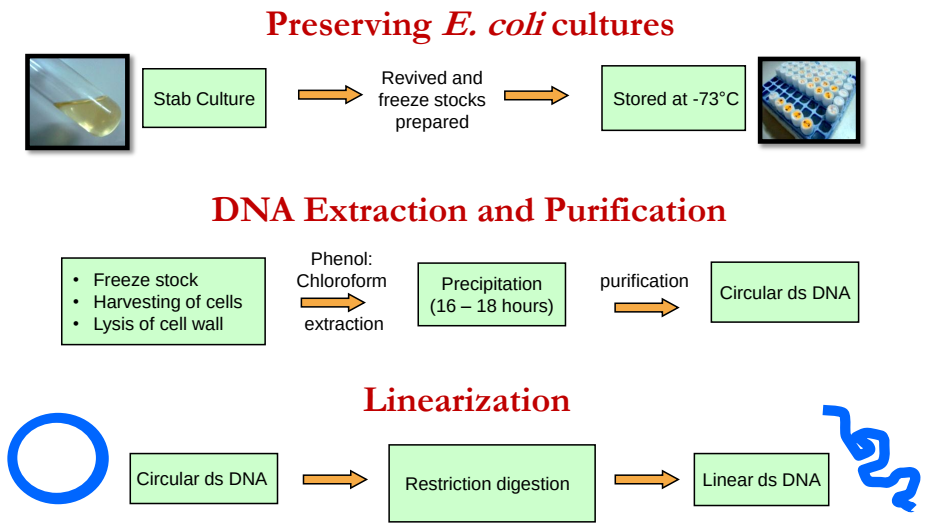

Figure 2.2: Major steps in the preparation of linear DNA molecules for the current work. From the revived and preserved freeze stock cultures of *E. coli*, the circular double stranded DNA was obtained following alkaline lysis, phenol chloroform extraction and ethanol precipitation. The linear double stranded DNA was obtained through restriction digestion (cutting) of the circular DNA using specific enzymes (restriction endonuclease) and subsequent purification. For details, see the text.

for 1 μg DNA (Sambrook and Russell, 2001). The samples were mixed well with micropippette (wide bore tips) for several times. The reaction mix (100μl) was incubated at 37°C for three hours. After restriction digestion / linearization, it is necessary to remove the enzymes / other reagents present in the reaction mix so that they do not interfere with the downstream application/s like light scattering studies, rheometry etc. For this, normal phenol-chloroform extraction followed by ethanol precipitation of DNA was carried out as described elsewhere (Sambrook and Russell, 2001). The purified DNA pellet for all DNA samples after linearization were dissolved in specific solvents (as described in the next section) for the light scattering and rheology experiments.

In addition to the above DNA samples, T4 bacteriophage linear genomic DNA (size 165.6 kbp) and λ-phage linear genomic DNA (size 48.5 kbp) were procured from Nippon Gene, Japan (#314-03973) and New England Biolabs, U.K. (#N3011L), respectively. For both T4 DNA and λ-phage DNA, with an anticipated purity of high order, the company specified values of 0.24 mg/ml and 0.5 mg/ml were used as their maximum concentrations, respectively.

Table 2.3: Composition of solvents used in the current work.

Light scattering and Shear studies	Extensional studies
10 mM Tris	10 mM Tris
1 mM EDTA	1 mM EDTA
0.5 M NaCl	0.5 M NaCl
Water	61.2 wt% Sucrose
	Water

2.1.1 Solvents used

Two different solvents were used in this study (see Table 2.3). For all the light scattering and shear rheological experiments, the solvent employed is predominantly the widely used Tris-EDTA (TE) buffer. The measured viscosity of this solvent at 20°C is 1.01 mPa.s. For all the uniaxial stretching (extensional) experiments, the same solvent has been used but with added sucrose (61.2 wt.%), mainly to increase the viscosity by approximately 60 times. The measured viscosity of this solvent at 21°C is 61 mPa.s. Both the solvent viscosities have been measured by a HAAKE MARS rheometer (Thermo Fisher Scientific). For each molecular weight, the purified linear DNA pellet was dissolved in these solvents, which have been commonly used in polymer physics and rheology experiments involving DNA solutions (Sunthar et al., 2005; Smith et al., 1996; Robertson et al., 2006; Smith and Chu, 1998). Both the solvents contain 0.5 M NaCl, to ensure charge screening (Marko and Siggia, 1995). Consequently, in both these solutions, the DNA molecules are expected to behave identically to charge neutral molecules.

2.1.2 Quantification of linear DNA samples

After the DNA samples were extracted and purified, their purity were determined using the Nano-Photometer (UV-VIS Spectrophotometer, IMPLEN, Germany, #UV-2450, Shimadzu). Optical Density (O.D.) readings were taken at three different wavelengths: 260 nm, 280 nm and 230 nm. The ratio of absorbance at 260 nm to that of 280 nm gives a rough indication of DNA purity (Sambrook and Rus-

sell, 2001). The concentrations were calculated from absorbance reading at 260 nm (DNA shows absorption peak at 260 nm) by Beer-Lambert's Law (Sambrook and Russell, 2001) and also by agarose gel electrophoresis through a serial dilution of DNA samples as suggested elsewhere (Laib et al., 2006). All the linear DNA samples demonstrated A_{260}/A_{280} ratio of 1.8 and above. This indicates good purity for DNA samples, though it is largely an assumption (Laib et al., 2006) and A_{260}/A_{230} ratio from 2.0 to 2.2 (absence of organic reagents like phenol, chloroform etc) (Laib et al., 2006). The low molecular weight linear DNA fragments (plasmids) were quantified through agarose gel electrophoresis with a known standard 1 kbp DNA marker (Fermentas). For low copy number fragments (fosmids) and very low copy number samples (BACs), it was confirmed that the samples were not sheared during extraction by running a very low concentration agarose gel for extended period at low voltage. A loss of 25 to 50% was observed in the amount of DNA samples after the linearization procedure. This is attributed to purification steps by phenol-chloroform extraction (Sambrook and Russell, 2001).

2.2 Static light scattering

2.2.1 Sample preparation

Solutions of linear purified 25 kbp DNA were used for the static light scattering (SLS) studies. The details of the preparation and quantification of this DNA and the solvent (see Table 2.3) used for making solutions and subsequent dilutions are mentioned in the above sections. For SLS, an extensive sample preparation method was followed to ensure repeatability. The methodology of sample preparation was modified from earlier studies (Sorlie and Pecora, 1990; Lewis et al., 1985; Selis and Pecora, 1995) and was repeated before each measurement. The cuvette was washed with ethanol (0.5 ml) for 5 times and kept for 15 minutes inside laminar air flow. It was followed by wash with milliQ grade water for 10 to 15 minutes continuously. In the meantime, the solvents were filtered with 0.45μ membrane-filter (PALL Corp., USA) with 2 different membranes consecutively. After filtration,

DNA was added to make final concentration of $c/c^* = 0.2$ to 0.4. Initial estimates of c^* were based on values of R_g as reported by Laib et al. (2006) for molecular weights that are identical to those used in this study. Typical c^* values for 25 kbp DNA in the solvent used for light scattering at different temperatures are summarized in Table 6.1 in Chapter 6. The SLS methodology has been explained in the following subsection.

2.2.2 Methodology

The static light scattering measurements were obtained from a BI-200SM Goniometer (Brookhaven Instruments Corporation, USA) with a 473 nm wavelength Argon ion laser from Coherent Inc. (USA) using BI-SLSW static light scattering software. A separate temperature control system (PolySc, USA) was used. The intensity of scattered light $I(q)$ was determined as a function of the scattering vector q , and polymer concentration c, at 5 different temperatures: 11.2°C, 13°C, 14°C, 15°C, and 20°C. The angle range was selected based on the sample concentration. For the highest concentration (0.0284 mg/ml) the following set of angles were used:15°, 16.5°, 18°, 19.5°, 21°, 22.5°, 24°, and 25°, while for the three other concentrations, the angles used were:15°, 16°, 17°, 18°, 19°, and 20°. Readings were taken in two temperature scans; with 5 repeats at each temperature. The mean of 10 repeats was taken as the final data point at each temperature. The SLS data was analysed according to the arguments given Chapter 3 in order to find the dependence of the second virial coefficient on temperature, and by this means, the θ-temperature.

2.3 Dynamic light scattering

2.3.1 Sample preparation

Solutions of linear purified DNA having a wide range of molecular weights (2.9, 5.9, 8.3, 11.1, 25, 45, 114.8 and 289 kbp) were used for the dynamic light scattering (DLS) studies. The preparation and quantification of all the DNA solutions and the solvent used are detailed in the above sections. All the DNA fragments

were characterized by DLS for measuring the hydrodynamic radii, R_H, at different temperatures: 5°C, 10°C, 15°C, 20°C, 25°C, 30°C and 35°C. The same sample preparation methodology for DLS has been adopted, as elaborated in the previous section for SLS. The final DNA solutions for all the different molecular weights had a concentration of $c/c^* = 0.1$. The initial estimates of c^* have been discussed in the above section. Typical c^* values for different DNA fragments used for dynamic light scattering at different temperatures are summarized in Table 6.1.

2.3.2 Methodology

The hydrodynamic radii were determined using a Zetasizer Nano ZS (ZEN3600, MALVERN, U.K.) particle size analyzer with temperature control fitted with a 633 nm He-Ne laser using back-scattering detection. This instrument uses dynamic light scattering to measure the diffusion coefficient $\mathcal{D}$, which is then converted to an average hydrodynamic size R_H of particles in solution using the Stokes-Einstein equation (Rubinstein and Colby, 2003)

$$R_H = \frac{k_B\, T}{6\pi\, \eta_s\, \mathcal{D}}, \tag{2.1}$$

where η_s is the solvent viscosity. A Standard Operating Procedure (SOP) was created using the Dispersion Technology Software (DTS 5.00, MALVERN, U.K.) to achieve the desired outcome (R_H) without manual intervention. Scattering of the DNA solutions was measured at a fixed 173° scattering angle (this enables measurements even at high sample concentrations and the effect of dust is greatly reduced). The temperature range investigated was from 5 to 35°C. The Zetasizer Nano ZS has the ability to measure a wide size range (0.6 to 6000 nm in diameter). In Chapter 4, we have reported sizes roughly in the range 140 to 2800 nm in diameter, which is within the size range of the instrument. Readings for the size were taken in three temperature scans (a sequence of High-Low, Low-High, and High-Low temperature settings); with 5 readings at each temperature. The mean of 15 readings was taken as final hydrodynamic radius at each temperature for each DNA fragment.

The DLS data was analysed according to the arguments given Chapter 4 in order to find the chemistry dependent constant k (see Equation 1.1), and by this means, the solvent quality z.

2.4 Shear rheometry

A Contraves Low Shear 30 rheometer with Couette geometry (1T/1T: Cup and bob; shear rate ($\dot{\gamma}$) range: 0.01 to 100 s^{-1}; temperature sensitivity: $\pm$ 0.1°C) has been used to obtain all the shear viscosity measurements reported in the present work because of two main advantages (Heo and Larson, 2005): it has a zero shear rate viscosity sensitivity even at a shear rate of 0.017 s^{-1} and thus can measure very low viscosities; and has a very small sample requirement (minimum 800 μl). Both of these are ideal for measuring viscosities of biological samples such as DNA solutions. Recently, Heo and Larson (2005) have given a detailed description of the measuring principles underlying the Contraves rheometer. The zero error was adjusted prior to each measurement. The rheometer was calibrated with appropriate Newtonian Standards (silicone oils) with known viscosities before measuring actual DNA samples. Values obtained fall within 5% of the company specified values.

Avoiding a continuous shear ramp, the steady state shear viscosities η were measured for the DNA solutions at different absolute concentrations and temperatures. To avert the problem of aggregation of long DNA chains, T4 and λ-phage DNA (at their maximum concentrations) were kept at 65°C for 10 minutes and instantly put into ice for 10 minutes (Heo and Larson, 2005). A manual delay of 30 seconds was applied at each shear rate to allow the DNA chains to relax to their equilibrium state and the sample was equilibrated for 30 minutes at each temperature. Some typical relaxation times observed in dilute and semidilute solutions are given in Table 2.1.

2.5 Filament stretching rheometer and extensional rheometry

For all extensional viscosity measurements, a Filament Stretching Rheometer or FSR (Tirtaatmadja and Sridhar, 1993; Gupta et al., 2000; Sunthar et al., 2005) was used, which is deemed to be the most efficient instrument to obtain reasonable estimates of the elongational stress growth of a polymer solution (McKinley and Sridhar, 2002). The instrument has a very small sample requirement (minimum 0.01 ml), which is ideal for measuring DNA solutions. The measuring principle of FSR is detailed (Gupta et al., 2000; McKinley and Sridhar, 2002) and standardized (Anna et al., 2001) in earlier studies and the theory of uniaxial extensional rheometry has also been discussed (Tirtaatmadja and Sridhar, 1993; McKinley and Sridhar, 2002). Briefly, the DNA samples were placed between two plates initially at rest and consequently moved in opposite directions at a controlled exponential rate. This produces an elongated liquid bridge that experiences a uniaxial extensional flow close to its midpoint, at a fixed strain-rate (Sridhar et al., 1991; Tirtaatmadja and Sridhar, 1993). The force needed for the separation depends on the stress due to the linear DNA molecules being extended from their equilibrium coil-like shape to elongated shapes. The stress is acquired by measuring this force at the end plates (Sunthar et al., 2005). By carefully choosing the extension rate for the solvent used in this study, the polymer contributions to the stress from other factors such as gravity, surface tension, and inertia were isolated, as suggested elsewhere (McKinley and Sridhar, 2002). The elongational stress growth coefficients (or the extensional viscosities) of the DNA solutions were obtained at different strain rates by a master-curve technique (Gupta et al., 2000). All experiments were conducted at a constant strain rate based on the mid-point diameter and carried out at the room temperature ($21 \pm 0.5^{\circ}$C).

PART I

EQUILIBRIUM CHARACTERIZATION

3

Determination of θ Temperature

3.1 Introduction

In both dilute and semidilute solutions, the scaling of static and dynamic properties of linear polymer chains are well explained in terms of the Flory exponent ν for the two extreme limits of θ and good solvents (de Gennes, 1979; Rubinstein and Colby, 2003), as pointed out in Chapter 1. Also, in the crossover region between these two extreme limits, the universality in a dilute solution has been long established by experiments (Tominaga et al., 2002; Miyaki and Fujita, 1981; Hayward and Graessley, 1999), theory (Yamakawa, 2001), and mesoscopic simulations (Kumar and Prakash, 2003; Sunthar and Prakash, 2006). However, this has not been demonstrated for dilute DNA solutions.

In order to characterize the crossover behaviour of DNA solutions, it is essential to determine both the θ-temperature T_θ and the solvent quality z, for these solutions at any temperature above the θ-temperature. In spite of the extensive use of DNA solutions, to our knowledge, the θ-temperature of any DNA solution has not been reported so far. To address this issue, first we establish that the salt concentration used in the solvent employed is well above the threshold value for observing charge screening effects. We find the θ-temperature using 25 kbp DNA

in this solvent (under excess salt conditions) with the help of static light scattering measurements in the dilute regime. We determine the absolute values of second virial coefficients A_2 from the SLS data at different temperatures and identify the temperature at which A_2 vanishes. We also attempt to collapse a suitable scaled A_2 on to a master curve for neutral synthetic polymers.

The plan of the chapter is as follows. In Section 3.2 we determine the salt concentration regime in which DNA behaves as a neutral polymer. The analysis of static light scattering data for dilute DNA solutions is discussed in Section 3.3. The determination of the θ-temperature is explained in Section 3.4. Finally, in Section 3.5, we summarize the principal conclusions of the present chapter.

3.2 Salt concentration independence

Before discussing the details of the estimation of θ-temperature, it is appropriate to first establish the salt concentration regime in which DNA behaves as a neutral polymer. DNA is a polyelectrolyte, so it is essential to ensure that sufficient salt is added to the DNA solutions such that all the charges are screened and they behave essentially like neutral synthetic polymer solutions. We have measured the hydrodynamic radii of two different linear DNA fragments across a range of salt concentrations (from 0.001 to 1 M) at 25°C using dynamic light scattering (DLS) experiments, and the results are displayed in Figure 3.1. Note that the methodology of DLS is given in Section 2.3. It is clear from the figure that complete charge screening occurs above 10 mM NaCl. This is in agreement with earlier dynamic light scattering studies on linear DNA (Soda and Wada, 1984; Langowski, 1987; Liu et al., 2000). Since the solvents used for the light scattering and rheology studies here contains 0.5 M NaCl, all the experiments performed are in a regime well above the threshold for observing charge screening effects.

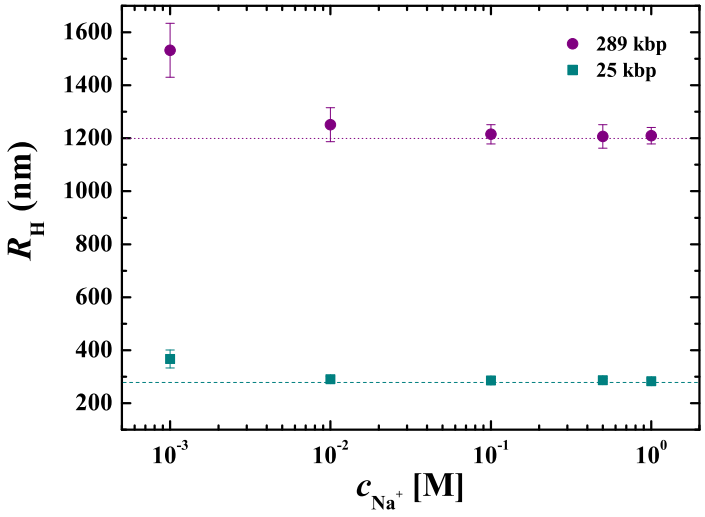

Figure 3.1: Dependence of R_H on salt concentration for two different molecular weights at 25°C.

3.3 Anaysis of SLS data for dilute DNA solutions

The sample preparation procedure and the methodology for SLS has been discussed in Section 2.2.

For solutions of macromolecules, the basic equation for the angular dependence of light scattering is the Debye-Zimm relation (Harding, 1994; Fishman and Patterson, 1996; Rubinstein and Colby, 2003),

$$\frac{Kc}{R_\theta} = \frac{1}{M}\left[1 + 2\,A_2\,c\,M\right]\frac{1}{P(q)}, \tag{3.1}$$

where, K is an optical constant, A_2 is the second virial coefficient, $P(q)$ is the form factor, and R_θ is the Rayleigh excess ratio, defined by the expression,

$$R_\theta = \frac{\bar{I} r^2}{I_i}, \tag{3.2}$$

where, $\bar{I} = I_{ex}/V$, is the excess scattered intensity I_{ex} per unit scattering volume V, the quantity I_i represents the incident intensity, and r is the distance from the sample to the detector. Here, we assume that the excess scattered intensity,

Table 3.1: The zero angle scattered intensity I_0 (in kilowatts/cm^2) for 25 kbp DNA, at various temperatures and a range of concentrations, determined using the Guinier approximation.

c ($\times 10^{-5}$g/ml)	11.2°C	13°C	14°C	15°C	20°C
2.84	12.7±1.45	7.0±0.4	5.3±0.23	3.8±0.21	2.2±0.16
2.485	9.3±0.72	5.9±0.27	4.4±0.1	3.2±0.17	2.1±0.1
2.13	6.5±0.73	4.8±0.33	3.8±0.27	2.84±0.089	1.54±0.089
1.42	3.2±0.29	2.8±0.33	2.4±0.15	1.9±0.15	1.08±0.058

$I_{\rm ex} = I(q) - I_{\rm s} \approx I(q)$, since the scattered intensity $I(q)$ from the DNA solution is much greater than the scattered intensity from pure solvent, $I_{\rm s}$. If we define the quantity,

$$K' = K\left(\frac{I_{\rm i}\, V}{r^2}\right) \tag{3.3}$$

it follows from Equations 3.1–3.3 that,

$$\frac{K'c}{I(q)} = \frac{1}{M}\left[1 + 2\,A_2\,c\,M\right]\frac{1}{P(q)}. \tag{3.4}$$

Denoting the scattered intensity in the limit of zero scattering angle by I_0 , then, since $\lim_{q\to 0} P(q) = 1$, Equation 3.4 implies,

$$I_0 \equiv \lim_{q\to 0} I(q) = \frac{K'c\,M}{[1 + 2\,A_2\,c\,M]} \tag{3.5}$$

and, Equation 3.4 can be rearranged in this limit to be,

$$\frac{c}{I_0} = \frac{1}{K'M} + \left[\frac{2A_2}{K'}\right]c. \tag{3.6}$$

If I_0 is known, then, it is clear from Equation 3.6 that a plot of c/I_0 versus the concentration c would be a straight line with intercept $1/(K'M)$ and slope $(2A_2/K')$. In the present instance, since we know M a priori for the 25 kbp sample used in the light scattering experiments, the constant K' can be determined from the intercept. As a result, the second virial coefficient A_2 can be determined from the slope. We address the question of determining I_0 as follows.

From Equations 3.4 and 3.5, it follows that,

$$\frac{I_0}{I(q)} = \frac{1}{P(q)}. \tag{3.7}$$

At low scattering angles, $q^2R_g^2 \sim \mathcal{O}(1)$, the form factor is often approximated by the Guinier function (Rubinstein and Colby, 2003),

$$P(q) = \exp\left[-\frac{q^2R_g^2}{3}\right]. \tag{3.8}$$

It then follows from Equation 3.7 that,

$$\ln\left(\frac{1}{I(q)}\right) = \ln\left(\frac{1}{I_0}\right) + \left(\frac{R_g^2}{3}\right) q^2. \tag{3.9}$$

As a result, a plot of $\ln(1/I(q))$ versus q^2 would be linear, and the zero angle scattered intensity I_0 could be determined from the intercept without a knowledge of either K', A_2 or R_g.

Figure 3.2 displays the intensity as a function of the scattering wave vector for 25 kbp DNA, at 14°C and four different concentrations (corresponding to $c/c^* =$ 0.2, 0.3, 0.35 and 0.4), plotted semilog. The fact that nearly all the measured intensity data, for various values of q^2, lies on the fitted lines indicates that the Guinier is a good approximation in this case. All the values of I_0, determined by extrapolating linear fits of $\ln(1/I(q))$ versus q^2 data to $q = 0$, at various temperatures and concentrations, are listed in Table 3.1.

Attempts to use an alternative procedure to find I_0 by assuming that $P(q)$ is a linear function of q^2, for $q^2R_g^2 \lesssim \mathcal{O}(1)$, i.e., $P(q) = 1 - (q^2R_g^2/3)$ and plotting $1/I(q)$ versus q^2 (as in a Zimm plot), or $\sqrt{1/I(q)}$ versus q^2 (as in a Berry plot) (Burchard, 2008) and extrapolating the fitted line through the data to $q = 0$, did not lead to consistent results in the subsequent analysis.

Once I_0 is known, the ratio c/I_0 can be plotted versus c, and both K' and A_2 determined, as discussed below Equation 3.6. Figure 3.3 is a plot of c/I_0 versus c for the values of I_0 listed in Table 3.1, at the various temperatures at which measure-

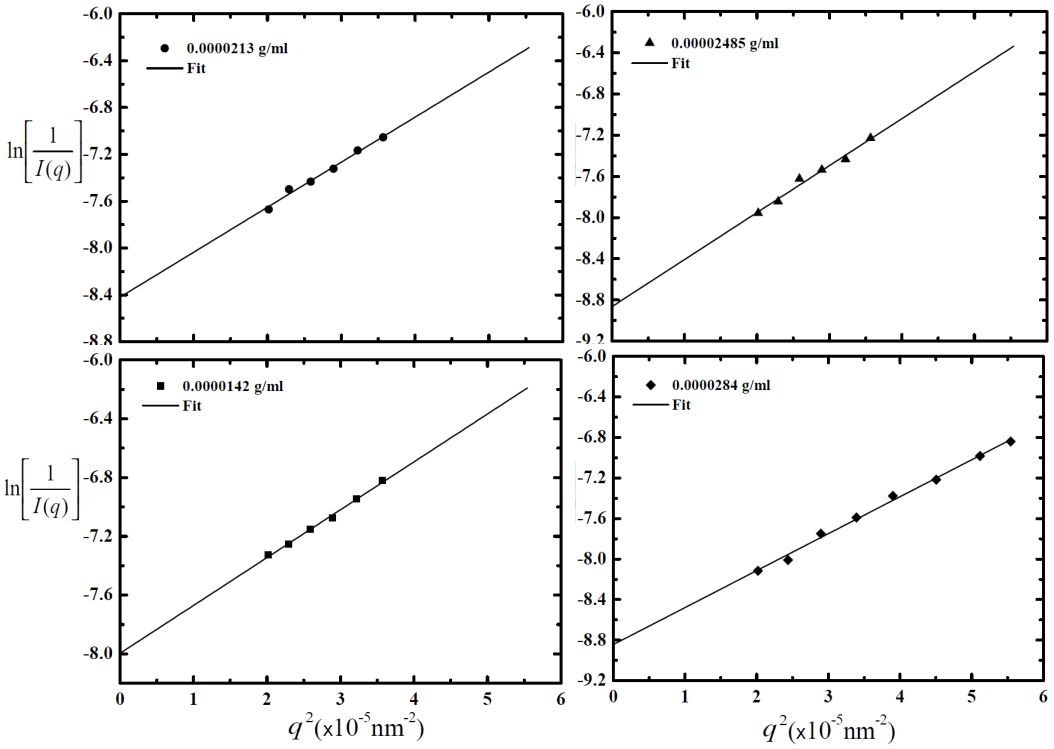

Figure 3.2: I_0 by Guinier approximation. Intensity as a function of scattering wave vector q, measured for 25 kbp DNA at 14°C and four different concentrations, corresponding to c/c^* = 0.2, 0.3, 0.35 and 0.4, extrapolated to q = 0.

ments were carried out. While in principle the data for all the temperatures should extrapolate to a unique intercept at c = 0, the scatter observed in Figure 3.3 reflects the uncertainty in the $I(q)$ data. Accounting for the spread in the values of the intercepts, leads to the value, $K' = 9.5 \pm 0.3$ mol cm watts/g^2. The dependence on temperature of the second virial coefficient A_2, determined from the slopes of the fitted lines in Figure 3.3, and the subsequent analysis, is discussed in the following section.

3.4 Determining the θ-temperature of DNA solutions

The θ-temperature for a polymer solution can be determined by finding the temperature at which the second virial coefficient A_2 vanishes. One of the methods often used to determine the temperature dependence of A_2 is static light scattering, since the intensity of scattered light, $I(q)$, at any temperature, concentration

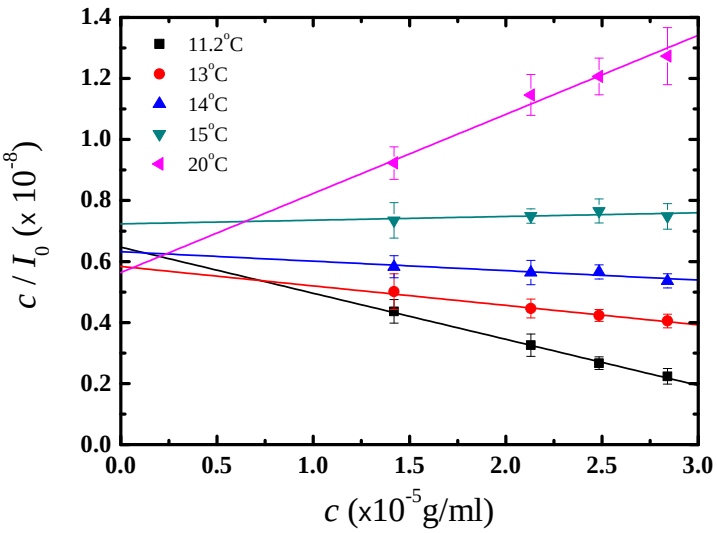

Figure 3.3: Linear dependence of the ratio c/I_0 on concentration, as expressed by Equation 3.6, for 25 kbp DNA at various temperatures. The constant K' is determined from the intercept, and the temperature dependence of the second virial coefficient is determined from the slope.

and molecular weight of the dissolved species, depends on $A_2(T)$. Details of the static light scattering experiments, the governing equation for $I(q)$, and the procedure adopted here to determine $A_2(T)$, have already been discussed in the above sections. The principal results of the analysis are presented here.

Figure 3.4, which is a plot of the second virial coefficient for 25 kbp DNA as a function of temperature in the range 10 to 20°C, shows that A_2 increases from being below zero to above zero in this range of temperatures. A linear least squares fit to the data in the vicinity of the θ temperature (where the dependence is expected to be linear) suggests that,

$$\boxed{T_\theta = 14.7 \pm 0.5^\circ\text{C}} \tag{3.10}$$

Note that this implies that a significant fraction of the temperatures at which measurements were carried out are in the poor solvent regime. The reliability of measurements in the poor solvent regime is discussed in detail in Appendix A.

As in the case of other polymer solution properties, the second virial coefficient, when represented in a suitably normalised form, is a universal function of the sol-

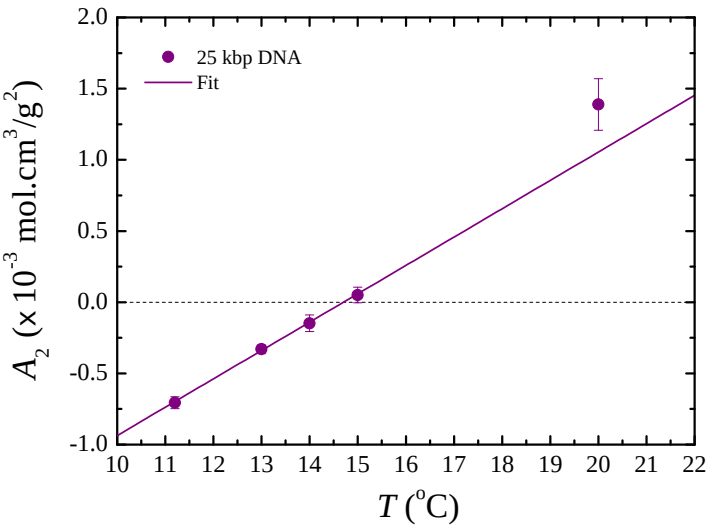

Figure 3.4: Determination of the θ-temperature, T_θ, for 25 kbp DNA. The equation of the fitted line to the temperature dependence of the second virial coefficient is: $A_2 = -3.15 \times 10^{-3} + 2.16 \times 10^{-4}\, T$, where T is in °C.

vent quality parameter in the crossover region. The specific form of the crossover function used to describe the dependence is,

$$\frac{A_2 M^{\frac{1}{2}} m_k^{\frac{3}{2}}}{N_A b_k^3} = 0.20 \left[\tilde{z}^{-2.64} + \tilde{z}^{-1.4}\right]^{-0.38}, \tag{3.11}$$

where, $\tilde{z} = N_k^{1/2}\left(1 - \frac{T_\theta}{T}\right)$ [see Equation 3.109 in Rubinstein and Colby (2003)]. The temperature and molecular weight dependence of the second virial coefficient, for a number of polymer-solvent combinations, and from computer simulations, is found to obey this universal crossover function. Figure 3.5 is a plot of this function, which is modelled after a similar figure in Rubinstein and Colby (2003), along with the data reported previously by Berry (1966) for linear polystyrenes in decalin. We have used a linear least squares fit to the 25 kbp DNA data displayed in Figure 3.4, and evaluated A_2 at a few temperatures between 14 and 20°C (indicated by the red triangles in Figure 3.5). Clearly the present data also appears to lie on the universal crossover function.

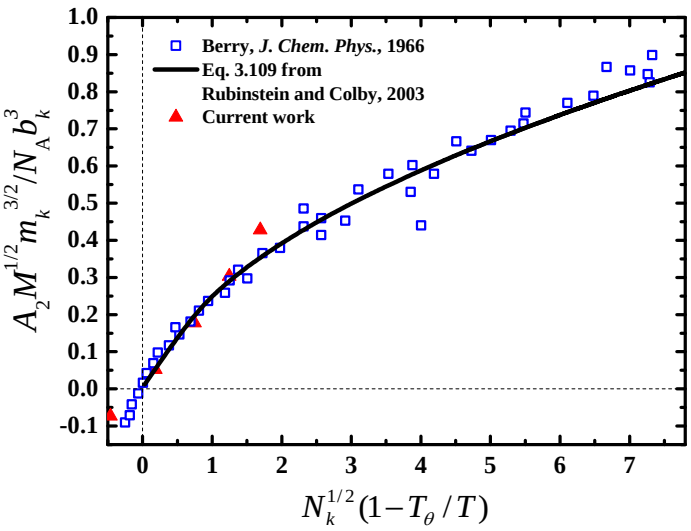

Figure 3.5: Universal crossover plot for the second virial coefficient. Values of A_2 for 25 kbp DNA (red triangles) are calculated from the fit function given in the caption to Figure 3.4 at 14, 15, 16, 17 and 18°C. The θ temperature is taken to be $T_\theta = 14.7$°C. The line is drawn according to Equation 3.11. The molar mass per Kuhn step is defined as $m_k = M/N_k$, and the Kuhn step length is $b_k = 2P$. Values of M, N_k, and P are given in Table 2.1. Open squares represent data from Berry (1966), for linear polystyrene in decalin.

At the θ-temperature, the precise form of the expression for the form factor, $P(q) = I(q)/I_0$, where, $I_0 = \lim_{q\to 0} I(q)$, is known to have the following form (referred to as the Debye function (Rubinstein and Colby, 2003)),

$$P(q) = \frac{2}{\left(q^2 R_g^{\theta 2}\right)^2}\left[\exp\left(-q^2 R_g^{\theta 2}\right) - 1 + q^2 R_g^{\theta 2}\right]. \tag{3.12}$$

Note that, since we know the contour length and the persistence length for 25 kbp DNA, we can estimate $R_g^\theta = 376$ nm, as displayed in Table 2.1. The determination of I_0 from the measured $I(q)$ data for 25 kbp DNA is discussed in the supplementary material. As a result, the dependence of $P(q)$ on q, for the current measurements on 25 kbp DNA, is known. The Debye function is also known to describe the angular dependence of the scattered intensity at temperatures away from the θ temperature very well, over a wide range of values of $q^2 {R_g}^2$ (Schäfer, 1999; Utiyama, 1971). As a result, the Debye function can be used to fit the $P(q)$ data to determine

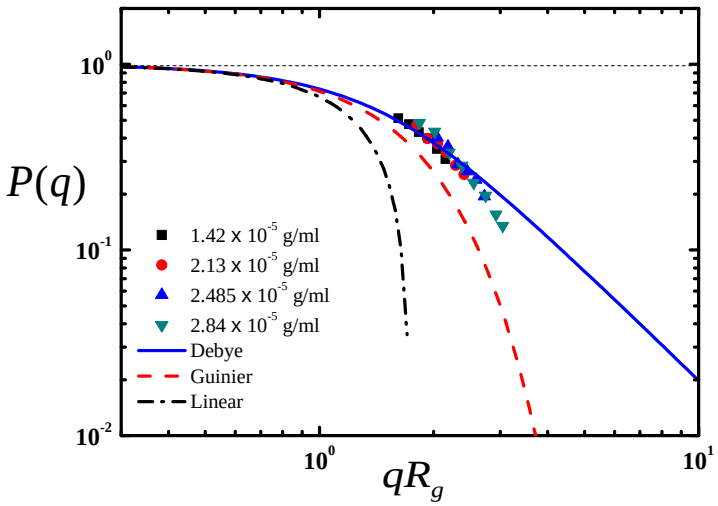

Figure 3.6: A Debye function fit to the form factor, $P(q)$, data for 25 kbp DNA, obtained at 14°C and four different concentrations. The Guinier approximation, $P(q) = exp(-q^2 {R_g}^2/3)$, and the linear approximation, $P(q) = 1 - (q^2 {R_g}^2/3)$ are also displayed.

R_g. Figure 3.6 displays the Debye function fit to the $P(q)$ data for 25 kbp DNA, at 14°C and four different concentrations, along with the Guinier approximation $P(q) = \exp\left(-q^2 {R_g}^2/3\right)$, and the linear approximation, $P(q) = 1 - \left(q^2 {R_g}^2/3\right)$. We can see that the Debye function describes the data reasonably accurately, independent of concentration, over a wide range of the measured values of $q^2 {R_g}^2$. We find that the fitted values of R_g are in the range 389.4 ± 68.1 nm across the four different concentrations. While this is reasonably close to the analytical value of $R_g^\theta = 376$ nm, as is expected at 14°C, the current data does not cover a sufficiently wide range of $q^2 {R_g}^2$ values to determine R_g more precisely.

3.5 Conclusions

Using static light scattering measurements, for the first time, the θ-temperature (T_θ) has been determined using a single, medium molecular weight DNA fragment, 25 kbp, from the absolute values of second virial coefficients A_2 at different temperatures in a solvent (10 mMTris, 1 mMEDTA, 0.5 M NaCl and water), that is com-

monly used for polymer physics and rheology studies. DNA, in this solvent, has T_θ = 14.7 $\pm$ 0.5°C. The absolute values of A_2 from the current work appear to lie on a universal crossover function of the second virial coefficient when plotted as a function of solvent quality, and are in agreement with reported data on linear polystyrene in decalin from Berry (1966). This is our first confirmation that double-stranded DNA under high salt concentration behaves similar to neutral synthetic polymers.

The knowledge of the θ-temperature of DNA in this solvent will facilitate the characterization of the z values of DNA in this solvent which is essential for proper characterization of the crossover behaviour of DNA solutions, both in dilute and semidilute regime. The estimation of solvent quality for DNA solutions using dynamic light scattering measurements is discussed in the next chapter.

4

Solvent Quality and Universal Swelling of the Hydrodynamic Radius

4.1 Introduction

We know that this universality in a dilute solution, in terms of dynamic properties for synthetic polymer-solvent systems, has already been demonstrated through experiments, simulations and theoretical predictions, as a function of the solvent quality parameter z in the crossover regime (see Section 3.1). However this is not the case with DNA solutions. As pointed out in Chapters 1 and 3, for characterizing the behaviour of DNA solutions in the crossover region, it is mandatory to determine the solvent quality z of the DNA solutions in the specific solvent that has been used in current experiments.

In this chapter, we establish the methodology for determining the solvent quality of the DNA solutions by systematically characterising the DNA molecules in an extended range of molecular weights from 2.9 to 289 kbp ($\approx 10^6$ to 10^8 g/mol), and at a variety of different temperatures by dynamic light scattering (DLS) measurements in the dilute regime. For determining the solvent quality parameter z for DNA solutions, we need to know both the θ-temperature and the chemistry depen-

dent constant k (see Equation 1.1). We have already determined the θ-temperature for DNA in a particular solvent (see Section 3.4 in the previous chapter). With the knowledge of T_θ we have determined k by finding the dependence of the swelling of the hydrodynamic radius α_{H} on the variable $\left(1 - \frac{T_\theta}{T}\right)\sqrt{M}$ in the same solvent, and by shifting the data for DNA with a shift factor such that it coincides with the BD simulation data from our group (Sunthar and Prakash, 2006) and also data for different synthetic polymer-solvent systems (Tominaga et al., 2002). We show that, similar to the behaviour exhibited by neutral synthetic polymer solutions, the swelling of DNA solutions in excess salt also exhibits universal behaviour in the context of α_{H}, which is a dynamic equilibrium property. More importantly, this will also enable us to properly characterize the temperature crossover behaviour of the zero shear rate viscosity for semidilute DNA solutions, as a function of z and to validate the scaling predictions by Jain et al. (2012a).

In this chapter, the estimation of the solvent quality z, the chemistry dependent constant k, and asymptotic swelling of the hydrodynamic radii as a function of z for dilute DNA solutions are discussed in various subsections of Section 4.3. In Section 4.4, we summarize the principal conclusions of the present work.

4.2 DLS of dilute DNA solutions

The sample preparation procedure and the methodology for DLS has been discussed in Section 2.3. A typical example of the "Correlation Coefficient" , $G(\tau) =< I(t)I(t+\tau) >$ measured by the instrument for 25 kbp DNA at various temperatures and $c/c^* = 0.1$ is shown in Figure 4.1. Here, I is the intensity of scattered light, and τ is the time difference of the correlator. The correlation function is processed by the instrument to obtain the size distribution as a plot of the relative intensity of light scattered by particles in various size classes. Typical intensity size distribution plots are shown in Figure 4.2 for 25 kbp DNA at various temperatures, where it can be seen that there is a single fairly smooth peak indicating the molecule's size. Measured values of R_{H} are reported in Table 4.1.

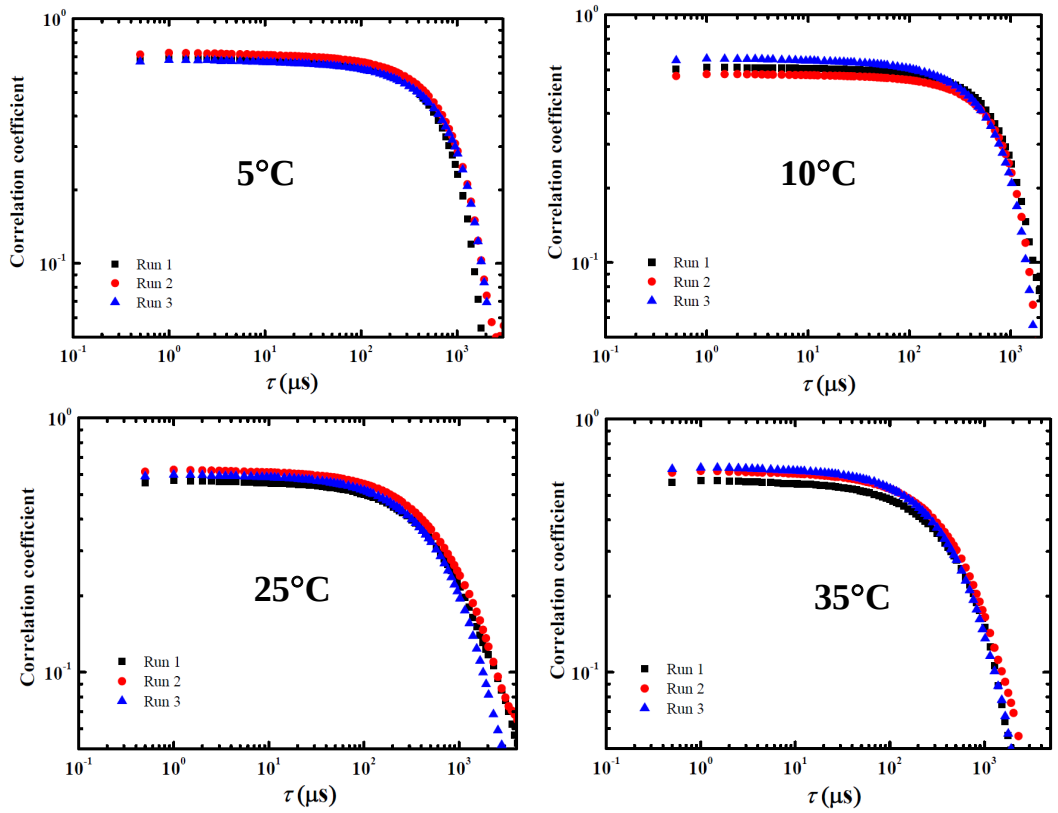

Figure 4.1: Intensity autocorrelation spectra for 25 kbp DNA at various temperatures (indicated within the figures) and $c/c^* = 0.1$.

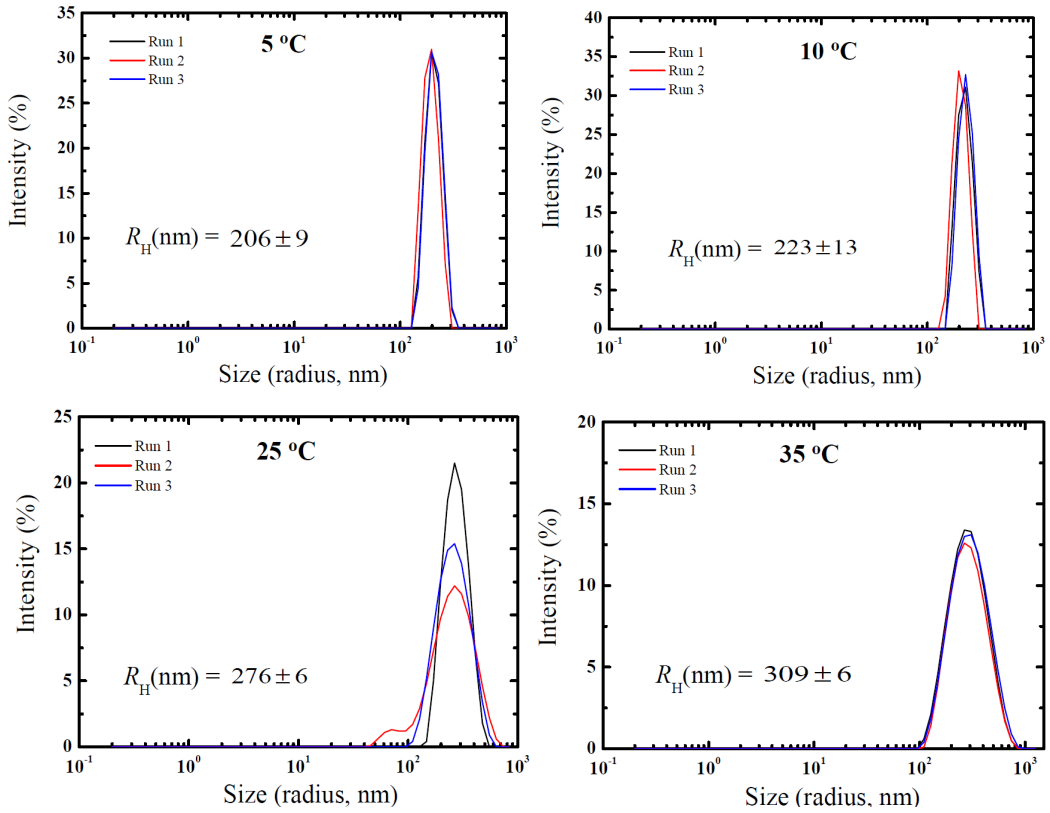

Figure 4.2: Intensity size distributions for 25 kbp DNA at various temperatures (indicated within the figures).

4.3 Estimating the solvent quality of DNA solutions

The scaling variable that describes the temperature crossover behaviour from θ solvents to very good solvents, is the solvent quality parameter z, defined in Equation 1.1. The significance of the variable z is that when data for any equilibrium property of a polymer-solvent system is plotted in terms of z in the crossover region, then regardless of the individual values of M and T, provided the value of z is the same, the equilibrium property will turn out to have the same value. Indeed, provided the values of k are chosen appropriately, equilibrium data for different polymer-solvent systems can be shown to collapse onto master plots, revealing the universal nature of polymer solution behaviour. Typically, a particular polymer-solvent system is chosen as the reference system and data for all other systems are shifted to coincide with the values of the reference system by an appropriate choice of k (Miyaki and Fujita, 1981; Tominaga et al., 2002; Hayward and Graessley, 1999). The same shifting procedure is also commonly used to compare experimental observations in the crossover regime with theoretical predictions or simulations results (Kumar and Prakash, 2003; Sunthar and Prakash, 2006). Basically, as will be demonstrated in greater detail subsequently, the values of k for an experimental system are chosen such that the experimental and theoretical values of z agree when the respective equilibrium property values are identical.

We have determined the value of z for the DNA solutions used here by comparing experimental measurements of the swelling α_H of the hydrodynamic radius R_H, with predictions of Brownian dynamics simulations reported previously (Sunthar and Prakash, 2006). The hydrodynamic radius has been measured by carrying out dynamic light scattering measurements over a range of temperatures and molecular weights at a concentration $c/c^* = 0.1$. Details of the dynamic light scattering measurements, including the instrument used, sample preparation procedure, and typical intensity plots are given in the above sections. Before discussing the details of the estimation of solvent quality, it is appropriate to first present some results of the measurements of the hydrodynamic radius.

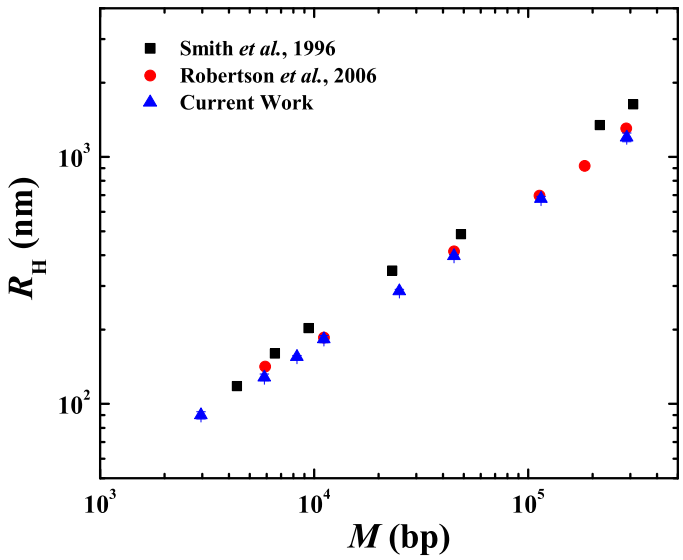

Figure 4.3: Comparison of the molecular weight dependence of hydrodynamic radius, obtained previously by Smith et al. (1996) and Robertson et al. (2006) at 25°C with the current work.

Figure 4.3 compares present measurements of the dependence of hydrodynamic radius on molecular weight, with previous measurements (Smith et al., 1996; Robertson et al., 2006) at 25°C. While Smith et al. (1996) used fragments and concatenates of λ-phage DNA to obtain molecules across the wide range of molecular weights that were studied, the measurements of Robertson et al. (2006) were carried out on molecules identical to those that have been used here. Both the earlier results were obtained by tracking fluorescently labeled linear DNA, in contrast to current measurements which were obtained by dynamic light scattering. The close agreement between results obtained by two entirely different techniques, across the entire range of molecular weights, establishes the reliability of the procedures adopted here.

Table 4.1 is a compilation of all the measurements of $R_{\rm H}$ carried out here, across all molecular weights and temperatures. Since we have established that $T_\theta = 14.7 \pm 0.5$°C, we expect the hydrodynamic radius to scale as $M^{0.5}$ at $T = 15$°C. Figure 4.4 is a plot of $R_{\rm H}^\theta$ versus M, which clearly confirms that indeed ideal chain statistics are

Table 4.1: Hydrodynamic Radius (R_H) of linear DNA at different temperatures. Each data point corresponds to the intensity peaks from DLS measurements. The mean of 15 readings was taken as final data point at each temperature for each DNA fragment. The values of R_H^θ, with the θ-temperature assumed to be 15°C, are indicated in italics.

Sequence length	2.9 kbp	5.9 kbp	8.3 kbp	11.1 kbp
Temperature	R_H (in nm)	R_H (in nm)	R_H (in nm)	R_H (in nm)
5°C	73±4	104±3	123±3	141±3
10°C	77±3	109±3	131±3	152±3
15°C	*85±3*	*121±3*	*145±3*	*167±3*
20°C	87±3	124±3	148±3	173±4
25°C	90±3	131±5	155±2	183±6
30°C	96±2	136±4	162±3	189±3
35°C	101±4	145±7	174±3	203±5

Sequence length	25 kbp	45 kbp	114.8 kbp	289 kbp
Temperature	R_H (in nm)	R_H (in nm)	R_H (in nm)	R_H (in nm)
5°C	203±4	258±5	385±13	540±35
10°C	226±5	303±6	473±14	718±46
15°C	*258±3*	*349±4*	*560±18*	*897±57*
20°C	267±8	367±4	607±13	1025±39
25°C	286±5	397±5	677±15	1201±49
30°C	297±4	417±6	722±13	1300±38
35°C	313±8	431±8	753±19	1363±57

obeyed in the neighbourhood of the estimated θ-temperature. It is remarkable that the θ-solvent scaling behaviour is seen in as low as a molecular weight as 2.9 kbp. This serves as our second confirmation of the double-stranded DNA behaviour like a neutral polymer.

Since both R_g^θ and R_H^θ scale with molecular weight as $M^{0.5}$ at the θ-temperature, their ratio should be a constant. As is well known, experimental observations and theoretical predictions indicate that $U_{RD}^\theta = R_g^\theta / R_H^\theta$ is a chemistry independent universal constant (for a recent compilation of values see Table I in Kröger et al. (2000)). Zimm theory predicts a universal value $U_{RD}^\theta \approx 1.47934$ (Zimm, 1956; Öttinger, 1996). Since we have estimated R_g^θ by assuming Gaussian chain statistics at the θ temperature, and have measured R_H^θ, we can calculate U_{RD}^θ for all the molecular weights used in this work. The expected molecular weight independence of U_{RD}^θ is displayed in Figure 4.5. The mean value of U_{RD}^θ is also seen to be close to the value

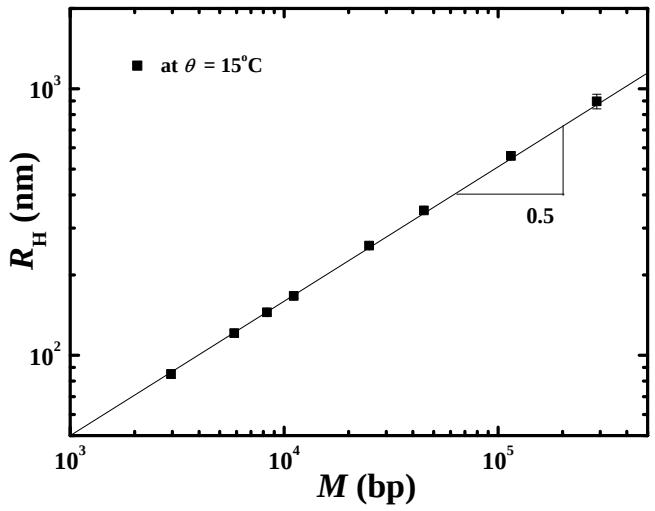

Figure 4.4: The variation of the hydrodynamic radius ($R_{\rm H}^{\theta}$) with molecular weight (in bp) at $T = 15^{\circ}$C, which is estimated to be close to the θ-temperature.

predicted by Zimm. This confirms that both the scaling with molecular weight, and the absolute values of $R_{\rm H}^{\theta}$, across the entire range of DNA molecular weights, are accurately captured by the dynamic light scattering experiments.

The swelling $\alpha_{\rm H}$ for any combination of M and T can be calculated from the values reported in Table 4.1, and plotted as a function of the scaling variable z, once a choice has been made for the value of the constant k. As mentioned in Section 4.1, k can be determined by comparison of experimental measurements with the results of Brownian dynamics simulations. We refer the interested reader to the relevant literature (Domb and Barrett, 1976; Barrett et al., 1991; Yamakawa, 2001; Schäfer, 1999; Kumar and Prakash, 2003; Sunthar and Prakash, 2006) for a discussion of how the solvent quality parameter z enters the structure of analytical theories and Brownian dynamics simulations. It suffices here to note that the theoretically predicted swelling of the hydrodynamic radius can be represented by the functional form $\alpha_{\rm H} = f_{\rm H}(z)$, where, $f_{\rm H}(z) = (1 + a\,z + b\,z^2 + c\,z^3)^{m/2}$, with the values of the constants a, b, c, m, etc., dependent on the particular context. The values of the various constants that fit the results of Brownian dynamics simulations, are reported

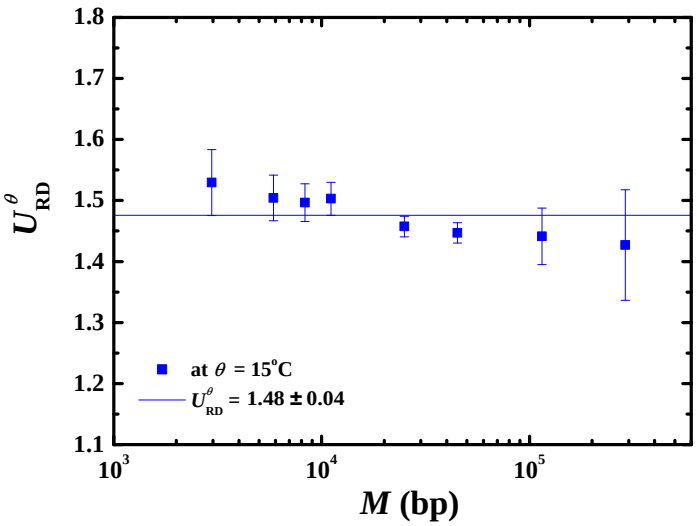

Figure 4.5: The molecular weight independence of $U^{\theta}_{\rm RD}$. The mean value is close to the Zimm model prediction in the long-chain limit, $U^{\theta}_{\rm RD} \approx 1.47934$ (Zimm, 1956; Öttinger, 1996).

in the caption to Figure 4.7. We find the constant k for DNA solutions by adopting the following procedure.

The value of the chemistry dependent constant k (appearing in the definition of the solvent quality parameter z) has been determined for the current solvent by adopting a procedure elaborated in an earlier work (Kumar and Prakash, 2003). Consider $\alpha_{\rm H}^{\rm expt}$ to be the experimental value of swelling at a particular value of temperature T and molecular weight M. It is then possible to find the Brownian dynamics value of z that would give rise to the same value of swelling from the expression $z = f_{\rm H}^{-1}(\alpha_{\rm H}^{\rm expt})$, where $f_{\rm H}^{-1}$ is the inverse of the function $f_{\rm H}(z)$. Since $z = k\,\hat{\tau}\,\sqrt{M}$, where $\hat{\tau} = \left(1 - \dfrac{T_\theta}{T}\right)$, it follows that a plot of $f_{\rm H}^{-1}(\alpha_{\rm H}^{\rm expt})/\sqrt{M}$ versus $\hat{\tau}$, obtained by using a number of values of $\alpha_{\rm H}^{\rm expt}$ at various values of T and M, would be a straight line with slope k (see Figure 4.6). The value of k found by this procedure is,

$$\boxed{k = 0.0047 \pm 0.0003\ (\mathrm{g/mol})^{-1/2}}. \tag{4.1}$$

Once the constant k is determined, both experimental measurements of swelling

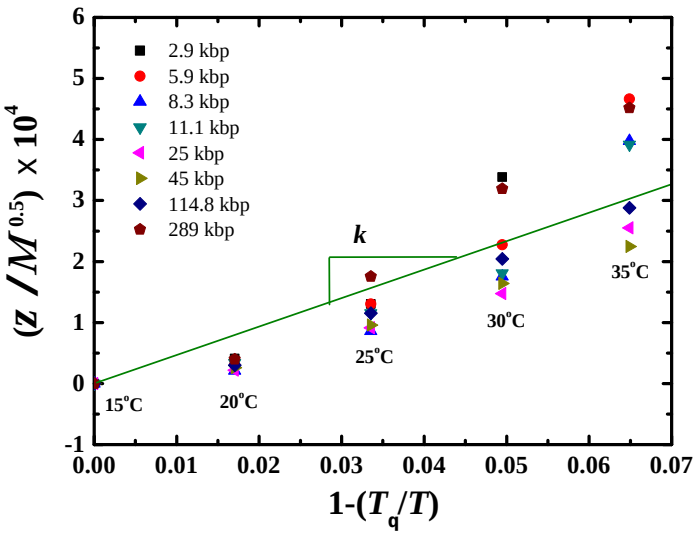

Figure 4.6: Determination of the chemistry dependent constant k for the current solvent by adopting a procedure elaborated in an earlier work (Kumar and Prakash, 2003). Only the temperatures above T_θ are considered here. The data points were least square fitted with a straight line, and the slope k was determined (Kumar and Prakash, 2003). A value of 15°C has been used for the θ-temperature. The value of k found by this procedure is given in Equation 4.1.

and results of Brownian dynamics simulations can be represented on the same plot. Assuming that the θ-temperature is 15°C for the solvent used in this study, we have determined the value of k by following this procedure. It follows that for any given molecular weight and temperature, the solvent quality z for the DNA solution can be determined. Typical values of z, at various M and T, obtained by this procedure are reported in Table 6.1.

The solvent quality crossover of α_H for DNA, determined from the current measurements, is shown in Figure 4.7, along with the predictions of Brownian dynamics simulations. Experimental data of Tominaga et al. (2002), which are considered to be highly accurate measurements of synthetic polymer swelling, are also plotted in the same figure. It is evident from the figure that, just as in the case of synthetic polymer solutions, irrespective of solvent chemistry, the swelling of DNA is universal in the crossover region between θ to good solvents. This is our third confirmation of double-stranded DNA good to be considered as a model polymer.

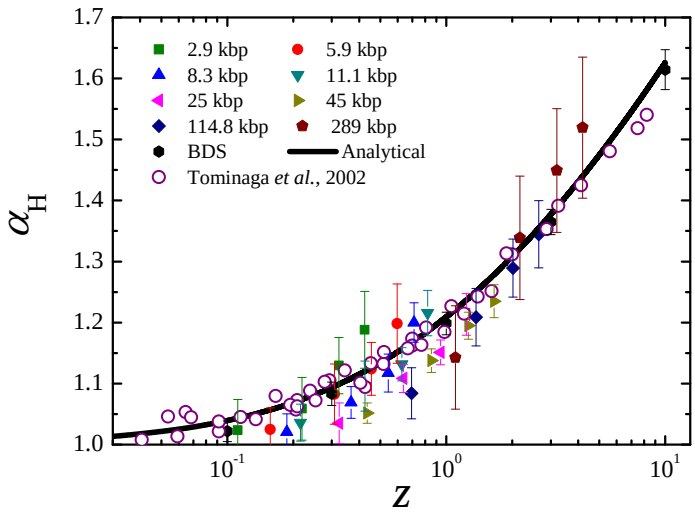

Figure 4.7: Swelling of the hydrodynamic radius. The filled coloured symbols represent experimental data for DNA. BDS refers to the predictions of Brownian dynamics simulations (Sunthar and Prakash, 2006), with the curve representing the function $f_H(z)$, with constants $a = 9.528$, $b = 19.48$, $c = 14.92$, and $m = 0.0999$. Empty circles represent several experimental data on synthetic polymers collated in Tominaga et al. (2002).

Having estimated the value of z for any values of M and T, it follows that other universal properties predicted by simulations or theory, at any particular value of z, can be compared with experimental results for DNA, at the same value of z.

4.4 Conclusions

In the current work, a dynamic property (R_H) of a range of DNA (2.9 to 289 kbp) in a commonly used solvent (same as in Chapter 3) have been characterized in terms of parameters used in dilute polymer solution theory. Using dynamic light scattering, the chemistry dependent constant k has been found out from the R_H values at different temperatures for different molecular weights, and the crossover of the swelling of the hydrodynamic radius (α_H) in good solvent conditions ($T > T_\theta$) was also demonstrated in the same solvent, as used for SLS studies. DNA in this solvent has $k = 0.0047 \pm 0.0003$ $(g/mol)^{-1/2}$.

As with the regular polymers, the dilute solution crossover data of DNA can also be collapsed into a unique function of a scaling variable z. The scaling functions also agree within experimental error with the functions for synthetic polymers and model chains in good solvents obtained using molecular simulations. With known values of T_θ (from Chapter 3) and k (from this chapter), it is now possible to accurately determine the value of z for a DNA of any M and at any T in this solvent. Also, by demonstrating the universal dynamic crossover of DNA, it was established that the crossover regime between θ and good solvents can only be characterized by a combined dependence of both molecular weight and temperature, in the form of z. This is crucial for the characterization of the semidilute unentangled solutions in the crossover regime, as will be shown in Chapter 6. These developments make it now possible to examine the crossover behaviour of any static or dynamic property of linear DNA molecules in the presence of excess salt.

5

Intrinsic Viscosity and the Swelling of the Viscosity Radius

5.1 Introduction

The swelling α_η (defined in Equation 1.6), of the viscosity radius R_η, defined as

$$R_\eta \equiv \left(\frac{3[\eta]M}{4\pi N_A}\right)^{\frac{1}{3}}, \tag{5.1}$$

has already been experimentally measured and shown to be a universal function of only the solvent quality parameter z in the crossover regime for synthetic polymer-solvent systems (Tominaga et al., 2002; Arai et al., 1995; Jamieson and Simha, 2010; Miyaki and Fujita, 1981; Hayward and Graessley, 1999). Notably, however, the universal curve for the swelling α_g of the gyration radius R_g as a function of z is significantly different from the universal curve for either α_η or swelling α_H of the hydrodynamic radius R_H (Miyaki and Fujita, 1981; Arai et al., 1995; Tominaga et al., 2002; Hayward and Graessley, 1999). However, to our knowledge, an experimental study demonstrating the universal crossover of α_η as a function of z for dilute DNA solutions is still lacking.

The approximate quasi-two-parameter theory of Yamakawa and co-workers (Yamakawa, 2001, 1997), which is based on pre-averaged hydrodynamic interactions (HI) (Barrett, 1984), is able to describe the crossover behaviour of α_η with reasonable accuracy (Tominaga et al., 2002; Jamieson and Simha, 2010). On the other hand, it fails to describe the crossover behaviour of α_{H}, even when modified to take into account fluctuations in HI (Yamakawa and Yoshizaki, 1995; Arai et al., 1995; Jamieson and Simha, 2010). By carrying out exact Brownian dynamics simulations, Sunthar and Prakash (2006) have shown that the fundamental difference between the crossover scaling behaviour of the static swelling α_{g}, and the dynamic swelling α_{H}, is in fact due to the presence of fluctuating HI. By suitably accounting for fluctuating HI and excluded volume (EV) interactions in the asymptotic long chain limit, Prakash and coworkers have been able to obtain quantitatively accurate, parameter free predictions of α_{g} and α_{H}, as functions of z (Kumar and Prakash, 2003; Sunthar and Prakash, 2006). Very recently, Prakash and coworkers have obtained parameter free predictions of α_η for flexible chains in dilute solutions by exact BD simulations and have examined the role of fluctuating HI (Ahirwal, 2009; Pan et al., 2014), in determining the observed difference between α_η and α_{g}, which also agree quantitatively with experimental observations.

The universal viscosity ratio , $U_{\eta\mathrm{R}}$, which is closely related to the Flory-Fox constant (Rubinstein and Colby, 2003; Jamieson and Simha, 2010) Φ , and which is frequently used to characterise dilute polymer solutions, is defined by (Öttinger, 1996; Kröger et al., 2000),

$$U_{\eta\mathrm{R}} \equiv \left(\frac{R_\eta}{R_{\mathrm{g}}}\right)^3 = \frac{6^{\frac{3}{2}}}{(4\pi/3)}\,\frac{\Phi}{N_{\mathrm{A}}}. \tag{5.2}$$

For θ solvents, experimental measurements (Miyaki et al., 1980; Kröger et al., 2000) indicate that $U^{\theta}_{\eta\mathrm{R}} = 1.49 \pm 0.06$, which corresponds to the well known value of the Flory-Fox constant for θ solvents (Rubinstein and Colby, 2003), $\Phi_0 = 2.6 \times 10^{23}$. As discussed by Jamieson and Simha (2010) in their recent review, a number of experimental measurements of the Flory-Fox constant under good solvent conditions have been reported in the literature. Nevertheless, the behaviour of Φ with vary-

ing solvent conditions appears not to be known with any great certainty. The approximate quasi-two-parameter theory seems to accurately describe (indirectly) the crossover of $U_{\eta R}$ from θ to very good solvents (Tominaga et al., 2002; Jamieson and Simha, 2010). Also, in addition to α_η, Prakash and coworkers have predicted the crossover behaviour of $U_{\eta R}$ through exact Brownian dynamics simulations, which account for fluctuating HI (Ahirwal, 2009; Pan et al., 2014). As in the case with α_η, the universal crossover of $U_{\eta R}$ as a function of z has not been demonstrated so far for dilute DNA solutions.

As mentioned earlier in this section, the reported observations of the swelling of the viscosity radius α_η and the Flory-Fox constant have largely been on synthetic polymer-solvent systems (Tominaga et al., 2002; Miyaki and Fujita, 1981; Hayward and Graessley, 1999). We have shown in Chapter 4 that the crossover swelling of R_H of linear DNA molecules in dilute solutions with excess salt can be collapsed onto earlier observations of the α_H of synthetic polymers. This now makes it possible to examine the crossover behaviour of any static or dynamic property of linear DNA solutions in the presence of excess salt. Since the solvent quality z for the DNA solutions has been determined (see Chapter 4), this enables us to verify the universal scaling of α_η with z, by comparison with experimental measurements for synthetic polymer systems. From its definition (see Equation 1.6), α_η for DNA solutions can be obtained from the measurement of $[\eta]$ at the θ-temperature and at several temperatures above the θ-temperature.

The aim of this work is two-fold. First, by carrying out systematic measurements of the intrinsic viscosity of two different molecular weight samples of linear double-stranded DNA at a range of temperatures in the presence of excess salt, we examine the crossover scaling of the swelling of the viscosity radius α_η, and the universal viscosity ratio, $U_{\eta R}$. Comparison with earlier observations of the behaviour of synthetic polymers enables not only the establishment of the universal scaling of DNA solutions, but also serves as an independent verification of the θ-temperature and solvent quality, as estimated in Chapters 3 and 4. Second, we also compare our results with the detailed BD simulations from Prakash and cowork-

ers (Ahirwal, 2009; Pan et al., 2014). This is a further step in validating the role of double-stranded DNA as a model flexible polymer.

The plan of the chapter is as follows. In subsection 5.3.1, we describe the measurement of the intrinsic viscosity of the DNA solutions, and tabulate values of intrinsic viscosity and the Huggins coefficient across a range of temperatures. In the remaining subsections of Section 5.3, we briefly discuss the prediction of α_η and $U_{\eta R}$ by BD simulations (Ahirwal, 2009; Pan et al., 2014) and compare simulation predictions with prior and current experimental measurements. Finally, in Section 5.4, we summarize the principal conclusions of the present work.

5.2 Methodology

5.2.1 Preparation of DNA solutions

We have measured the shear viscosities of two DNA samples: 25 kbp and T4 DNA at various temperatures (15 to 35°C) and concentrations (0.0038 to 0.118 mg/ml) in the dilute regime. The procurement of the T4 DNA and and protocols for preparation and purification of the 25 kbp DNA solutions including the solvent used have been discussed in Section 2.1. The maximum concentration used for T4 DNA was the same as mentioned in Section 2.1. The maximum concentration used for 25 kbp was 0.24 mg/ml.

5.2.2 Shear rheometry

Details about the rheometer used, measuring principle, temperature sensitivity, shear rheometry procedure, precautions taken while measurements, instrument calibration, shear rate range employed and avoidance of shear ramp, sample equilibration time, dependence on rheometer geometry etc., have been elaborated in Section 2.4.

The shear rate dependence of the measured steady state shear viscosity η of the solutions is shown in Figure 5.1. From the figure, it is clear that the solution viscosity is virtually independent of the shear rate at very low shear rates, which

Table 5.1: Steady state zero shear rate viscosities, η_0 (mPa.s) for 25 kbp and T4 DNA at various concentrations, c (mg/ml) and temperatures, T (°C) in the dilute regime. Note that $T_\theta \approx 15$°C.

25 kbp			
c	T	c/c^*	η_0
0.112	15	0.91	2.95 ± 0.01
0.07	15	0.57	1.76 ± 0.01
	18	0.74	1.75 ± 0.01
	21	0.85	1.72 ± 0.01
	25	0.97	1.58 ± 0.02
0.0441	15	0.36	1.53 ± 0.01
	18	0.46	1.49 ± 0.01
	21	0.54	1.43 ± 0.01
	25	0.61	1.31 ± 0.01
	30	0.7	1.27 ± 0.01
	35	0.76	1.2 ± 0.01
0.028	15	0.23	1.38 ± 0.01
	18	0.29	1.31 ± 0.01
	21	0.34	1.25 ± 0.01
	25	0.39	1.15 ± 0.01
	30	0.44	1.09 ± 0.01
	35	0.48	1.01 ± 0.01
0.0175	15	0.14	1.29 ± 0.01
	18	0.18	1.2 ± 0.01
	21	0.21	1.14 ± 0.01
	25	0.24	1.05 ± 0.01
	30	0.28	0.98 ± 0.01
	35	0.3	0.9 ± 0.01

T4 DNA			
c	T	c/c^*	η_0
0.038	15	0.79	5.38 ± 0.13
0.023	15.7	0.58	2.43 ± 0.01
	17.3	0.72	2.33 ± 0.01
	19.4	0.85	2.23 ± 0.01
0.015	15.7	0.38	1.96 ± 0.01
	17.3	0.47	1.86 ± 0.01
	19.4	0.56	1.79 ± 0.01
	22	0.65	1.68 ± 0.01
	24.5	0.71	1.6 ± 0.01
0.0094	15	0.2	1.51 ± 0.01
	20	0.36	1.48 ± 0.01
	25	0.39	1.43 ± 0.01
	30	0.52	1.4 ± 0.01
	35	0.59	1.37 ± 0.01
0.0059	15	0.12	1.36 ± 0.01
	20	0.23	1.29 ± 0.01
	25	0.25	1.22 ± 0.01
	30	0.33	1.16 ± 0.01
	35	0.37	1.09 ± 0.01
0.0038	15	0.08	1.27 ± 0.01
	20	0.14	1.18 ± 0.01
	25	0.15	1.09 ± 0.01
	30	0.21	1.02 ± 0.01
	35	0.23	0.96 ± 0.01

is expected for dilute polymer solutions. The zero shear rate solution viscosities η_0 were determined by least-square fitting of the viscosity values in the plateau region of very low shear rates with a straight line and then extrapolating it to zero shear rate, as shown in the figures. Table 5.1 displays all the zero shear rate viscosities obtained this way for the two molecular weights across the range of concentrations and temperatures examined in the current work. We have also established that the measured viscosity does not depend on rheometer geometry in the range of shear rates employed (in terms of the 'gap' between the cup and the bob), by measuring the viscosity of T4 DNA at two different gaps at two different temperatures as shown in Figure 5.2.

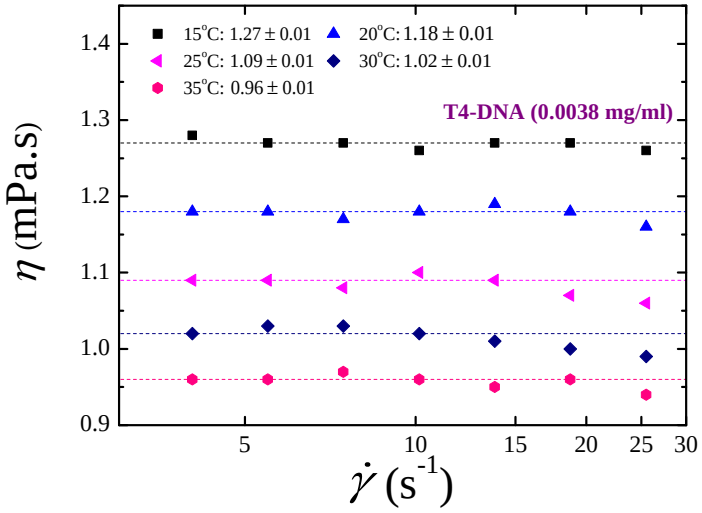

(a)

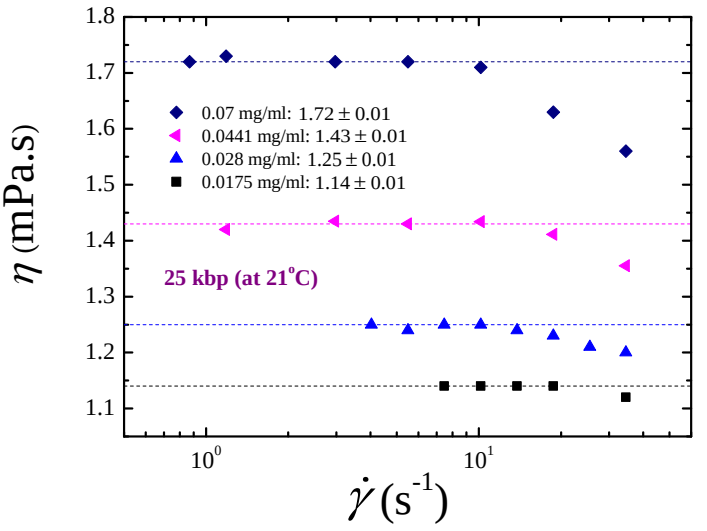

(b)

Figure 5.1: Determination of the zero shear rate solution viscosity η_0. The shear rate dependence of solution viscosity η in the region of low shear rate is extrapolated to zero shear rate (a) for T4 DNA at a fixed concentration, for a range of temperatures and (b) for 25 kbp DNA at a fixed temperature, for a range of concentrations. The extrapolated values in the limit of zero shear rate are indicated in the legends.

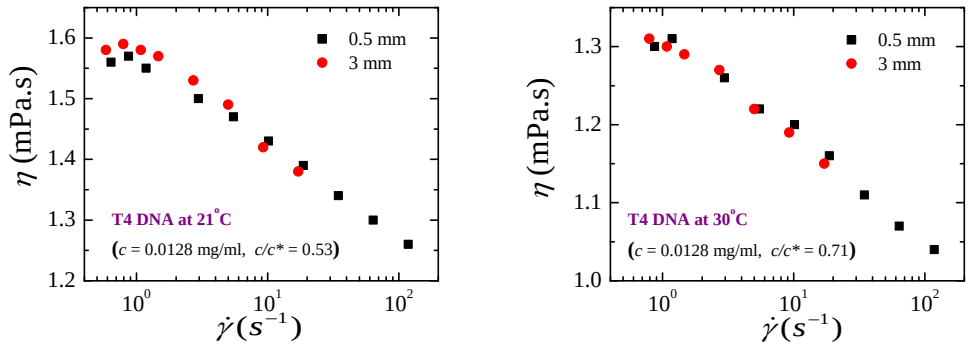

Figure 5.2: Measured solution shear viscosity η as a function of shear rate $\dot{\gamma}$ for a dilute solution of T4 DNA at two different 'gaps' (between the cup and the bob) and at two different temperatures: (a) 21°C and (b) 30°C. The measurement with the gap of 0.5 mm corresponds to the 1T/1T geometry that has been used for all the measurements in the current work.

5.2.3 Simulations

The Brownian dynamics simulations are not a part of this thesis, but were carried out as a separate study by our group and the predictions (Ahirwal, 2009; Pan et al., 2014) have been used for comparison with the experimental data on linear DNA solutions from the current work and previously reported experimental data on synthetic polymer-solvent systems. A detailed description of the BD simulation methodology, universal properties derived from the viscosity radius, variance reduced simulations and integration of the correlation functions is given in Appendix B.

5.3 Results and Discussion

5.3.1 Intrinsic viscosity

The intrinsic viscosity of a polymer solution is typically obtained from a virial expansion of the dilute solution viscosity as a function of concentration. Two commonly used forms of the virial expansion are the Huggins equation,

$$\eta_{sp} \equiv \frac{\eta_{p,0}}{\eta_s} = [\eta]\, c + k_H\, ([\eta]\, c)^2 + k'_H\, ([\eta]\, c)^3 + \cdots \tag{5.3}$$

and Kraemer's equation,

$$\ln \frac{\eta_0}{\eta_s} = [\eta]\, c - k_K \left([\eta]\, c\right)^2 + k'_K \left([\eta]\, c\right)^3 + \cdots \tag{5.4}$$

where, η_{sp} is the specific viscosity, η_0 is the zero shear rate viscosity , the coefficient k_H in the quadratic term in Huggins equation (Equation 5.3) is the Huggins constant, and is analogous to the second virial coefficient for viscosity (Rubinstein and Colby, 2003), while k_K is the equivalent coefficient in Kraemer's equation. The parameters k'_H and k'_K are coefficients of the cubic terms in the Huggins and Kraemer's equations, respectively.

Substituting the Huggins expansion in terms of η_0 from Equation 5.3 into the left hand side of Kraemer's equation (Equation 5.4), and comparing terms of similar order leads to,

$$k_K = \frac{1}{2} - k_H\,, \quad \text{and} \quad k'_K = k'_H - k_H + \frac{1}{3}. \tag{5.5}$$

Typically, dilute solution viscosities are measured at low values of concentration, where the contribution of the cubic terms in the Huggins equation are negligible. As a result, by plotting η_{sp}/c versus concentration, the intrinsic viscosity can be obtained from the intercept on the y-axis of a straight line fitted to the data, while k_H can be determined from the slope of the line, since,

$$\frac{\eta_{sp}}{c} = [\eta] \; + k_H\, [\eta]^2 c. \tag{5.6}$$

As pointed out by Pamies et al. (2008) even though $k'_H \left([\eta]\, c\right)^3 \approx 0$, the contribution of the cubic terms in Kraemer's equation need not be zero (unless, $k_H \approx 1/3$, see Equation 5.5). At sufficiently low concentrations, however, Kraemer's equation (Equation 5.4) suggests that a plot of $\ln(\eta_0/\eta_s)/c$ will be linear in concentration,

$$\frac{1}{c} \ln \frac{\eta_0}{\eta_s} = [\eta] \; - k_K\, [\eta]^2 c, \tag{5.7}$$

with the intrinsic viscosity obtained by extrapolating to zero concentration, while k_K can be determined from the slope of the line through the data.

Since the leading order term in the expansions for both η_{sp} and $\ln(\eta_0/\eta_s)$ is $[\eta]c$, Solomon and Ciută (1962) suggested that the virial expansion of the difference $\eta_{sp} - \ln(\eta_0/\eta_s)$ would have a weaker dependence on concentration ,

$$\eta_{sp} - \ln \frac{\eta_0}{\eta_s} = k_{SC} \left([\eta]\, c\right)^2 + k'_{SC} \left([\eta]\, c\right)^3 + \cdots \tag{5.8}$$

$$\text{with,} \quad k_{SC} = \frac{1}{2}, \quad \text{and} \quad k'_{SC} = k_H - \frac{1}{3} \tag{5.9}$$

As a result, by defining the quantity,

$$[\eta]_c = \frac{1}{c}\sqrt{2\left(\eta_{sp} - \ln\left(\eta_0/\eta_s\right)\right)} \tag{5.10}$$

it follows that,

$$[\eta]_c = [\eta] + k'_{SC}[\eta]^2\, c + \cdots \tag{5.11}$$

As discussed in some detail by Pamies et al. (2008) under the special circumstances when $k'_{SC}[\eta]^2\, c \approx 0$, or $k_H \approx 1/3$ (see Equation 5.9), the intrinsic viscosity can be determined from the Solomon-Ciută equation (Equation 5.11) by measuring the viscosity at a single concentration, without the necessity of an extrapolation procedure. The departure of $[\eta]_c$ from a constant value when $[\eta]_c$ is plotted as a function of c, can be seen as indicating the departure of k_H from a value of $1/3$.

Plots of the relevant variables in the linear versions of the Huggins equation (Equation 5.6), the Kraemer equation (Equation 5.7) and the Solomon-Ciută equation (Equation 5.11), as a function of concentration, can now be interpreted in the light of the discussion above. Figure 5.3 displays plots of η_{sp}/c, $\ln(\eta_0/\eta_s)/c$, and $[\eta]_c$, obtained using results of the zero shear rate solution viscosity measurements described previously in Section 5.2 (see Table 5.1), as a function of concentration. Values of $[\eta]$ obtained by extrapolating linear fits to the finite concentration data to the limit of zero concentration are listed in Table 5.2, where the subscript on $[\eta]$ indicates the equation used to obtain the value. The mean values of $[\eta]$ obtained from the three methods are also indicated in the table. It is clear that the three extrapolation methods give values that are fairly close to each other.

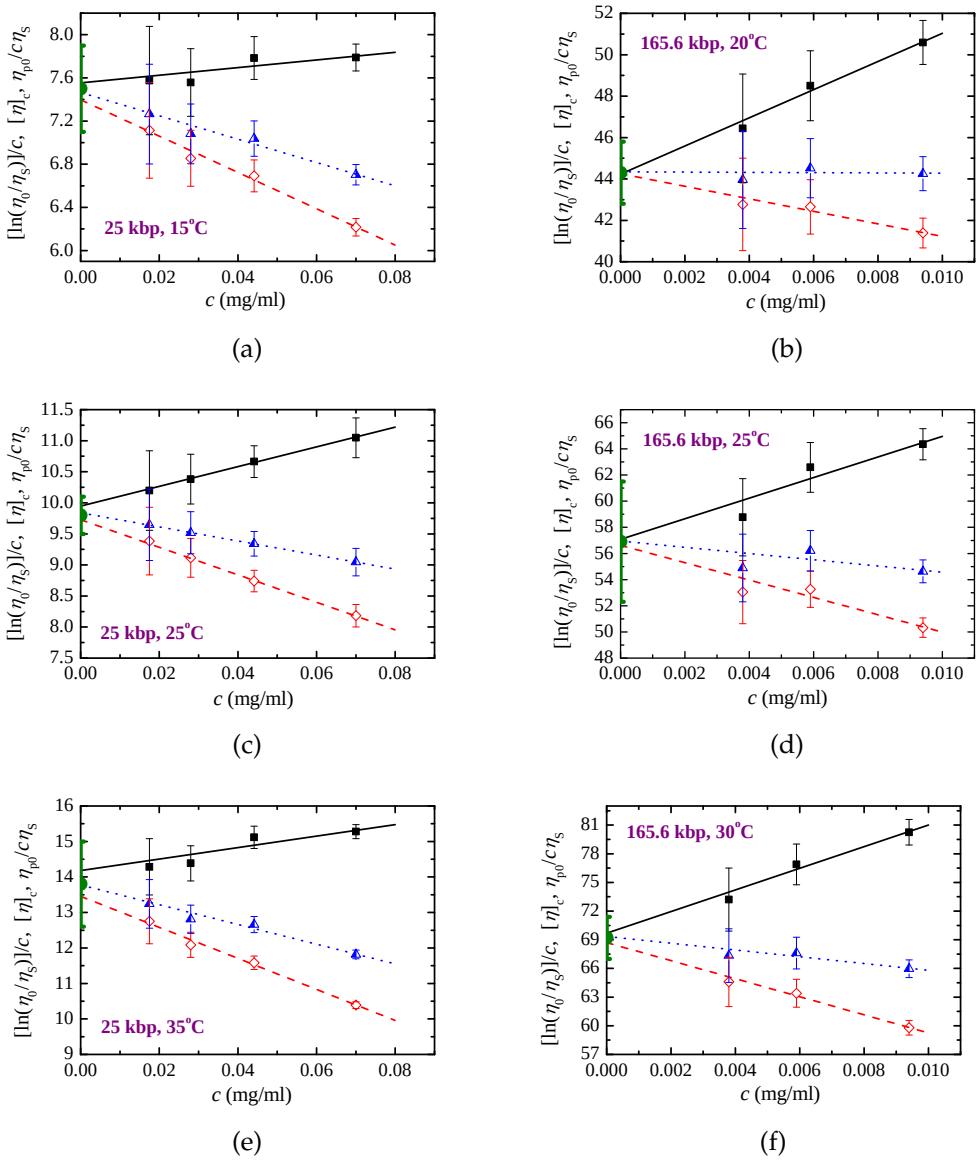

Figure 5.3: Determination of $[\eta]$ for 25 kbp and T4 DNA. The left and right column of figures represent 25 kbp and T4 DNA respectively at different temperatures (indicated within the figures). The solid, dashed and dotted lines are least-squares linear fits to the data points extrapolated to zero concentration in accordance with the Huggins, Kraemer and Solomon-Ciută equations, respectively. In each figure, the mean value of $[\eta]$ obtained by extrapolating data for $[\ln(\eta_0/\eta_s)]/c$ (open diamonds), $\eta_{p0}/c\eta_s$ (opaque squares) and $[\eta]_c$ (half-filled triangles), is represented by an opaque circle (the common intercept on the y-axis). Note that the unit of y-axis is ml/mg, the same as $[\eta]$.

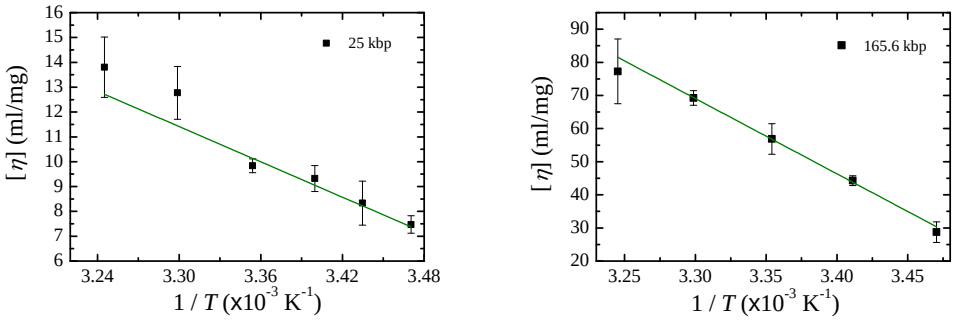

Figure 5.4: Temperature dependence of $[\eta]$ for (a) 25 kbp DNA and (b) T4 DNA. The lines are the least-squares linear fits to the data.

Recently, Rushing and Hester (2003) have shown that the intrinsic viscosity of a number of different polymer-solvent systems scales linearly with inverse temperature, in line with a relationship proposed originally by Stockmayer and Fixman (1963). Figure 5.4 indicates that the mean value of $[\eta]$, for both the DNA samples, scales linearly with inverse temperature, as T increases from T_θ to good solvent conditions, in agreement with the observations of Rushing and Hester (2003) for synthetic polymer solutions.

As discussed earlier, the values of k_{H} can be obtained from the slopes of the lines in Figure 5.3. While it is obtained directly from the slope of the line through the Huggins data, Kraemer's data gives k_{H} from k_{K} (see Equation 5.5), and the Solomon-Ciută data gives k_{H} from k'_{SC} (see Equation 5.9). The values of k_{H} obtained from these different methods are listed in Table 5.3. We first discuss the data for T4 DNA, which appears to be more in line with previous observations on synthetic polymer solutions.

Pamies et al. (2008) have recently tabulated values of k_{H} for several systems by collating data reported previously in literature (see Table 1 in Pamies et al. (2008)). For flexible polymers, k_{H} is observed to lie in the range $0.4 - 0.7$ for θ-solvents, and in the range $0.2 - 0.4$ for good solvents. Clearly, values of k_{H} reported for T4 DNA in Table 5.3 lie in the expected ranges for θ and good solvents, with the θ-solvent value greater than that for good solvents. The three different means of

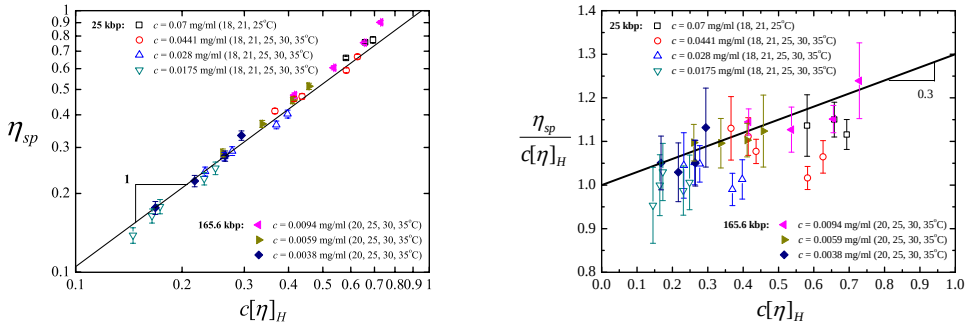

Figure 5.5: (a) Dependence of the specific viscosity $\eta_{\rm sp}$ on the non-dimensional concentration $c[\eta]_{\rm H}$, and, (b) dependence of the dimensionless ratio $\eta_{\rm sp}/c[\eta]_{\rm H}$ on $c[\eta]_{\rm H}$, for the two DNA used in this work at different absolute concentrations, each of which is at different temperatures in good solvents.

estimating $k_{\rm H}$ also give values reasonably close to each other. Since $k_{\rm H} \approx 1/3$, we expect from the Solomon-Ciută equation (Equation 5.11) that the slope of the line through values of $[\eta]_{\rm c}$ is close to zero. This is indeed the case, as can be seen from Figures (b), (d) and (f) for T4 DNA in Figure 5.3.

When terms of order $([\eta]c)^3$ are negligible, we expect a plot of $\eta_{\rm sp}$ versus $c[\eta]$ to depend quadratically on $c[\eta]$ for increasing values of $c[\eta]$ (see Equation 5.3). The departure from linearity can be observed for the T4 DNA data in Figure 5.5 (a) for $c[\eta] \gtrsim 0.3$ (filled symbols). The importance of the quadratic term can be seen more clearly by plotting $\eta_{\rm sp}/(c[\eta])$ versus $(c[\eta])$, as shown in Figure 5.5 (b), since,

$$\frac{\eta_{\rm sp}}{c[\eta]} = 1 + k_{\rm H}\, c[\eta]. \tag{5.12}$$

The data for T4 DNA is scattered around a line with slope = 1/3, as expected from the values of $k_{\rm H}$ listed for T4 DNA in Table 5.3.

Values of $k_{\rm H}$ extracted from the dilute solution viscosity data for 25 kbp DNA using the Huggin's method have a greater degree of uncertainty associated with them compared to those for T4 DNA (see first column in Table 5.3). Even though the values obtained from the Kraemer and Solomon-Ciută equations lie closer to the expected range of values for good solvents, the θ-solvent values are smaller

than the good solvent values. Figure 5.5 (a) indicates that the dependence of η_{sp} on $c[\eta]_H$ for 25 kbp DNA appears to be linear in the entire range of values of $c[\eta]_H$ observed here (empty symbols), which suggests that it would be harder to extract the values of k_H with confidence using the Huggin's method. This is also clearly reflected in Figure 5.5 (b), where the data indicates that the value of the Huggins constant is highly scattered, and in most cases smaller than 1/3. More extensive measurements at a larger range of concentrations would be required to obtain k_H with greater accuracy for 25 kbp DNA.

The intrinsic viscosity data obtained at various temperatures can be used to calculate the viscosity radius of 25 kbp and T4 DNA. Of the two properties of interest in the present work, namely, $U_{\eta R}$ and α_η, the latter is directly calculable from experimental measurements. Values of α_η for the two DNA samples are reported in Table 5.2. On the other hand, the direct estimation of $U_{\eta R}$ at different values of z requires the additional knowledge of R_g as a function of z. While the prediction of $U_{\eta R}$ here by simulations is based on the determination of both the viscosity and the radius of gyration as a function of solvent quality, we do not have experimental information on R_g for the DNA samples studied here. The ratio $(U_{\eta R}/U^{\theta}_{\eta R})$, however, which is also equal to the ratio of the Flory-Fox constants in good and θ-solvents, can be calculated without a knowledge of R_g. From Equations 1.6 and 5.2, we can write

$$\alpha_\eta = \frac{R_\eta}{R_g}\frac{R_g}{R^{\theta}_g}\frac{R^{\theta}_g}{R^{\theta}_\eta} = \left(\frac{U_{\eta R}}{U^{\theta}_{\eta R}}\right)^{1/3}\alpha_g, \tag{5.13}$$

or

$$\frac{U_{\eta R}}{U^{\theta}_{\eta R}} = \frac{\Phi}{\Phi_0} = \left(\frac{\alpha_\eta}{\alpha_g}\right)^3. \tag{5.14}$$

Table 5.2: Intrinsic viscosities $[\eta]$ (in ml/mg) for 25 kbp and T4 DNA at various temperatures (T), as obtained from different extrapolation methods: Huggins ($[\eta]_{\mathrm{H}}$), Kraemer ($[\eta]_{\mathrm{K}}$) and Solomon-Ciută ($[\eta]_{\mathrm{SC}}$). The mean of the $[\eta]$ values from these extrapolations are also indicated at each temperature. The swelling ratio α_η is also listed for each DNA at each temperature and has been calculated based on the $[\eta]_{\mathrm{mean}}$ values. Note that T_θ = 15 °C.

T	25 kbp					T4 DNA				
(°C)	$[\eta]_{\mathrm{H}}$	$[\eta]_{\mathrm{K}}$	$[\eta]_{\mathrm{SC}}$	$[\eta]_{\mathrm{mean}}$	α_η	$[\eta]_{\mathrm{H}}$	$[\eta]_{\mathrm{K}}$	$[\eta]_{\mathrm{SC}}$	$[\eta]_{\mathrm{mean}}$	α_η
15	7.6 ± 0.1	7.4 ± 0.1	7.5 ± 0.1	7.5 ± 0.4	1 ± 0.03	28.5 ± 1.4	28.9 ± 1.3	28.8 ± 1.3	28.7 ± 3.1	1 ± 0.05
18	8.3 ± 0.5	8.3 ± 0.4	8.4 ± 0.4	8.3 ± 0.9	1.03 ± 0.04	–	–	–	–	–
20	–	–	–	–	–	44.2 ± 0.7	44.3 ± 0.6	44.3 ± 0.6	44.3 ± 1.5	1.15 ± 0.04
21	9.4 ± 0.3	9.3 ± 0.2	9.3 ± 0.2	9.3 ± 0.5	1.07 ± 0.03	–	–	–	–	–
25	9.9 ± 0.1	9.7 ± 0.1	9.8 ± 0.1	9.8 ± 0.3	1.09 ± 0.02	57.1 ± 2.4	56.6 ± 1.7	57 ± 2	56.9 ± 4.6	1.26 ± 0.06
30	13.2 ± 0.2	12.4 ± 0.1	12.7 ± 0.1	12.8 ± 1.1	1.19 ± 0.04	69.7 ± 1.5	68.7 ± 0.8	69.3 ± 1.1	69.2 ± 2.2	1.34 ± 0.05
35	14.2 ± 0.4	13.5 ± 0.1	13.8 ± 0.2	13.8 ± 1.2	1.22 ± 0.04	77.5 ± 5.3	76.8 ± 3.7	77.5 ± 4.1	77.3 ± 9.8	1.39 ± 0.08

Table 5.3: k_{H} as obtained from Huggins, Kraemer and Solomon-Ciută equations for 25 and T4 DNA at different temperatures (T).

T (°C)	k_{H} (Huggins)		k_{H} (From Kraemer, see Equation 5.5)		k_{H} (From Solomon-Ciută, see Equation 5.9)	
	25 kbp	T4 DNA	25 kbp	T4 DNA	25 kbp	T4 DNA
15 (T_θ)	0.06 ± 0.04	0.82 ± 0.22	0.19 ± 0.02	0.64 ± 0.18	0.14 ± 0.3	0.68 ± 0.19
18	0.24 ± 0.13	–	0.28 ± 0.09	–	0.25 ± 0.1	–
20	–	0.35 ± 0.05	–	0.35 ± 0.03	–	0.33 ± 0.04
21	0.24 ± 0.05	–	0.3 ± 0.03	–	0.26 ± 0.04	–
25	0.16 ± 0.01	0.24 ± 0.09	0.27 ± 0.01	0.29 ± 0.06	0.21 ± 0.01	0.26 ± 0.07
30	0.01 ± 0.02	0.23 ± 0.04	0.22 ± 0.01	0.3 ± 0.02	0.14 ± 0.01	0.26 ± 0.03
35	0.08 ± 0.03	0.32 ± 0.12	0.26 ± 0.01	0.35 ± 0.08	0.18 ± 0.02	0.31 ± 0.08

The swelling α_η is known from the present experimental measurements at various values of M and T. Since, in Chapter 4, the mapping between T and M and the solvent quality parameter z has already been established, α_η can be determined as a function of z, while α_g can be obtained from the following equation (Domb and Barrett, 1976; Schäfer, 1999; Kumar and Prakash, 2003),

$$\alpha_g = (1 + az + bz^2 + cz^3)^{m/2} \tag{5.15}$$

at any value of z. As a result, experimentally determined values of $(U_{\eta R}/U^{\theta}_{\eta R})$ and α_η for DNA can be compared at identical values of the solvent quality z, with earlier observations for synthetic polymer solutions and with results of Brownian dynamics simulations, as discussed in the following subsections.

5.3.2 Solvent quality crossover of $U_{\eta R}$

Experimental observations of the dependence of the Flory-Fox constant on solvent quality for a number of different polymer-solvent systems have been summarised in the recent review by Jamieson and Simha (2010). The general consensus appears to be that the ratio Φ/Φ_0 decreases rapidly with increasing solvent quality, and with increasing molecular weight in good solvents. Using Equation 5.14, Jamieson and Simha (2010) argue that analytical predictions of the z dependence of α_η and α_g by Barrett (1984), and the experimental observations of these crossover functions by Tominaga et al. (2002) support these conclusions on the dependence of the ratio Φ/Φ_0 on solvent quality. Very recently, Prakash and coworkers (Ahirwal, 2009; Pan et al., 2014) have carried out exact simulations predictions by extrapolating finite chain data to the long chain limit, while simultaneously keeping the hydrodynamic interaction parameter h^* and solvent quality z constant, that lead to asymptotic predictions of crossover behaviour of $U_{\eta R}$in the non-draining limit (see Appendix B). Though the simulations are not a part of the current work, it is important to understand the predictions of solvent quality dependence of $U_{\eta R}$, particularly for comparison with the experiments.

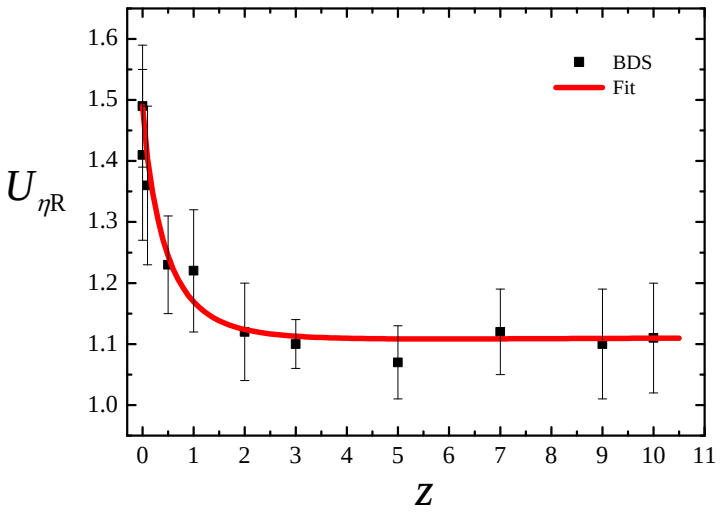

Figure 5.6: Predicted values of the universal viscosity ratio $U_{\eta R}$ as a function of the solvent quality parameter z. Black squares are the results of BD simulations obtained by extrapolating finite chain data to the long chain limit (Ahirwal, 2009; Pan et al., 2014). The red curve is a fit to the simulation data with the expression given in Equation 5.16. Reproduced with permission from Ahirwal (2009); Pan et al. (2014).

Figure 5.6 displays the dependence on z of the asymptotic values of $U_{\eta R}$ obtained in this manner (Ahirwal, 2009; Pan et al., 2014). Starting at $U^{\theta}_{\eta R} = 1.49 \pm 0.1$ at $z = 0$, the universal ratio appears to decrease rapidly with increasing values of z, levelling off to an excluded volume limit value of $U^{\infty}_{\eta R} = 1.1 \pm 0.1$ for $z \gtrsim 5$. This behaviour is in agreement with the qualitative trend expected from experimental observations Jamieson and Simha (2010).

The dependence of the swelling α_{η} on the solvent quality z, predicted by BD simulations, can be represented by a functional form identical to that for α_g, described elsewhere (Kumar and Prakash, 2003), with values of the parameters a, b and c as given in Table 5.4. The value of the exponent m, however, is the same in the expressions for both the crossover functions α_{η} and α_g, since (as can be seen from Equation 5.14), this must be true in order for $U_{\eta R}$ to level off to a constant value for large values of z, as observed in the BD simulations displayed in Figure 5.6. Using

Table 5.4: Values of the parameters a, b, c and m in the functional form $f(z) = (1 + az + bz^2 + cz^3)^{m/2}$ used to fit the Brownian dynamics simulations data for the crossover functions α_g (Kumar and Prakash, 2003), α_η(Current work) and α_H (see Chapter 4).

	α_g	α_η	α_H
a	9.5286	5.4475 ± 1.776	9.528
b	19.48 ± 1.28	3.156 ± 1.982	19.48
c	14.92 ± 0.93	3.536 ± 0.277	14.92
m	0.133913 ± 0.0006	0.1339	0.0995 ± 0.0014

the functional forms for α_η and α_g, and Equation 5.14, it follows that,

$$U_{\eta R} = U^{\theta}_{\eta R} \left(\frac{1 + a_\eta z + b_\eta z^2 + c_\eta z^3}{1 + a_g z + b_g z^2 + c_g z^3} \right)^{3m/2} \tag{5.16}$$

where, the suffixes on the parameters a, b and c indicate the relevant crossover function. The red curve in Figure 5.6 is a fit to the BD simulation data using Equation 5.16, along with $U^{\theta}_{\eta R} = 1.49$, and the appropriate values for the fitting parameters listed in Table 5.4. As seen from Figure 5.6, the fit is very good, as can be expected from the excellence of the fits for the crossover functions for α_η and α_g.

Tominaga et al. (2002) have reported the crossover behaviour of α_η in terms of a solvent quality parameter they denote as $\tilde{z}$. Since the data in Tominaga et al. (2002) is for a wide range of polymer-solvent systems, including helical polymer chains, the definition of $\tilde{z}$ is more general than the quantity z used here. However, as pointed out in by Tominaga et al. (2002), $\tilde{z} = z$ in the random-coil limit. Additionally, Tominaga et al. (2002) have also directly plotted $\log \alpha_\eta^3$ versus $\log \alpha_g^3$. As a result, using Equation 5.14, the dependence of $(U_{\eta R}/U^{\theta}_{\eta R})$ on z can be determined for the polymer-solvent systems studied in Tominaga et al. (2002). As discussed earlier in subsection 5.3.1, this ratio can also be determined for the 25 kbp and T4 DNA samples studied here. Figure 5.7 displays a comparison of these experimental observations, with the curve fit to the BD simulations data. The experimental data can be seen to be scattered around the BD simulation curve, and closely follow the trend of rapid decrease in $(U_{\eta R}/U^{\theta}_{\eta R})$ with increasing solvent quality. In particular, experimental measurements for the two DNA samples lie

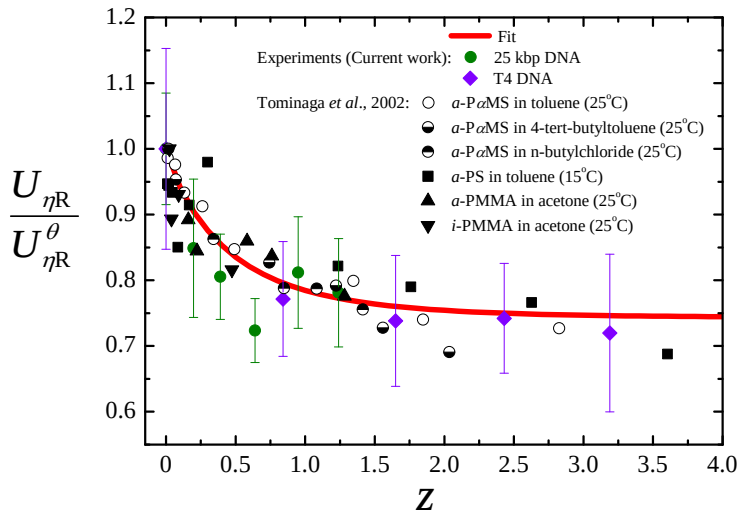

Figure 5.7: Comparison of experimental observations of the universal viscosity ratio $U_{\eta R}$ as a function of the solvent quality parameter z, obtained from current measurements on DNA solutions and data collated in Tominaga et al. (2002). The solid curve is a fit to experimental data using Equation 5.16.

close to the observations for synthetic polymer-solvent systems, and to the BD simulation curve. For large values of z, Equation 5.16 implies that the excluded volume limit value of the ratio, from fitting Brownian dynamics simulations is, $(U^{\infty}_{\eta R}/U^{\theta}_{\eta R}) = (c_{\eta}/c_g)^{3m/2} = 0.749$. Experimental measurements appear to indicate a value of the ratio, $\Phi/\Phi_0 \approx 0.773$ (Jamieson and Simha, 2010).

5.3.3 Swelling of the viscosity radius

A comparison of the experimental measurements of α_{η} as a function of z, for 25 kbp and T4 DNA obtained in the present work, with the results of current BD simulations, and with previous measurements on synthetic polymer-solvent systems collated in Tominaga et al. (2002), is displayed in Figure 5.8.

The excellent agreement between the swelling of DNA, and synthetic polymer-solvent systems implies that the swelling of the viscosity radius of DNA, in dilute solutions with excess salt, is universal. This was also observed with the swelling of the hydrodynamic radius of DNA in similar solutions (see Chapter 4). Impor-

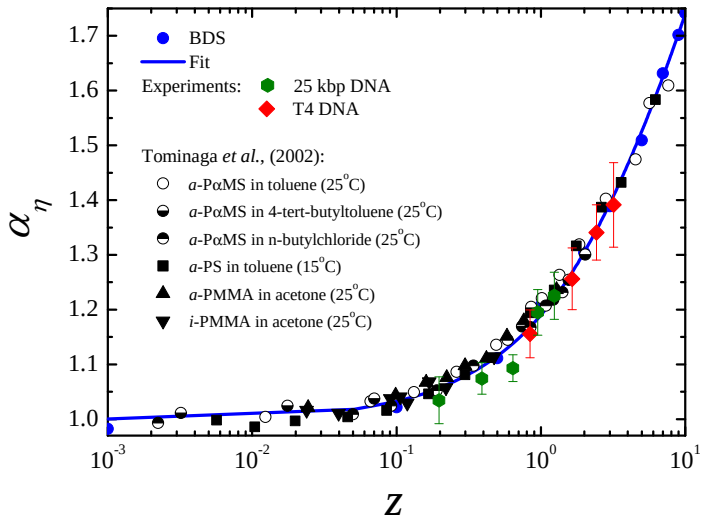

Figure 5.8: Swelling of the viscosity radius in the crossover region from θ to good solvents. The filled blue circles are the predictions of the current BD simulations. The line represents the fitting function described in the caption to Table 5.4. Experimental measurements of the swelling of 25 kbp and T4 DNA are represented by the filled hexagons and diamonds, respectively, while the remaining symbols represent data on various synthetic polymer-solvent systems collated in Tominaga et al. (2002).

tantly, the collapse of the data onto a master plot validates the estimation of the θ-temperature to be $T_\theta \approx 15°C$, as shown in Chapter 3, and the determination of the solvent quality z, at any given molecular weight M and temperature T, for DNA solutions in the presence of excess salt. The agreement between experimental observations and current BD simulations (Ahirwal, 2009; Pan et al., 2014) displayed in Figure 5.8 suggests that the simulation framework is highly suited to obtain accurate predictions of universal behaviour of dilute polymer solutions in the entire solvent quality crossover regime.

5.4 Conclusions

The intrinsic viscosities of dilute DNA solutions, of two different molecular weight samples (25 kbp and T4 DNA), have been measured at different temperatures in a commonly used solvent under excess salt conditions. The measurements have been used to calculate the swelling of the viscosity radius α_η and the universal viscosity

ratio $U_{\eta \mathrm{R}}$, as a function of the solvent quality z. Also, the experimental results are compared with the universal predictions of these crossover functions obtained with the help of BD simulations (Ahirwal, 2009; Pan et al., 2014) that incorporate fluctuating hydrodynamic interactions, in the non-draining limit.

The experimental measurements of $U_{\eta \mathrm{R}}$ and α_η for the DNA solutions are found to collapse onto previously reported data for synthetic polymer-solvent systems, and onto the BD simulations predictions. The close agreement between prior experiments, current experiments and simulations suggests that the DNA solutions in the presence of excess salt exhibit universal behaviour in line with similar observations for synthetic polymer solutions and the model used by our group (Ahirwal, 2009; Pan et al., 2014), incorporates all the important mesoscopic physics necessary to capture the universal behaviour of equilibrium static and dynamic properties of dilute polymer solutions.

6

Zero Shear Rate Viscosity and Scaling in Semidilute Solutions

6.1 Introduction

Like dilute polymer solutions, various large scale properties of semidilute solutions too obey power law scaling in the limits of θ and good solvents. In semidilute solutions, for viscosity, one observes for instance, $\eta_{p0}/\eta_s \sim (c/c^*)^2$ in θ solvents, while $\eta_{p0}/\eta_s \sim (c/c^*)^{1/(3\nu-1)}$ in very good solvents (de Gennes, 1979; Rubinstein and Colby, 2003). Power law scaling is, however, *not* obeyed in the crossover regime between θ and very good solvents. Instead, the polymer solution in this regime is described in terms of universal crossover scaling functions (Schäfer, 1999). Though in case of dilute solutions, the nature of these scaling functions is very well understood in terms of scaling arguments, analytical theories, experimental observations and computer simulations (see Section 5.1); to the best of our knowledge, a comprehensive characterization of the crossover scaling functions for semidilute polymer solutions is yet to be achieved. In this work, the systematic measurement of the crossover scaling function for the zero shear rate viscosity of semidilute polymer solutions is discussed, using DNA molecules as model polymers. It is shown that

the crossover behaviour of the zero shear rate viscosity can also be described in terms of a power law, albeit with an exponent that depends on where the solution lies in the crossover regime. This behaviour is shown to be in quantitative agreement with recent Brownian dynamics simulation predictions (Jain et al., 2012a,b).

From the definition of the solvent quality parameter z (see Equation 1.1), it may be noted that $z = 0$ in θ-solvents and $z \to \infty$ in very good solvents, so that the scaling of many dilute polymer solution properties in the crossover regime is typically represented in terms of functions of z (Schäfer, 1999; Rubinstein and Colby, 2003). For instance, the swelling of the gyration radius α_g, can be expressed as function of z in the crossover regime, as shown in Equation 5.15, where the constants (a, b, c, m, etc.) are either theoretically or experimentally determined constants (Domb and Barrett, 1976; Schäfer, 1999; Kumar and Prakash, 2003). This expression reduces to the appropriate power laws in the limits $z \to 0$ and $z \to \infty$. The crossover scaling functions for semidilute solutions have an additional dependence on the scaled concentration c/c^*. We expect, for instance, $\eta_{p0}/\eta_s = f(z, c/c^*)$ in the double crossover regime of temperature and concentration. The specific *power law* forms of these scaling functions in the phase space of solvent quality and concentration, far away from the crossover boundaries, has been predicted previously by scaling theories (de Gennes, 1979; Grosberg and Khokhlov, 1994; Rubinstein and Colby, 2003). More recently, using scaling theory based on the blob picture of polymer solutions, Prakash and coworkers (Jain et al., 2012a,b) have made a number of predictions regarding the behaviour of scaling functions in the entire $(z, c/c^*)$ phase space, and, by carrying out Brownian dynamics simulations, have demonstrated the validity of their predictions for the scaling of the polymer size and diffusivity in the semidilute regime. In this work, we investigate experimentally, the scaling of the zero shear rate viscosity of semidilute polymer solutions in the double crossover regime of the variables z and c/c^*, to examine if the observed scaling behaviour is indeed as predicted by blob scaling arguments.

Two central conclusions from Jain et al. (2012a) are of relevance to this work. The first is that there is only one unique scaling function in the double crossover

regime of semidilute polymer solutions. In other words, if the scaling function for any one property is known, the scaling function for other properties can be inferred from it. The second conclusion, which comes from the results of Brownian dynamics simulations (since scaling theories cannot predict precise functional forms), is that the crossover scaling functions (in a significant range of values of c/c^*) can also be represented as power laws, but with an effective exponent that depends on z. By combining these two observations, one can anticipate that in the semidilute regime, $\eta_{p0}/\eta_s \sim (c/c^*)^{1/(3\nu_{\text{eff}}(z)-1)}$, where the effective exponent $\nu_{\text{eff}}(z)$ is identical to the exponent which characterises the power laws for both the polymer size and the diffusivity. The aim of the experiments carried out here is to establish if such is indeed the case.

In order to examine the scaling behaviour of the zero shear rate viscosity of semidilute polymer solutions in the double crossover regime, it is necessary to measure the viscosity as a function of concentration and temperature for a range of molecular weights, and to represent this behaviour in terms of z and c/c^*. As pointed out in Chapter 1, c^* depends on R_{g} (Rubinstein and Colby, 2003), which according to the function $f_{\text{g}}(z)$, also varies between θ and very good solvent conditions. Therefore, it is evident that a comparison of the experimental data with the BD simulation predictions or scaling predictions for semidilute solutions is possible only with the knowledge of the solvent quality z at given values of T and M. Also, the determination of the scaled concentration c/c^*, that determines the location of a solution in the concentration crossover between dilute and concentrated solutions, will depend on the estimates of z in the limit of dilute solutions. To address these issues, we have already established a method to accurately estimate the θ-temperature and consequently the solvent quality for DNA solutions in Chapters 3 and 4. In the current work, by systematically measuring the zero shear rate viscosities for semidilute solutions of 25 kbp, λ-phage and T4 DNA, across a range of temperatures and concentrations, we show that the scaling predictions of Jain et al. (2012a) are correct. By doing so, we also simultaneously assert the universal nature of double-stranded DNA solutions.

The plan of the chapter is as follows. In various subsections of Section 6.3, the double crossover behaviour of semidilute solutions is examined. First it is demonstrated that at the θ-temperature, the power law scaling is obeyed, as predicted by blob scaling theory. The dependence of the zero shear rate viscosity on z and c/c^* is then examined in the light of the scaling predictions of Jain et al. (2012a), and the validity of these predictions in the double crossover regime is established. Finally, in Section 6.4, we compare measurements of the longest relaxation time λ_η obtained in this work, defined in terms of the zero shear rate viscosity, with the recent measurements of the longest relaxation time λ_1 by Steinberg and coworkers (Liu et al., 2009), who observed the relaxation of stained T4 DNA molecules in semidilute solutions following the imposition of a stretching deformation. In Section 6.5, we summarize the principal conclusions of the present work.

6.2 Methodology

6.2.1 Preparation of DNA solutions

We have measured the shear viscosities of three DNA samples: 25 kbp, λ-phage and T4 DNA at various temperatures (10 to 44.6°C) and concentrations (0.023 to 0.441 mg/ml) in the semidilute regime. The procurement of the T4 DNA and λ-DNA, the protocols for preparation and purification of the 25 kbp DNA solutions including the solvent used, and the maximum concentrations used for T4 and λ-DNA have been discussed in Section 2.1. The same maximum concentration was used for 25 kbp DNA as mentioned in Section 5.2.

6.2.2 Shear rheometry

Details about the rheometer used, measuring principle, temperature sensitivity, shear rheometry procedure, precautions taken while measurements, instrument calibration, shear rate range employed and avoidance of shear ramp, sample equilibration time, dependence on rheometer geometry etc., have been elaborated in Section 2.4.

Table 6.1: Solvent quality parameter z and the overlap concentration c^* (in mg/ml) for several DNA samples, at various temperatures. The θ-temperature is taken to be 15°C.

		15°C	20°C	25°C	30°C	35°C
2.9 kbp	z	0	0.11	0.22	0.32	0.43
	c^*	0.371	0.313	0.278	0.253	0.234
5.9 kbp	z	0	0.16	0.31	0.46	0.60
	c^*	0.251	0.201	0.173	0.155	0.142
8.3 kbp	z	0	0.19	0.37	0.54	0.71
	c^*	0.214	0.165	0.141	0.125	0.114
11.1 kbp	z	0	0.22	0.43	0.63	0.83
	c^*	0.184	0.139	0.117	0.103	0.093
25 kbp	z	0	0.33	0.64	0.95	1.24
	c^*	0.123	0.084	0.068	0.059	0.052
45 kbp	z	0	0.44	0.86	1.27	1.66
	c^*	0.092	0.058	0.045	0.039	0.034
114.8 kbp	z	0	0.69	1.37	2.03	2.66
	c^*	0.057	0.031	0.023	0.019	0.017
289 kbp	z	0	1.11	2.18	3.22	4.22
	c^*	0.036	0.016	0.012	0.010	0.008

6.3 Solvent quality crossover of the zero shear rate viscosity

6.3.1 Zero shear rate viscosity of semidilute DNA solutions

The scaling behaviour of the zero shear rate viscosity of semidilute polymer solutions can be determined by measuring the viscosity as a function of concentration and temperature for a range of molecular weights, and then representing this behaviour in terms of the crossover variables z and c/c^*. In Chapter 3, we have shown that for the solvent used in current experiments, the θ-temperature of DNA is 14.7 ± 0.5 °C. A value of $T_\theta = 15$°C has been used in all the calculations carried out here, since measurements have been done at this temperature. We have also established a procedure for determining the solvent quality z for DNA in the same solvent (see Chapter 4). Representative values of z, obtained by this procedure at various values of M and T and for several DNA, are displayed in Table 6.1.

The estimation of the overlap concentration, c^* depends on the radius of gyration, R_g (see Equation 1.8). R_g can be determined from the expression $R_g = R_g^\theta \alpha_g(z)$, for any M and T. Since the chain confirmations at the θ-temperature are expected to be ideal Gaussian chains, the analytical value for R_g at T_θ is, $R_g^\theta = L_o/\sqrt{6N_k}$. The respective values of L_o and N_k have been consistently used for all the molecular weights used here, to determine R_g^θ (as displayed in Table 2.1). Further, since we know z, α_g can be determined from Equation 5.15, where the constants, $a = 9.528$, $b = 19.48$, $c = 14.92$, and $m = 0.1339$ have been determined earlier by Brownian dynamics simulations (Kumar and Prakash, 2003). Representative values of c^* found using this procedure, at various M and T and for several DNA, are displayed in Table 6.1. Note that we expect the estimated values of R_g to be close to the actual values for DNA, since measured crossover values for the hydrodynamic and viscosity radii agree with the results of Brownian dynamics simulations at identical values of z (as demonstrated in Chapters 4 and 5).

Figure 6.1 displays examples of the dependence of the measured steady state shear viscosity on the shear rate. The zero shear rate viscosities have been determined by the same procedure as discussed in Section 5.2. All the zero shear rate viscosities determined in this manner, across the range of molecular weights, temperatures and concentrations examined here, are displayed in Table 6.2.

6.3.2 Power law scaling at the θ-temperature

Under θ-solvent conditions, the polymer contribution to the zero shear rate viscosity is expected to obey the following scaling law in the semidilute unentangled regime (Jain et al., 2012a),

$$\frac{\eta_{p0}}{\eta_{p0}^*} \sim \left(\frac{c}{c^*}\right)^2, \tag{6.1}$$

where, η_{p0}^* is the value of η_{p0} at $c = c^*$. Jain et al. (2012a) have shown that it is more convenient to used η_{p0}^* rather than η_s as the normalising variable in the development of some of their scaling arguments. Additionally, it ensures that the ratio $\eta_{p0}/\eta_{p0}^* = 1$ when $c/c^* = 1$, for all the systems studied here. Clearly, when the bare zero shear rate viscosity versus concentration data (displayed in Figure 6.2), is replotted in terms of scaled variables in Figure 6.3, data for different molecular

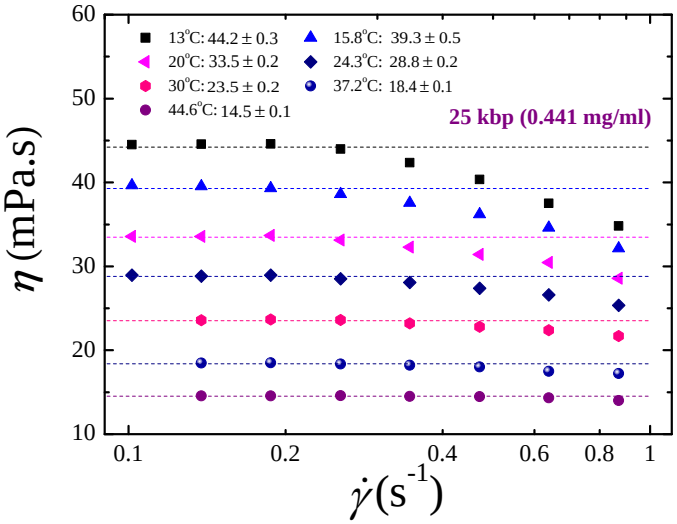

(a)

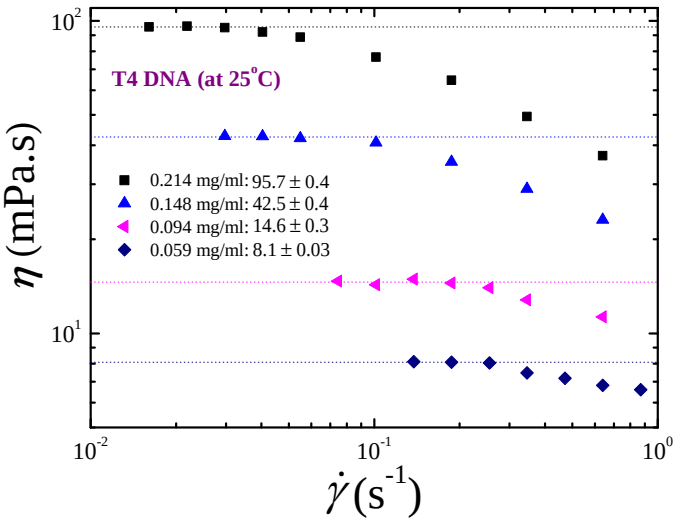

(b)

Figure 6.1: Determination of the zero shear rate solution viscosity η_0. The shear rate dependence of solution viscosity η in the region of low shear rate is extrapolated to zero shear rate (a) for 25 kbp DNA at a fixed concentration, for a range of temperatures and (b) for T4 DNA at a fixed temperature, for a range of concentrations. The extrapolated values in the limit of zero shear rate are indicated in the legends.

Table 6.2: Zero shear rate steady state viscosities (mPa.s) for 25 kbp, λ-phage, and T4 DNA at various concentrations (mg/ml) and temperatures (°C) in the semidilute regime.

25 kbp

c	T	c/c^*	η_0
0.441	13	2.12	44.2 ± 0.3
	15.8	3.9	39.3 ± 0.5
	20	5.13	33.5 ± 0.2
	24.3	6.04	28.8 ± 0.2
	30	7	23.5 ± 0.2
	37.2	7.88	18.4 ± 0.1
	44.6	8.65	14.5 ± 0.1
0.364	13	1.75	22.6 ± 0.1
	15.8	3.22	20.4 ± 0.1
	20	4.23	17.7 ± 0.1
	24.3	4.99	15.5 ± 0.1
	30	5.78	12.8 ± 0.1
	37.2	6.5	10.5 ± 0.1
	44.6	7.14	8.5 ± 0.01
0.315	13	1.51	15.8 ± 0.1
	15.8	2.79	14.7 ± 0.04
	20	3.66	12.7 ± 0.1
	24.3	4.32	11.2 ± 0.01
	30	5	9.3 ± 0.03
	37.2	5.63	7.7 ± 0.05
	44.6	6.18	6.6 ± 0.05
0.112	18	1.18	2.7 ± 0.02
	21	1.37	2.5 ± 0.01
	25	1.56	2.3 ± 0.02
	30	1.78	2 ± 0.02
	35	1.93	1.8 ± 0.01
0.07	30	1.11	1.5 ± 0.01
	35	1.21	1.5 ± 0.01

λ-DNA

c	T	c/c^*	η_0
0.5	10	–	408.7 ± 9.7
	13	–	357.7 ± 5.9
	21	9.26	334.8 ± 10
	25	10.87	291.2 ± 15.1
0.315	10	–	82.6 ± 0.5
	13	–	71.5 ± 2.1
	21	5.83	61.4 ± 1.05
	25	6.85	57.9 ± 0.9
0.2	10	–	19.4 ± 0.2
	13	–	16.2 ± 0.7
	15	2.25	16 ± 0.1
	21	3.7	14.6 ± 0.3
	25	4.35	12.3 ± 0.6
	30	4.88	11.3 ± 0.3
	35	5.41	10 ± 0.2
0.125	10	–	9.1 ± 0.1
	13	–	8 ± 0.1
	21	2.31	6.1 ± 0.1
	25	2.72	5.6 ± 0.2
	30	3.05	5 ± 0.1
	35	3.38	4.4 ± 0.1
0.08	10	–	4.4 ± 0.1
	13	–	4.1 ± 0.02
	21	1.48	3.4 ± 0.02
	25	1.74	3.1 ± 0.01
	30	1.95	2.8 ± 0.01
	35	2.16	2.5 ± 0.03
0.05	25	1.09	1.9 ± 0.01
	30	1.22	1.7 ± 0.01
	35	1.35	1.6 ± 0.02

T4 DNA

c	T	c/c^*	η_0
0.214	13	2.08	128.4 ± 0.1
	25	10.82	95.7 ± 0.4
	30	11.89	85.3 ± 0.4
	35	13.76	75.6 ± 0.4
0.148	10	–	66.7 ± 0.3
	13	1.44	58.5 ± 0.4
	15	3.08	55.9 ± 0.7
	18	4.93	50.7 ± 0.5
	21	6.14	46.7 ± 0.5
	25	7.48	42.5 ± 0.4
	30	8.22	37.1 ± 0.2
	35	9.52	32.5 ± 0.3
0.094	10	–	21.9 ± 0.6
	13	0.57	20.2 ± 0.8
	15	1.96	19.2 ± 0.6
	18	3.13	17.6 ± 0.4
	21	3.92	16.6 ± 0.1
	25	4.75	14.6 ± 0.3
	30	5.22	12.9 ± 0.2
	35	6.05	11.6 ± 0.2
0.059	15	1.23	10.2 ± 0.2
	18	1.97	9.6 ± 0.1
	21	2.46	8.9 ± 0.1
	25	2.98	8.1 ± 0.03
	30	3.28	7.3 ± 0.1
	35	3.79	6.6 ± 0.1
0.038	18	1.27	4.9 ± 0.2
	21	1.58	4.6 ± 0.2
	25	1.92	4.2 ± 0.2
	30	2.11	3.8 ± 0.2
	35	2.44	3.3 ± 0.05
0.023	22	1	2.1 ± 0.01
	24.5	1.1	2 ± 0.01

weights of DNA collapse on top of each other, with the viscosity ratio depending linearly on c/c^* in the dilute regime, followed by the expected power law scaling (with an exponent of 2) in the semidilute regime. Note that the values of viscosity at T_θ = 15°C, displayed in Figure 6.3, were obtained by interpolation from values at nearby T reported in Table 6.2.

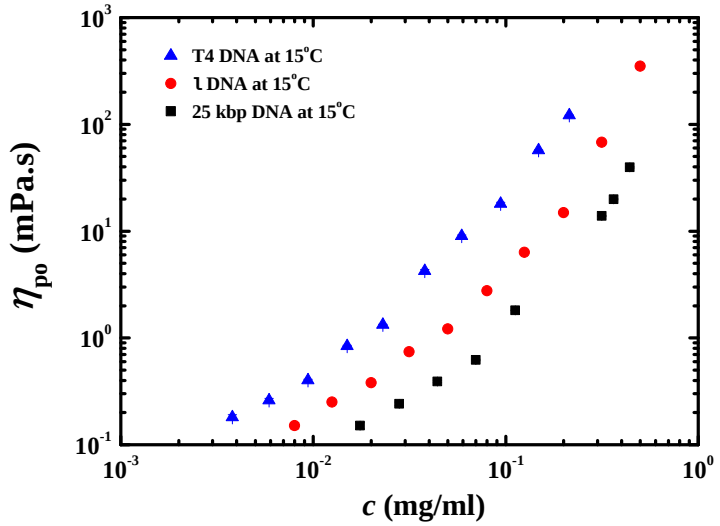

Figure 6.2: Dependence of the raw polymer contribution to viscosity η_{p0} on raw concentration c for 25 kbp, λ and T4 DNA, at the θ-temperature.

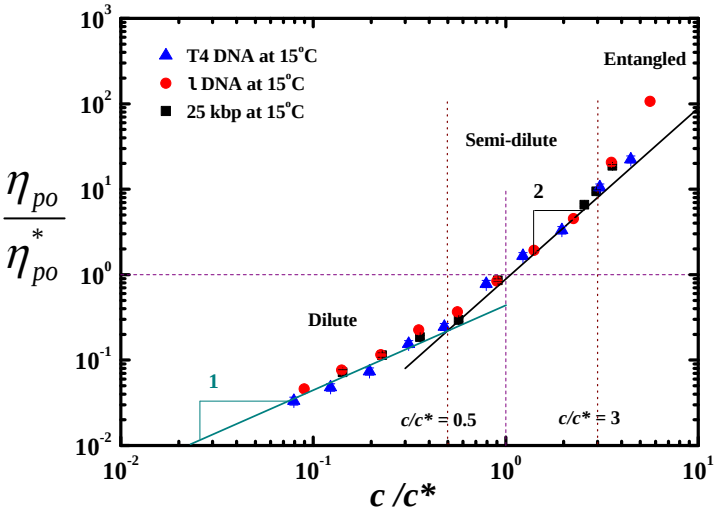

Figure 6.3: Dependence of the viscosity ratio η_{p0}/η^*_{p0} (where η^*_{p0} is the value of η_{p0} at $c = c^*$) on the scaled concentration c/c^*, for 25 kbp, λ and T4 DNA, at the θ-temperature.

The semidilute unentangled regime is typically expected to span the range from $c/c^* = 1$ to 10 (Graessley, 1980; Rubinstein and Colby, 2003). Figure 6.3 suggests that for θ-solutions, the onset of the semidilute regime for the viscosity ratio, which is dynamic property that is influenced by the presence of hydrodynamic interactions, occurs with a relatively small crossover at a concentration less than $c/c^* = 1$. Further, T4 DNA, which is the longest molecule in the series studied here, appears to follow the semidilute unentangled scaling for the largest concentration range, while the 25 kbp and λ-phage DNA crossover into the entangled regime beyond a concentration $c/c^* \gtrsim 3$. The difference in the behaviour of the different DNA can be understood by the following qualitative argument.

Chain entanglement is likely to occur when monomers from different chains interact with each other. In a semidilute solution, this would require a monomer within a concentration blob of a particular chain encountering a monomer within the concentration blob of another chain. A simple scaling argument suggests that at a fixed value of c/c^*, such encounters become less likely as the molecular weight of the chains increases. For a fixed value of c/c^*, it can be shown that the number of concentration blobs in a chain remains constant, independent of the molecular weight of the chain (Jain et al., 2012a). As a result, the size of a concentration blob increases with increasing molecular weight, while at the same time the concentration of monomers within a blob reduces. This decreasing concentration within a blob makes entanglements less likely to occur in systems with longer chains compared to systems with shorter chains, at the *same value* of c/c^*. This can also be seen from the fact that, since in a semidilute solution the concentration within a blob c_{blob} is the same as the overall solution concentration c, we can write $c_{\text{blob}} = (c/c^*) \times c^* \sim (c/c^*)\, M^{1-3\nu}$.

The scaling of the zero shear rate viscosity in semidilute solutions under θ solvent conditions, displayed in Figure 6.3, has been observed previously (Rubinstein and Colby, 2003) for synthetic polymer solutions. However, there have been very few explorations in the experimental literature of the scaling of the zero shear rate viscosity in the crossover region above the θ-temperature (Berry, 1996). The ex-

Table 6.3: Temperature range investigated in the shear experiments for different molecular weights. Temperatures in each row correspond to the same solvent quality.

T4 DNA	λ-DNA	25 kbp DNA	z
15°C	15°C	15°C	0
16.8°C	18.4°C	19.7°C	0.3
19.2°C	22.9°C	26.1°C	0.7
21.7°C	27.5°C	32.8°C	1.1
25.4°C	34.8°C	43.4°C	1.7

perimental results that we have obtained in this regime are discussed within the framework of scaling theory in the section below.

6.3.3 Power law scaling in the crossover regime

The concentration dependence of the scaled polymer contribution to the viscosity in the semidilute regime, $\eta_{\mathrm{p0}}\ /\eta^*_{\mathrm{p0}}$, for three different molecular weights of DNA, is presented in Figure 6.4, for four different values of the solvent quality z. In order to maintain the same value of solvent quality across the various molecular weights, it is necessary to carry out the experiments at the appropriate temperature for each molecular weight (see Table 6.3). This procedure would not be possible without the systematic characterisation of solvent quality. Remarkably, Figure 6.4 indicates that, provided z is the same, the data collapses onto universal power laws, independent of DNA molecular weight. Also worth noting is that while the crossover into entangled regime for θ-solutions occurs at around $c/c^* = 3$, Figure 6.4 appears to suggest that the threshold for the onset of entanglement effects increases with increasing z.

As discussed earlier in Section 6.1, recent scaling theory and Brownian dynamics simulations (Jain et al., 2012a) suggest that the viscosity ratio should scale according to the power law,

$$\frac{\eta_{p0}}{\eta^*_{p0}} \sim \left(\frac{c}{c^*}\right)^{1/(3\nu_{\mathrm{eff}}(z)-1)}, \tag{6.2}$$

where, the dependence of the effective exponent ν_{eff} on the solvent quality z should

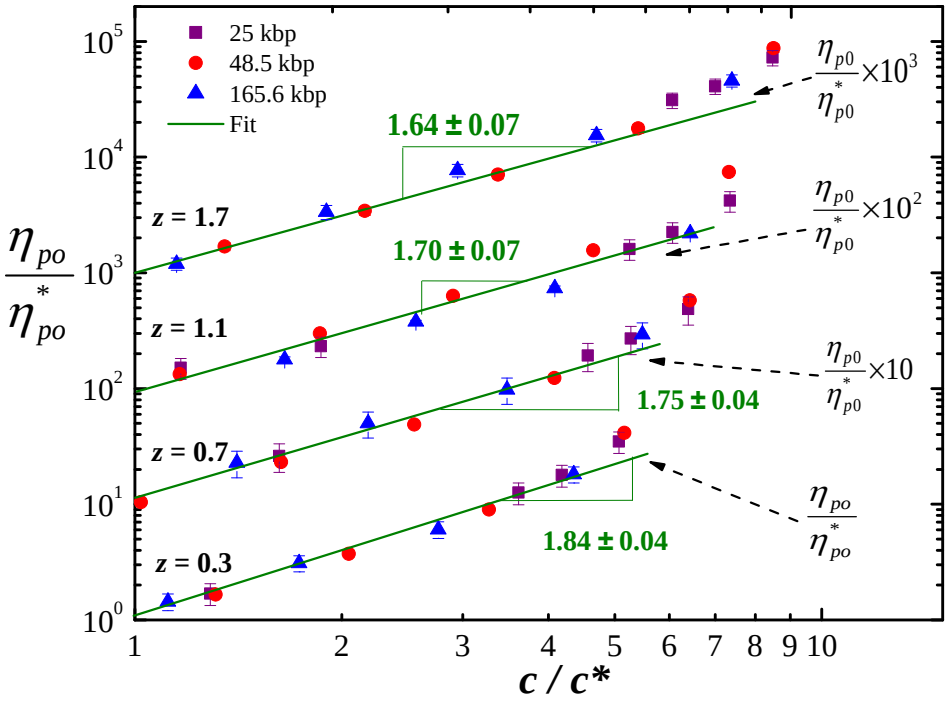

Figure 6.4: Dependence of the viscosity ratio $\eta_{p0}\,/\eta^*_{p0}$ on the scaled concentration c/c^* in the semidilute regime, for 25 kbp, λ and T4 DNA, at fixed values of the solvent quality z. In order to display all the measurements on a single plot, viscosity ratios for the different values of z have been multiplied by different fixed factors as indicated. Lines through the data are fits to the experimental data, with slopes and error in the fitted slope as shown.

Table 6.4: Values of the effective exponent $\nu_{\text{eff}}(z)$ determined experimentally at z = 0.3, 0.7, 1.1, 1.7 and by Brownian dynamics simulations at z = 0.7, 1.7

z	25 kbp	λ-DNA	T4 DNA	$\frac{\partial \ln(\eta_{p0}/\eta^*_{p0})}{\partial \ln(c/c^*)}$	ν_{eff}	ν_{eff}
	T	T	T	(experiments)	(experiments)	(BDS)
0.3	19.7°C	18.4°C	16.8°C	1.84 ± 0.04	0.51 ± 0.01	–
0.7	26.1°C	22.9°C	19.2°C	1.75 ± 0.04	0.52 ± 0.01	0.54 ± 0.02
1.1	32.8°C	27.5°C	21.7°C	1.70 ± 0.07	0.53 ± 0.01	–
1.7	43.4°C	34.8°C	25.4°C	1.64 ± 0.07	0.54 ± 0.01	0.58 ± 0.03

be identical to that which characterizes the power laws for both the polymer size and the diffusivity. From the set of values of z for which Brownian dynamics simulations results have been reported by Jain et al. (2012a), there are two values at which this conclusion can be tested by comparison with experiment (z = 0.7 and z = 1.7). [Note that at each value of z, the experimental value of ν_{eff} can be determined by equating the slope of the fitted lines in Figure 6.4 to $1/(3\ \nu_{\text{eff}}$ -1).] The values of $\nu_{\text{eff}}(z)$ listed in Table 6.4, at z = 0.7 and 1.7, suggest that simulation and experimental exponents agree with each other to within error bars.

6.4 Universal ratio of relaxation times

Blob scaling arguments can be used to show that, away from the crossover boundaries, the concentration dependence of the longest relaxation time, λ_1 , obeys the power law,

$$\lambda_1 \sim \left(\frac{c}{c^*}\right)^{(2-3\nu)/(3\nu-1)}. \tag{6.3}$$

In very good solvents, since $\nu \approx 0.59$, this would imply $\lambda_1 \sim (c/c^*)^{0.3}$, while in θ-solutions, $\lambda_1 \sim c/c^*$.

Liu et al. (2009) have recently examined the concentration dependence of λ_1 by studying the relaxation of stretched single T4 DNA molecules in semidilute solutions. They find that at 22°C, the longest relaxation time obeys the power law,

$$\frac{\lambda_1}{\lambda_{1,z}} \sim \left(\frac{c}{c^*}\right)^{0.5}, \tag{6.4}$$

where, $\lambda_{1,z}$ is the longest relaxation time in the dilute limit. This clearly suggests that, (i) for the solution of T4 DNA considered in their work, 22°C is in the crossover regime, and (ii) the relaxation time also obeys a power law in the crossover regime (as observed here for viscosity), with an effective exponent $\nu_{\text{eff}} \approx 0.56$.

It is worth noting that, for T4 DNA molecules dissolved in the solvent used in the present work, 22°C corresponds to a values of the solvent quality parameter z = 1.17.

It is common to define an alternative large scale relaxation time λ_η, based on the polymer contribution to the zero shear rate viscosity η_{p0}, as shown in Equation 1.9. It is straight forward to show that, in the semidilute unentangled regime, λ_η obeys the same power law scaling with concentration as obeyed by λ_1 (see Equation 6.3). Figure 6.5 compares the concentration dependence of the ratio $\lambda_1/\lambda_{1,z}$ in the semidilute regime, obtained by Liu et al. (2009), with that of the ratio $\lambda_\eta/\lambda_{\eta,z}$, measured by the current experiments at 22°C. Here, $\lambda_{\eta,z}$ is a large scale relaxation time in the dilute limit, based on $[\eta]$ (Sunthar et al., 2005)

$$\lambda_{\eta,z} = \frac{M[\eta]\,\eta_{\text{s}}}{N_{\text{A}}\,k_{\text{B}}\,T}. \tag{6.5}$$

It is clear that both relaxation times exhibit identical scaling with concentration in the semidilute regime at 22°C.

It is well known that for dilute polymer solutions, the ratio of the two large scale relaxation times ,

$$U_{\eta\lambda} = \frac{\lambda_{\eta,z}}{\lambda_{1,z}}, \tag{6.6}$$

is a universal constant, independent of polymer and solvent chemistry. Predicted values of $U_{\eta\lambda}$ vary from 1.645 by Rouse theory to 2.39 by Zimm theory, with predictions by other approximate theories lying somewhere in between (Kröger et al., 2000). Recently, Somani et al. (2010) have predicted the dependence of $U_{\eta\lambda}$ on the solvent quality z, in the dilute limit, with the help of Brownian dynamics simulations. This enables us to calculate the value of the ratio λ_η/λ_1 at 22°C using the present measurements and the measurements of Liu et al. (2009), by the following

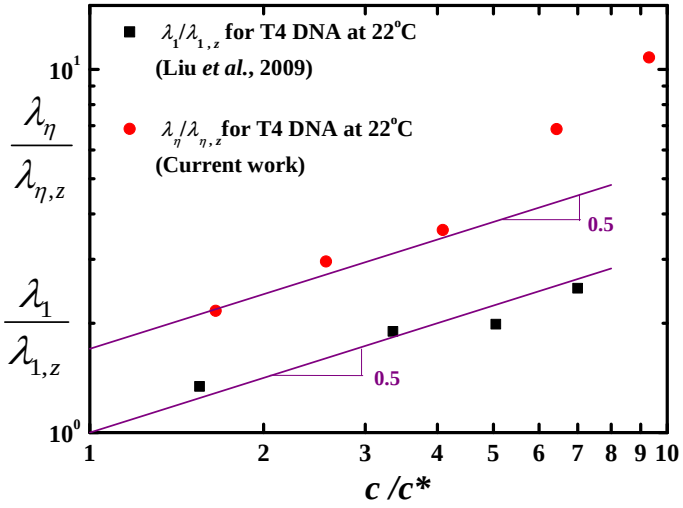

Figure 6.5: The concentration dependence of the ratio $\lambda_1/\lambda_{1,z}$ in the semidilute regime, obtained by Liu et al. (2009), compared with the dependence of the ratio $\lambda_\eta/\lambda_{\eta,z}$, measured by current experiments at 22°C.

argument. Clearly,

$$\frac{\lambda_\eta}{\lambda_1} = \left(\frac{\lambda_\eta}{\lambda_{\eta,z}}\right)\left(\frac{\lambda_{1,z}}{\lambda_1}\right) U_{\eta\lambda}(z). \tag{6.7}$$

Since the effective exponent in the experiments of Liu et al. (2009) and the present experiments is the same ($\nu_{\text{eff}} = 0.56$), we assume that the two solutions have the same value of z = 1.17. At this value of z, the simulations of Somani et al. (2010) suggest that $U_{\eta\lambda}\,(z = 1.17) = 1.79$. Equation 6.7 can then be used to find the ratio λ_η/λ_1 at the various values of concentration at which the ratios $\lambda_\eta/\lambda_{\eta,z}$ and $\lambda_1/\lambda_{1,z}$ have been measured in the two sets of experiments.

Figure 6.6 displays the ratio λ_η/λ_1 obtained in this manner in the dilute and semidilute regimes. Since both the ratios $\lambda_\eta/\lambda_{\eta,z}$ and $\lambda_1/\lambda_{1,z}$ are nearly equal to 1 in the limit of small c, it is not surprising that $\lambda_\eta/\lambda_1 \approx U_{\eta\lambda}\,(z)$ for concentrations in the dilute regime. However, while λ_η/λ_1 is constant in the semidilute regime, as expected from the similar scaling with concentration exhibited in the two sets of experiments, its value is not identical to the value in the dilute limit. This appears to be because $\lambda_\eta/\lambda_{\eta,z}$ increases more rapidly with concentration in the crossover regime between dilute and semidilute, than $\lambda_1/\lambda_{1,z}$. More experiments carried out for different polymer solvent systems are required to substantiate this observation.

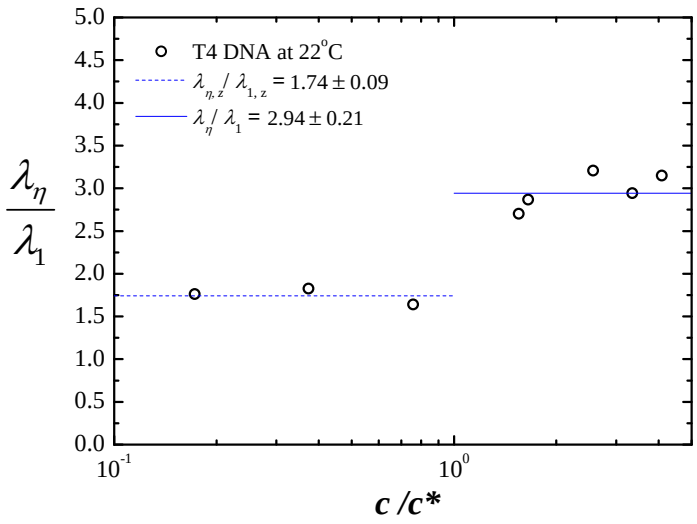

Figure 6.6: Universal ratio of λ_η (measured in the present work) to λ_1 (measured by Liu et al. (2009)) for T4 DNA at 22°C (which corresponds to a value of solvent quality $z = 1.17$), for a range of concentrations spanning the dilute and semidilute regime.

6.5 Conclusions

By carrying out accurate measurements of the polymer contribution to the zero shear rate viscosity of semidilute DNA solutions in the double crossover regime, the scaled polymer contribution to the viscosity is shown to obey the expression,

$$\frac{\eta_{\mathrm{p0}}}{\eta^*_{\mathrm{p0}}} \sim (c/c^*)^{\frac{1}{3\nu_{\mathrm{eff}}\,(z)-1}}$$

in line with recent predictions on the form of universal crossover scaling functions for semidilute solutions (Jain et al., 2012a). The experimentally determined values of the effective exponent ν_{eff}, for two values of $z = 0.7$ and 1.7, agree within error bars, with values determined from Brownian dynamics simulations. This suggests, in accordance with the prediction of scaling theory (Jain et al., 2012a), that the exponent $\nu_{\mathrm{eff}}(z)$ that governs the scaling of viscosity is identical to the exponent which characterizes the power laws for polymer size and the diffusivity.

The results obtained here clearly demonstrate that the solvent quality parameter z, and the scaled concentration c/c^*, are the two scaling variables that are

essential in order to properly understand and characterise the concentration and temperature dependent dynamics of a linear viscoelastic property, such as the zero shear rate viscosity, of semidilute polymer solutions.

PART II

NON-EQUILIBRIUM CHARACTERIZATION

7

Shear Flow of Semidilute and Dilute DNA Solutions

7.1 Introduction

In spite of the occurrence of polymer solutions at semidilute concentrations in a number of industrially relevant flows such as in inkjet printing, to date, there are very few systematic studies of the rheological behaviour of semidilute solutions either experimentally (Hur et al., 2001), or via simulations (Huang et al., 2010; Stoltz et al., 2006). On the other hand, dilute polymer solutions have been studied much more extensively. In particular, the dependence of the polymer contribution to viscosity, η_{p}, on the Weissenberg number, $\mathrm{Wi} = \lambda\dot{\gamma}$ (where λ is the measure of the largest relaxation time of the solution), has been thoroughly investigated, and various scaling relationships have been derived analytically (Winkler, 2006; Rubinstein and Colby, 2003; Winkler, 2010; Bird et al., 1987; Öttinger, 1996), measured experimentally (Schroeder et al., 2005; Bird et al., 1987), and estimated by simulations (Schroeder et al., 2005; Aust et al., 1999). In this chapter, results of measurements of the shear viscosity of DNA solutions (discussed in Chapters 5 and 6), are presented as a function of flow strength, across a range of temperatures, concen-

trations and molecular weights, in the semidilute and dilute regimes. The central purpose of this part of the study is to identify the relevant scaling variables with which to represent the data, such that the universal behaviour of polymer solutions in flow (if it exists) can be revealed.

In order to place the present work in context, it is necessary to summarize the results of earlier studies, both in the dilute and semidilute regimes.

A number of different analytical approaches to predicting the dependence of η_p on Wi for *dilute* polymer solutions suggest that for $Wi \gg 1$, $\eta_p \sim Wi^{-2/3}$ (Bird et al., 1987; Doyle et al., 1997; Winkler, 2006, 2010). There are very few experimental studies validating this prediction. A recent study by Hua and Wu of polystyrene in DOP (Hua and Wu, 2006) observed this scaling only for the largest molecular weight sample considered by them (2 Million molecular weight). Samples of lower molecular weight polystyrene appear to follow a scaling $\eta_p \sim Wi^{-\alpha}$, with α varying with molecular weight, but is always less than 2/3. Simulation studies of dilute bead-spring solutions (with finitely extensible springs) (Jendrejack et al., 2002; Schroeder et al., 2005) observe the existence of two power law regimes, $\eta_p \sim Wi^{-0.5}$ (for $10^2 < Wi < 10^3$) and $\eta_p \sim Wi^{-2/3}$ (for $Wi > 10^4$), regardless of whether nonlinear effects such as HI and EV are included or absent. On the other hand, simulations of dilute bead-rod solutions only appear to observe the $Wi^{-0.5}$ regime (Liu, 1989; Hur et al., 2001; Doyle et al., 1997).

At very high Weissenberg numbers, in the experiments of Hua and Wu (2006) and in bead-rod simulations, η_p for dilute polymer solutions is observed to level off and approach a constant asymptotic value. On the other hand, predictions of η_p from BD simulations of FENE chains (Jendrejack et al., 2002; Schroeder et al., 2005), and analytical solutions of constitutive equations with an approximate treatment of the FENE spring force law, give rise to power law shear thinning for $Wi > \mathcal{O}(1)$ that persists for arbitrarily high Wi.

The only experimental measurements of the shear rheology of semidilute polymer solutions appears to be the pioneering study of Hur et al. (2001), who examined the behaviour of λ-phage DNA at concentrations equal to $1c^*$, $3c^*$ and $6c^*$.

In all these cases, they found $\eta_p \sim Wi^{-\alpha}$, with α close to -0.5, independent of the concentration, and in agreement with simulation predictions for dilute bead-rod chains. It should be noted here, that for semidilute solutions, a decision needs to be made regarding the choice of relaxation time λ, to use in the definition of the Weissenberg number. Hur et al. (2001) use the longest relaxation time λ_1, at the particular concentration of interest, which they determined by carrying out stretch relaxation experiments on stained DNA molecules.

Very recently, there have been two simulation studies of semidilute solutions in shear flow. The first study is by Stoltz et al. (2006), who have used BD simulations to predict the behaviour of bead-spring chains with roughly 20 beads per chain. They find that in the range of c/c^* from 0 to 2, $\eta_p \sim Wi^{-0.51}$ (when HI is included), in close agreement with the observations of Hur et al. (2001). Individual curves for the different values of c/c^*, however, were found not to collapse on top of each other. As in the case of Hur et al. (2001), the Weissenberg number is defined in terms of the longest relaxation time λ_1, determined by stretch relaxation simulations.

Using massively parallel multi-particle collision dynamics, Huang et al. (2010) have carried out an exhaustive study of semidilute solutions at equilibrium and in shear flow. In particular, they have paid close attention to validating all the simulation results with known scaling predictions for semidilute solutions (under good solvent conditions) that have been derived from blob theory. For instance, they establish that the longest relaxation time in their simulations scales as $(c/c^*)^{(2-3\nu)/(3\nu-1)}$ as expected from scaling arguments. When their simulation data is represented in terms of η_p / η_{p0} versus Wi, where the concentration dependent longest relaxation time is used in the definition of Wi, they observe a data collapse on to a master curve, independent of $c/c^*$and chain length. Subsequent to the onset of shear thinning, they find η_p /$\eta_{p0} \sim Wi^{-0.3}$ for $1 < Wi < 100$, and a steeper power law, with η_p /$\eta_{p0} \sim Wi^{-0.45}$ for high shear rates. The scaling with Wi at high Weissenberg number is consequently in agreement with the earlier simulations by Stoltz et al. (2006), and the experimental observations of Hur et al. (2001).

Since we have not carried out stretch relaxation experiments, we cannot use λ_1 in our definition of Wi. However, since λ_η (defined in Equation 1.9) obeys the same scaling with concentration as λ_1, (as demonstrated in Figure 6.5), it is entirely equivalent to define the Weissenberg number as $\lambda_\eta\ \dot{\gamma}$.

In the subsequent sections of this chapter, we first examine if $\eta_\mathrm{p}\ /\ \eta_{\mathrm{p}0}$ versus $\lambda_\eta\ \dot{\gamma}$ leads to data collapse for various values of c/c^* and molecular weight in the semidilute regime. We find that, contrary to the simulation predictions by Huang et al. (2010), this is not the case, both for DNA as well as synthetic polystyrene solutions. We then develop a scaling argument, which exploits the existence of Pincus blobs in shear flow, that leads to an alternative definition of a relaxation time, based on which data collapse is observed independent of the solvent quality and c/c^*. Finally, we present results for the viscosity of dilute DNA solutions, and discuss the observed behaviour in the light of the previous results on synthetic polymer solutions by Hua and Wu (2006).

7.2 Results and Discussion

7.2.1 Semidilute solutions in shear flow

We have measured the shear viscosities of three DNA samples: 25 kbp, λ-phage and T4 DNA at various temperatures and concentrations, same as in Sections 5.2 and 6.2. The experimental details of the shear rheometry are not discussed here, since they have already been discussed earlier in Section 2.4.

Two examples of the dependence of solution viscosity on shear rate $\dot{\gamma}$ are given in Figures 7.1 (a) and (b). The former displays the viscosity of 25 kbp DNA at a fixed concentration c = 0.441 mg/ml and at various temperatures ranging from T = 13 to 44.6°C. Since c^* varies with temperature, this corresponds to values of c/c^* ranging from 2.12 to 8.65 (see Table 6.2 in Chapter 6), all of which are in the semidilute regime. In Figure 7.1 (b), the dependence of η on $\dot{\gamma}$ of T4 DNA at a fixed temperature T = 25°C, is displayed at various concentrations c, varying from 0.059 to 0.214 mg/ml. This corresponds to a c/c^* range of 2.98 to 10.82, as displayed in Table 6.2.

We have estimated the overlap concentrations (c^*) for all the DNA samples at different temperatures from the z values, as explained in Section 6.3. Representative values of c^* found from the z values, at various M and T and for several DNA, are displayed in Table 6.1. The general pattern of the viscosity curves is typical of the behaviour observed for polymer solutions, with a constant plateau region at low shear rates denoting Newtonian behaviour, followed by shear thinning at high shear rates, with a power law decay. We have not observed the viscosity levelling off in any of our measurements at the highest shear rate used in our experiments, which is typically of the order 10^2 s^{-1}.

Figure 7.2 displays the dependence of the scaled viscosity η_p/η_{p0} on the shear rate $\dot{\gamma}$, for 25 kbp and λ-DNA, and Figure 7.3 the same for T4 DNA. Each of the subfigures in these two plots corresponds to a different concentration, with the individual symbols in the subfigures representing different temperatures. All the concentrations correspond to the solutions in the semidilute regime, as can be comfirmed from the values of c/c^* listed in Table 6.2. The reason the scaled viscosity appears to *increase* with temperature is because of the division of η_p by η_{p0}. While η_p decreases with temperature, as expected (see Figure 7.1 (a)), the shear rate dependence of η_p is more pronounced over the same range of shear rates for solutions at a lower temperature.

The dependence of the scaled viscosity η_p/η_{p0} on the Weissenberg number $\lambda_\eta\dot{\gamma}$ for 25 kbp, λ-phage and T4 DNA, is displayed in Figures 7.4, 7.5 and 7.6, respectively. There are several striking features in these figures that we discuss in turn.

The first noticeable fact is that the various curves for η_p/η_{p0} at *different* temperatures, but at the *same* concentration collapse on top of each other when the data is represented in this form. This implies that using λ_η as the relaxation time to scale the shear rate leads to *time-temperature* superposition, i.e., all the different curves seen in the individual subfigures of Figures 7.2 and 7.3 collapse on to a single curve for each concentration, independent of temperature.

The dependence of λ_η on inverse temperature $1/T$ is displayed in Figures 7.7 to 7.9 for each of the three DNA samples. There is clearly a linear relationship

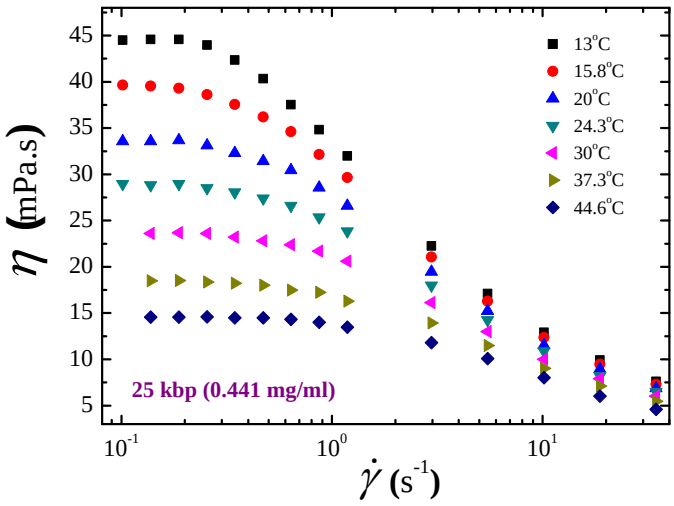

(a)

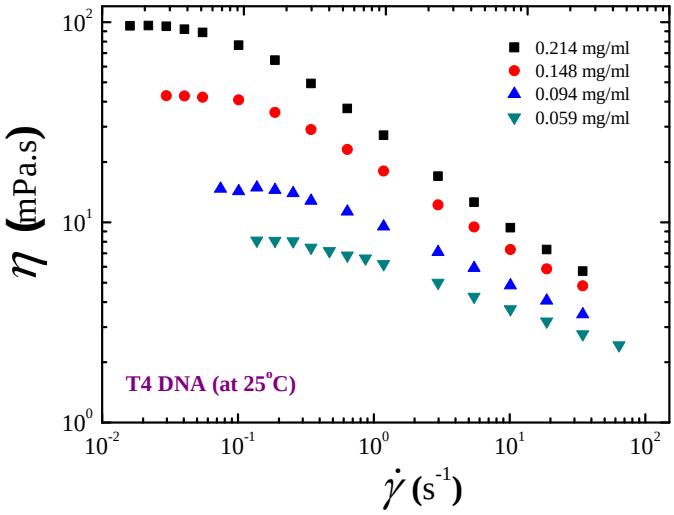

(b)

Figure 7.1: (a) Shear rate dependence of the steady state shear viscosity for 25 kbp DNA at a fixed absolute concentration for different temperatures. (b) Shear rate dependence of the steady state shear viscosity for T4 DNA at a fixed temperature for different absolute concentrations.

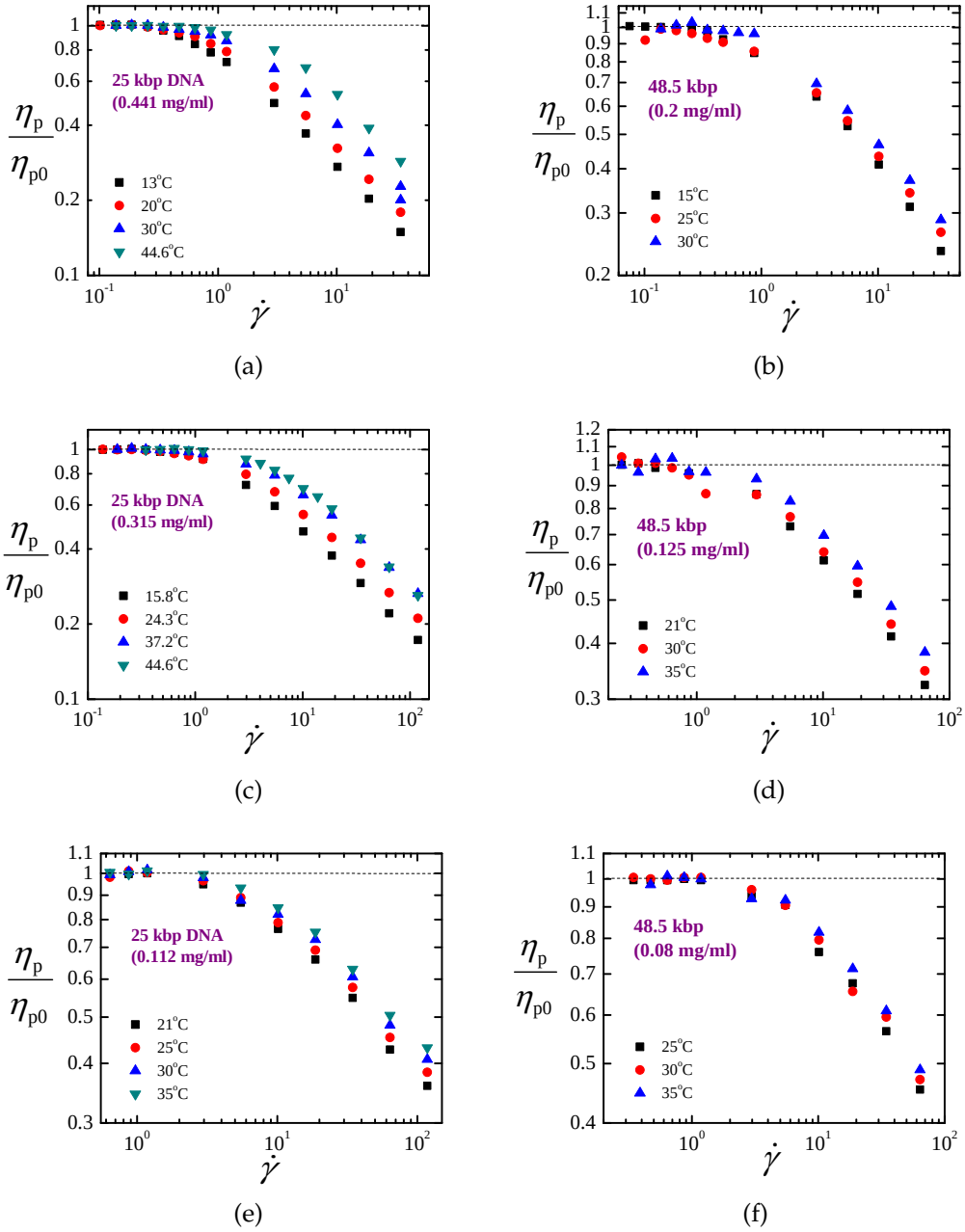

Figure 7.2: η_p/η_{p0} as a function of shear rate $\dot{\gamma}$ for 25 kbp and 48.5 kbp DNA, each at a fixed absolute concentration and at different temperatures. The temperatures are indicated in the legends and the concentrations are mentioned in individual figures.

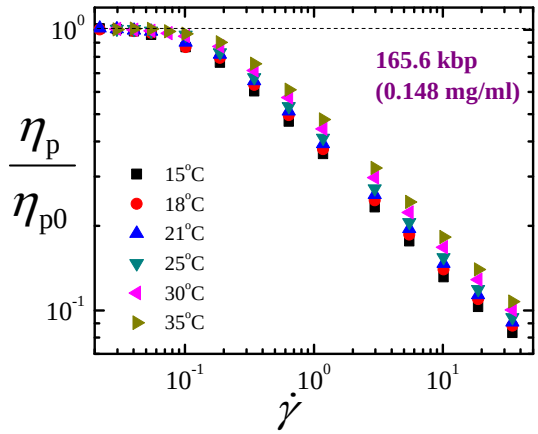

(a)

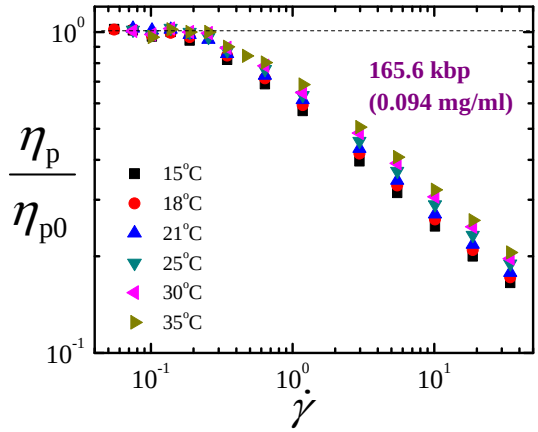

(b)

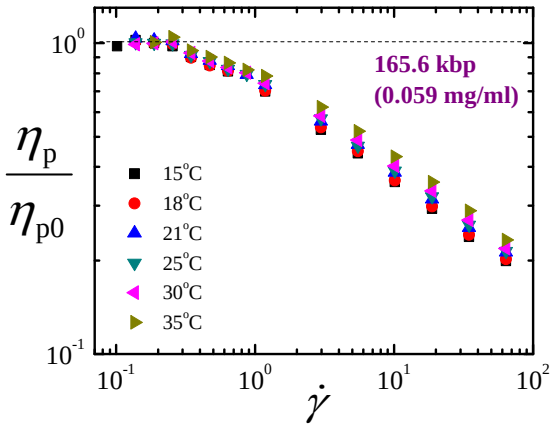

(c)

Figure 7.3: η_p/η_{p0} as a function of shear rate $\dot{\gamma}$ for T4 DNA, each at a fixed absolute concentration and at different temperatures. The temperatures are indicated in the legends and the concentrations are mentioned in individual figures.

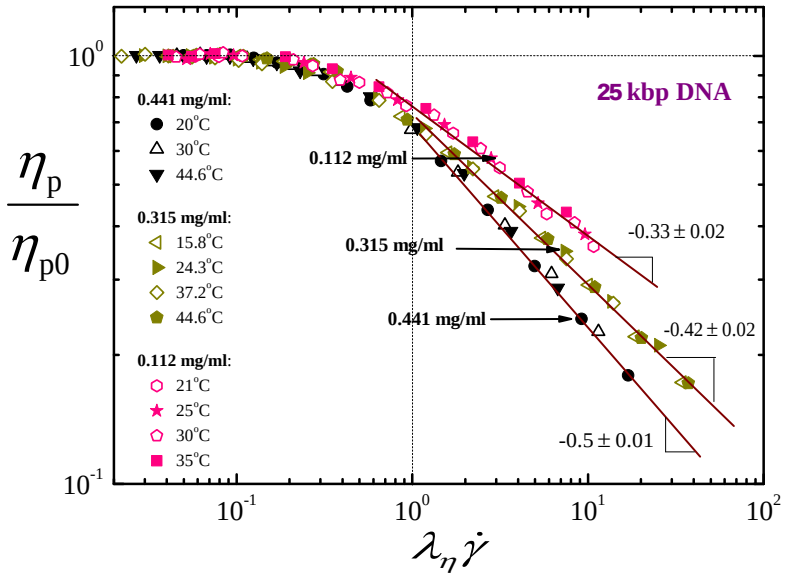

Figure 7.4: Shear rate dependence of scaled polymer contribution to shear viscosity for linear 25 kbp DNA at different temperatures and concentrations. There is a definite temperature superposition across the range of concentrations. A broad power law regime exists as we move from higher to lower concentrations. The lines are least quare fits of data in the shear thinning region.

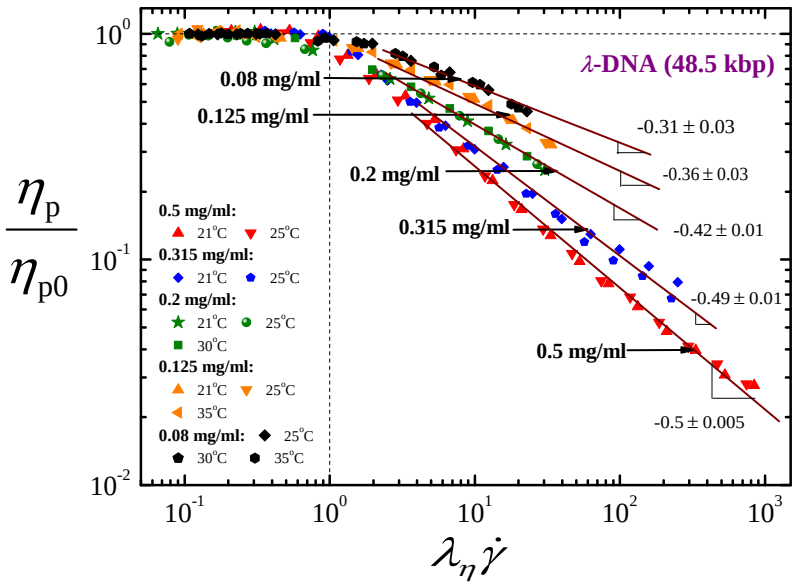

Figure 7.5: Shear rate dependence of scaled polymer contribution to shear viscosity for linear λ DNA at different temperatures and concentrations. There is a definite temperature superposition across the range of concentrations. A broad power law regime exists as we move from higher to lower concentrations. The lines are least quare fits of data in the shear thinning region.

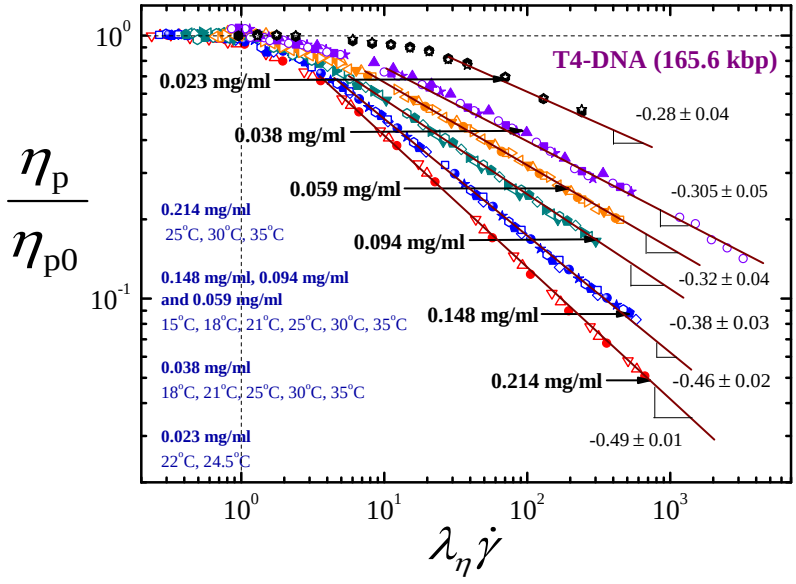

Figure 7.6: Shear rate dependence of scaled polymer contribution to shear viscosity for linear T4 DNA at different temperatures and concentrations. There is a definite temperature superposition across the range of concentrations with a broad power law regime as we move from higher to lower concentrations. The lines are least quare fits of data in the shear thinning region.

between λ_η and $1/T$, which can be anticipated from our earlier observation of the linear dependence of $[\eta]$ on $1/T$ displayed in Figure 5.4 in Chapter 5.

The usefulness of λ_η as a scaling variable, in leading to time-temperature superposition of the scaled viscosity versus shear rate data, can also be seen for the case of semidilute solutions of two other polymer-solvent systems. In the following chapter on elongational flow Chapter 8, we use a more viscous solvent for suspending the DNA molecules as shown in Table 2.3. We have also characterised its shear rate dependence. The dependence of the scaled viscosity η_p/η_{p0} on the Weissenberg number $\lambda_\eta\dot{\gamma}$ for 25 kbp, λ-phage and T4 DNA, is displayed in Figures 7.10, 7.11 and 7.12, respectively. We see that the various curves for η_p/η_{p0} at *different* temperatures, but at the *same* absolute concentration collapse on top of each other when the data is represented in this form. Also, irrespective of the DNA molecular weight, the terminal slope in the power law region at high shear rates increases with increasing concentration.

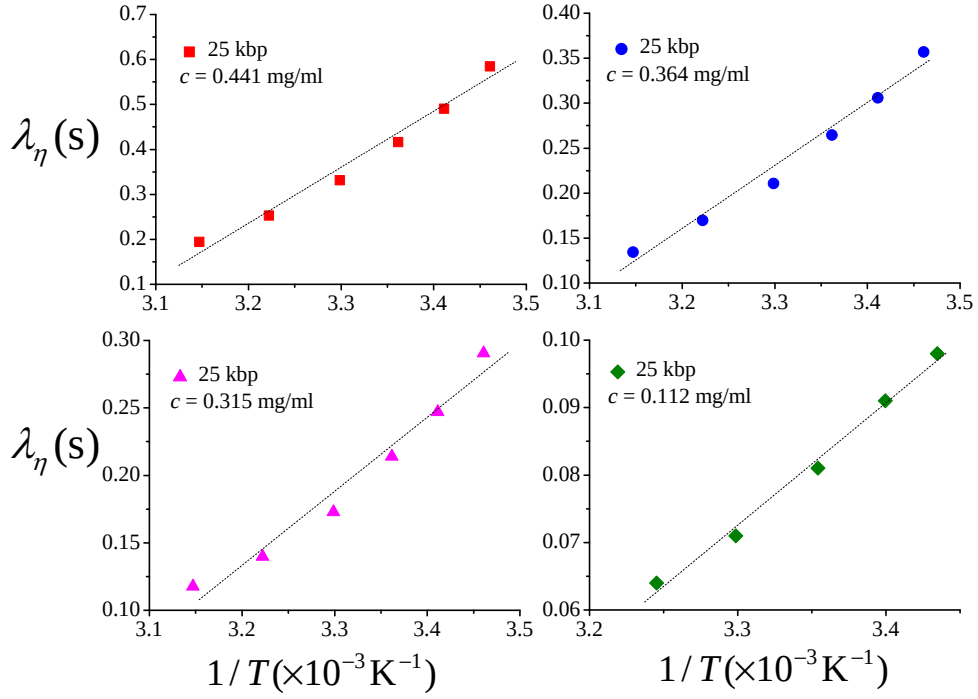

Figure 7.7: λ_η vs $1/T$ at a fixed c for 25 kbp DNA. The lines are the linear least squares fit to the data.

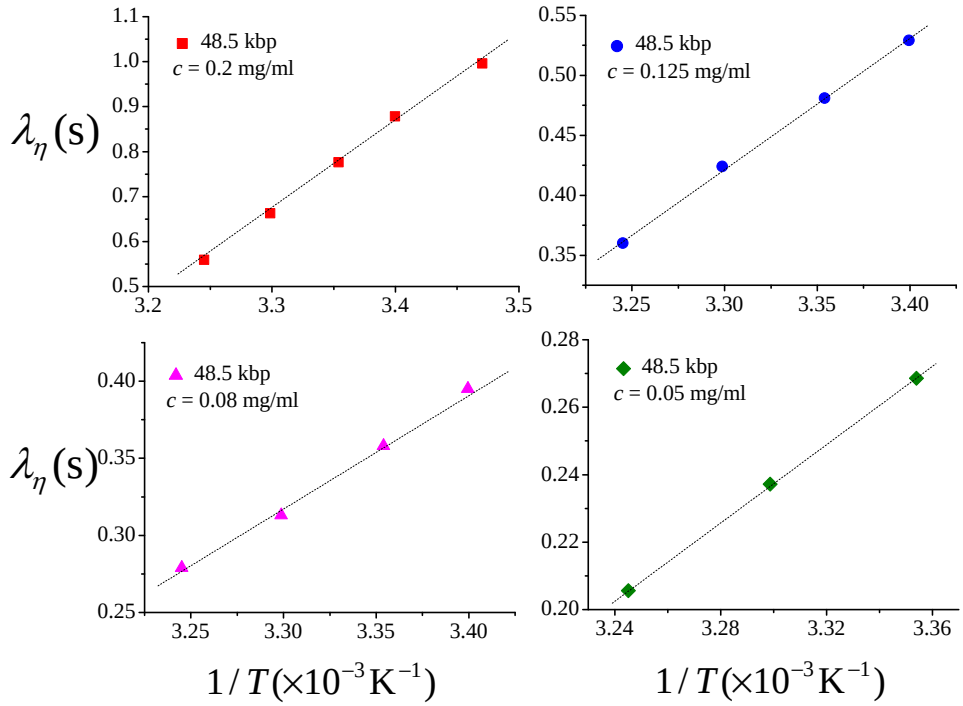

Figure 7.8: λ_η vs $1/T$ at a fixed c for 48.5 kbp DNA. The lines are the linear least squares fit to the data.

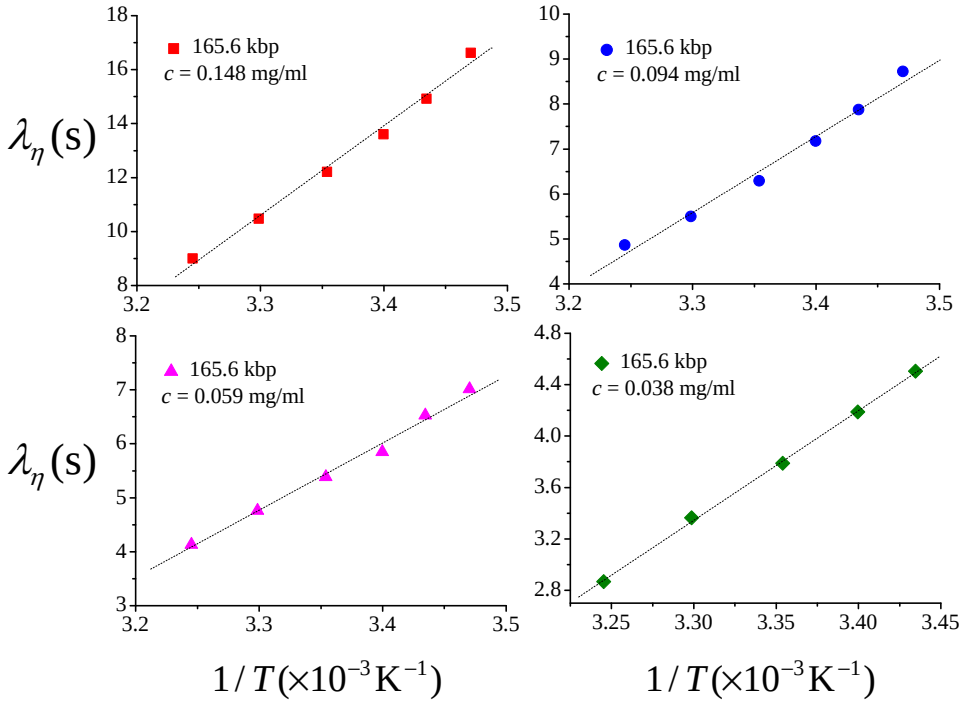

Figure 7.9: λ_η vs $1/T$ at a fixed c for 165.6 kbp DNA. The lines are the linear least squares fit to the data.

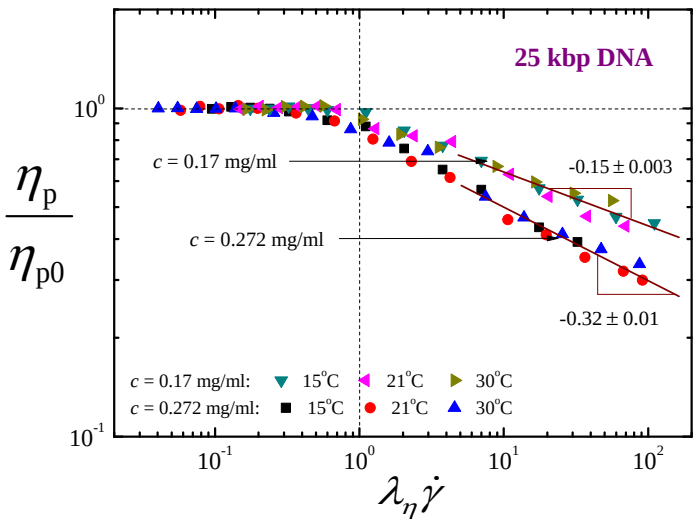

Figure 7.10: Shear rate dependence of scaled polymer contribution to shear viscosity for linear 25 kbp DNA at different temperatures and concentrations in the viscous solvent used for extensional studies, Table 2.3. There is a definite temperature superposition across the range of concentrations. A broad power law regime exists as we move from higher to lower concentrations. The lines are least quare fits of data in the shear thinning region.

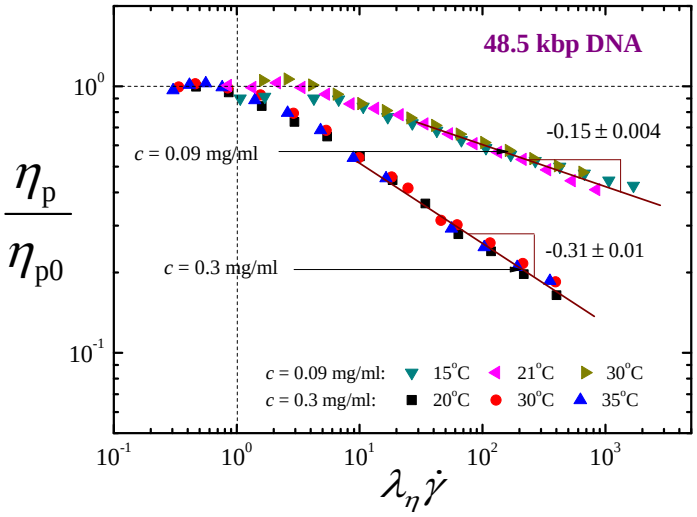

Figure 7.11: Shear rate dependence of scaled polymer contribution to shear viscosity for linear λ-DNA at different temperatures and concentrations in the viscous solvent used for extensional studies, Table 2.3. There is a definite temperature superposition across the range of concentrations. A broad power law regime exists as we move from higher to lower concentrations. The lines are least quare fits of data in the shear thinning region.

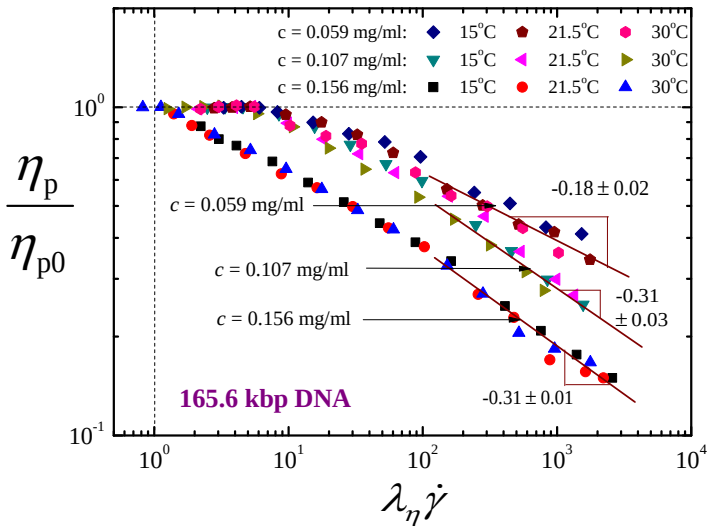

Figure 7.12: Shear rate dependence of scaled polymer contribution to shear viscosity for linear T4 DNA at different temperatures and concentrations in the viscous solvent used for extensional studies, Table 2.3. There is a definite temperature superposition across the range of concentrations with a broad power law regime as we move from higher to lower concentrations. The lines are least quare fits of data in the shear thinning region.

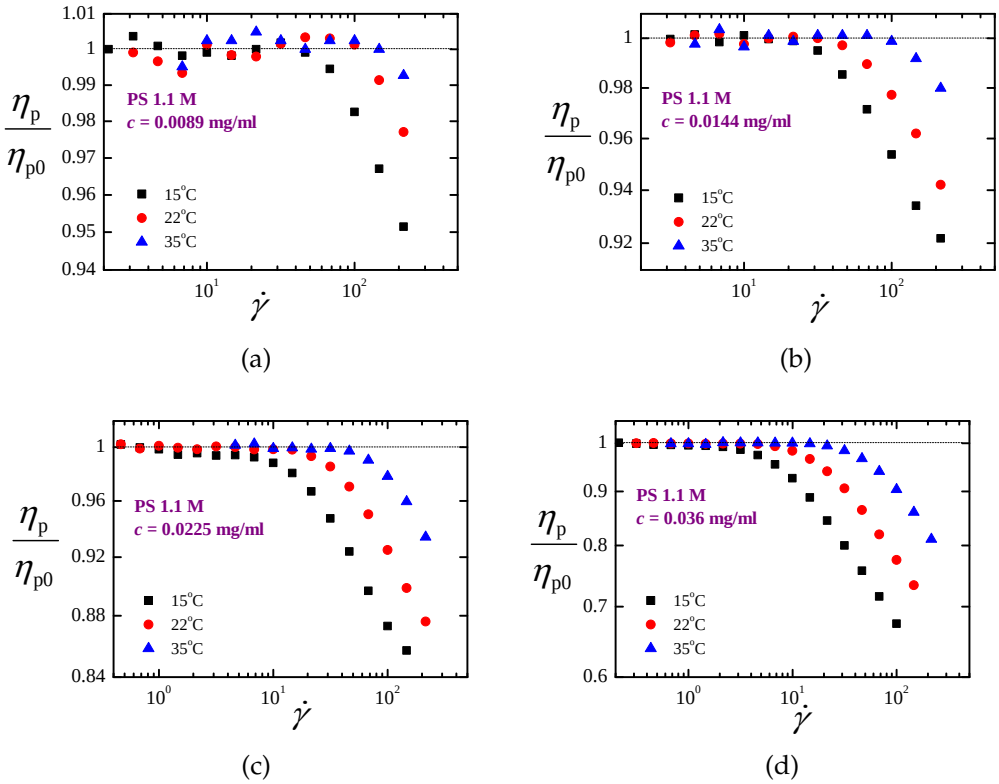

Figure 7.13: η_p/η_{p0} as a function of shear rate $\dot{\gamma}$ for linear 1.1 M polystyrene, each at a fixed absolute concentration and at different temperatures. The temperatures are indicated in the legends and the concentrations are mentioned in individual figures.

We have also studied the time-temperature superposition for linear polystyrene in DiOctyl Phthalate (DOP), displayed in Figures 7.13 to 7.15. The various subfigures in Figures 7.13 and 7.14 display the shear rate dependence of the scaled viscosity η_p/η_{p0} at fixed concentrations c and various temperatures, for two different molecular weights of polystyrene, namely 1.1 M and 15.4 M. Figures 7.15 (a) and (b) show the time-temperature superposition of this data when represented in terms of $\lambda_\eta\dot{\gamma}$, for these two molecular weights, respectively. As in the case of the DNA solutions, provided the concentration is fixed, data collapses on to a single curve, regardless of the temperature, with more pronounced shear thinning with increased concentration.

The concentrations and temperatures at which the measurements reported in Figures 7.13 and 7.14 were carried out, correspond to a range of c/c^* from 1 to

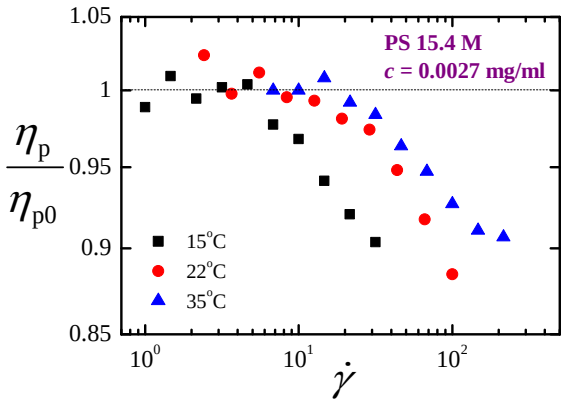

Figure 7.14: η_p/η_{p0} as a function of shear rate $\dot{\gamma}$ for linear 15.4 M polystyrene, each at a fixed absolute concentration and at different temperatures. The temperatures are indicated in the legends and the concentrations are mentioned in individual figures.

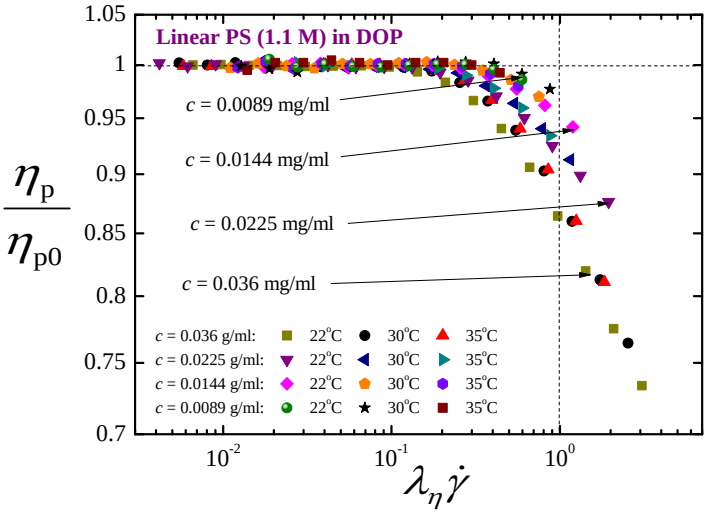

(a)

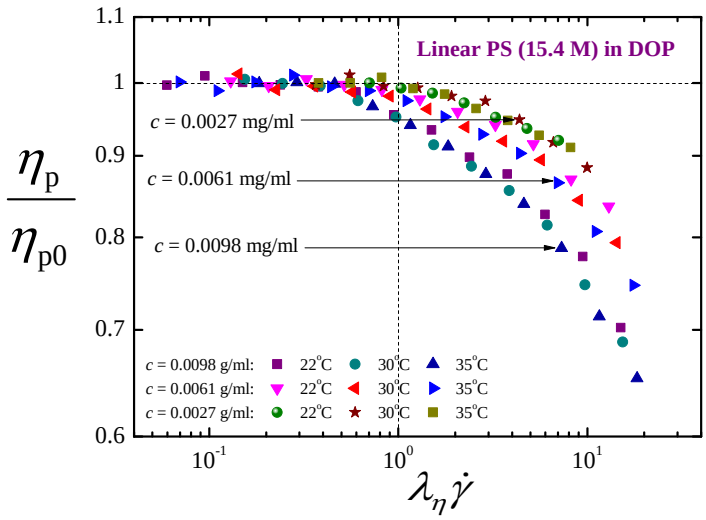

(b)

Figure 7.15: (a) Shear rate dependence of scaled polymer contribution to shear viscosity for linear 1.1 M polystyrene at different temperatures and concentrations. (b) Shear rate dependence of scaled polymer contribution to shear viscosity for linear 15.4 M polystyrene at different temperatures and concentrations. For both molecular weights, there is a definite temperature superposition across the range of concentrations and a broad power law regime as we move from higher to lower concentrations.

Table 7.1: Steady state zero shear rate viscosities, η_0 (mPa.s) for 1.1 M and 15.4 M linear polystyrene in DOP at various concentrations, c (mg/ml) and temperatures, T (°C) in the semidilute regime. Note that T_θ for polystyrene in DOP is 22°C (Brandrup et al., 1999). The c/c^* values at T_θ has been estimated from the $[\eta]$ values at T_θ from Li et al. (2000) using the relation $c^* \approx 1/[\eta]$.

1.1 M				15.4 M			
c	T	c/c^* (at T_θ)	η_0	c	T	c/c^* (at T_θ)	η_0
0.036	15	–	3043.8 ± 13.3	0.0098	15	–	666.6 ± 2.8
	22	4	1686.5 ± 1.3		22	4	443.4 ± 2.8
	35	–	721.6 ± 0.9		35	–	223.6 ± 0.2
0.0225	15	–	796.1 ± 2.3	0.0061	15	–	286.2 ± 1.4
	22	2.5	505.6 ± 0.6		22	2.5	196.9 ± 0.6
	35	–	238.6 ± 0.3		35	–	105 ± 0.6
0.0144	15	–	370.2 ± 0.3	0.0038	15	–	195.6 ± 1.9
	22	1.6	240.4 ± 0.2		22	1.6	139.3 ± 0.4
	35	–	118.3 ± 0.2		35	–	72.3 ± 0.3
0.0144	15	–	220 ± 0.2	0.0027	15	–	163.8 ± 0.4
	22	1	147.4 ± 0.2		22	1	112 ± 0.6
	35	–	74.6 ± 0.1		35	–	58.3 ± 0.2

4 (at $T = T_\theta$), as displayed in Table 7.1. Two linear polystyrene polymers have been used in this study: (i) a molecular weight of 1.14×10^6 g/mol (1.1 M) with a polydispersity index (pdi = M_w/M_n) of 1.09 purchased from Polymer Source Inc. (Canada) and (ii) a molecular weight of 1.54×10^7 g/mol (15.4 M) (pdi = 1.04) purchased from Varian (England). Both the polystyrene samples were dissolved in DOP, which is considered a θ-solvent for polystyrene at 22°C (Brandrup et al., 1999). To assist dissolving of polystyrene in DOP, methylene chloride was used as a co-solvent and the mixture was mixed for 24 hours. Methylene chloride was then completely evaporated in a vacuum oven at 40°C over the course of several days until no further weight loss was registered.

The most significant aspect of Figures 7.4 to 7.6 and Figures 7.10 to 7.12 for DNA, and Figures 7.15 (a) and (b) for polystyrene, is that the data does not collapse on to master curves, independent of c/c^* or molecular weight, as has been observed previously in the MPCD simulations of Huang et al. (2010). Nor is the slope in the power-law region close to 0.5 as observed in the simulations and experiments of Hur et al. (2001). Indeed, there is a significant power law regime over several decades of $\lambda_\eta\dot{\gamma}$, with the slope increasing with increasing concentration.

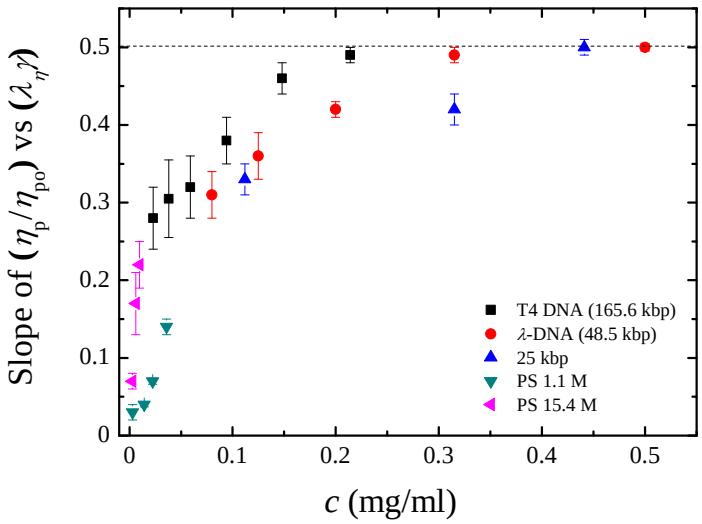

Figure 7.16: Slope of η_p/η_{p0} vs $\lambda_\eta\dot{\gamma}$ plots from Figures 7.4–7.6 for DNA and from Figure 7.15 for polystyrene as a function of absolute concentration c.

The dependence of the slope of the η_p/η_{p0} vs $\lambda_\eta\dot{\gamma}$ curves for DNA and polystyrene, in the power law regime, on concentration, is displayed in Figure 7.16. As can be seen, the magnitude of the slope for DNA appears to increase almost linearly before saturating to a value of 0.5. It should be noted that each of the symbols in the figure correspond to several temperatures, and as a result, to several values of c/c^*. Consequently while for each of the DNA, the asymptotic value of 0.5 is reached for increasing values of c/c^*, there is no meaningful threshold value in terms of c/c^*.

The source of the lack of agreement between the current experimental observations on DNA and polystyrene, with the predictions of the MPCD simulations of Huang et al. (2010), in terms of the ability of a concentration dependent large scale relaxation time to obtain data collapse across different values of c/c^*, is not clear to us. In particular, since both λ_1 and λ_η exhibit the same scaling with c/c^*. This was demonstrated for the special case of 22°C in Figure 6.5 in Chapter 6, since the experiments by Liu et al. (2009) were carried out at this temperature. Figure 7.17

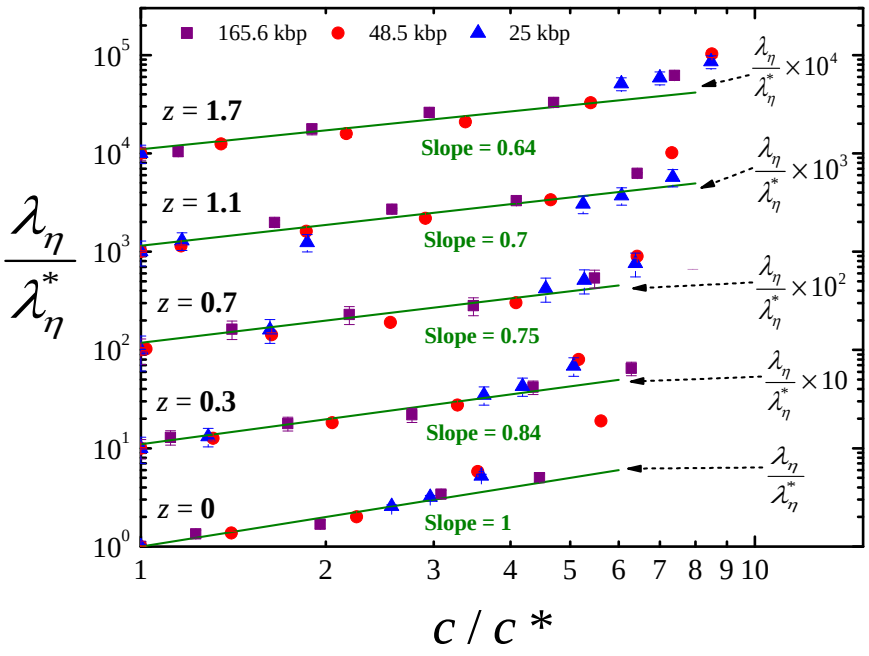

Figure 7.17: Crossover plot of λ_η for the three DNA at different values of z. The experiments have been conducted at different temperatures (see Table 6.3 in Chapter 6) for different DNA keeping the z constant. The collapse of different M at different T are seen when $\lambda_\eta/\lambda_\eta^*$ is plotted against c/c^*, keeping the z constant. Here λ_η^* is the value of λ_η at $c = c^*$. In order to display all the measurements on a single plot, the ratios of relaxation times for the different values of z have been multiplied by different fixed factors as indicated. Lines through the data have been drawn with a slope calculated from the value of ν_{eff} (z), listed in Table 6.4.

illustrates that indeed the scaled variable

$$\frac{\lambda_\eta}{\lambda_\eta^*} \sim \left(\frac{c}{c^*}\right)^{\frac{2-3\nu_{\text{eff}}}{3\nu_{\text{eff}}-1}},$$

with $\nu_{\text{eff}} = \nu_{\text{eff}}$ (z) being an affective exponent discussed earlier in the context of Figure 6.4. The lines through the symbols (representing the experimental data) in Figure 7.17, have been drawn with a slope calculated with values of ν_{eff} (z) listed in Table 6.4 in Chapter 6.

In the next subsection, we develop a scaling argument that suggests that an alternative relaxation time may be more appropriate to represent the universal behaviour observed in the shear flow of semidilute polymer solutions.

7.2.2 The derivation of an appropriate relaxation time

In the absence of shear flow, in semidilute solutions, the chain conformation consists of a series of 'correlation' blobs, with size ξ_c , such that chain segments below this length scale are under dilute solution conditions, while chain segments at larger length scales are under concentrated solution conditions. As a result, within the correlation blob, chain segments experience hydrodynamic (HI) and excluded volume (EV) interactions, while they are absent between the correlation blobs themselves due to the screening of these interactions. A consequence of the absence of EV, is that the correlation blobs obey random walk statistics. Furthermore, since the correlation blobs are space filling, semidilute solutions are often treated as a melt of correlation blobs.

The postulation of the correlation blob ansatz gives rise to some simple scaling arguments. If a chain consists of N_c correlation blobs, then random walk statistics imply,

$$R_{eq} \sim \xi_c N_c^{\frac{1}{2}} \tag{7.1}$$

where, R_{eq} is the mean size of the chain at equilibrium. If $\tilde{c}$ is the number of monomers N per unit volume, then $(\tilde{c}/N)$ is the number of polymers per unit volume, and

$$\frac{\tilde{c}}{N} = \frac{N_p}{V}, \tag{7.2}$$

where, N_p is the total number of polymers in the system, and V is the system volume. Since the correlation blobs are space filling, this implies,

$$\xi_c^3 N_c N_p = V,$$

or, from Equation 7.2,

$$\frac{\tilde{c}}{N} = \frac{1}{\xi_c^3 N_c}. \tag{7.3}$$

Solving for ξ_c^3 we get,

$$\xi_c^3 = \left(\frac{N}{N_c}\right)\frac{1}{\tilde{c}}. \tag{7.4}$$

At the overlap concentration we know that ,

$$\tilde{c}^* \frac{N}{R_{\mathrm{eq}}^3} \sim b^{-3} N^{1-3\nu}. \tag{7.5}$$

Multiplying and dividing the right hand side of Equation 7.4 with $\tilde{c}^*$, and using Equation 7.5, we get,

$$\xi_{\mathrm{c}}^3 = \left(\frac{N}{N_{\mathrm{c}}}\right)\left(\frac{\tilde{c}^*}{\tilde{c}}\right) b^3 N^{3\nu-1}. \tag{7.6}$$

For semidilute solutions, it can be shown that (see Supplementary material in Jain et al. (2012a)),

$$N_{\mathrm{c}} = \left(\frac{\tilde{c}}{\tilde{c}^*}\right)^{\frac{1}{3\nu-1}}. \tag{7.7}$$

As a result,

$$\xi_{\mathrm{c}}^3 = b^3 N^{3\nu} \left(\frac{\tilde{c}}{\tilde{c}^*}\right)^{-1} \left(\frac{\tilde{c}}{\tilde{c}^*}\right)^{\frac{-1}{3\nu-1}},$$

which simplifies to,

$$\xi_{\mathrm{c}}^3 = b^3 N^{3\nu} \left(\frac{c}{c^*}\right)^{\frac{-3\nu}{3\nu-1}}, \tag{7.8}$$

where, we have used c/c^* in place of $\tilde{c}/\tilde{c^*}$ since they are identical ($c = \tilde{c} m_{\mathrm{k}}$, where m_{k} is the mass of a monomer).

The diffusivity of a correlation blob is given by

$$\mathcal{D}_{\mathrm{c}} = \frac{k_{\mathrm{B}}\, T}{\zeta_{\mathrm{c}}}, \tag{7.9}$$

where, ζ_{c} is the friction coefficient for the blob. Since the chain segment within a correlation blob obeys Zimm dynamics,

$$\zeta_{\mathrm{c}} \sim \eta_{\mathrm{s}}\, \xi_{\mathrm{c}}. \tag{7.10}$$

As a result ,

$$\mathcal{D}_{\mathrm{c}} = \frac{k_{\mathrm{B}}\, T}{\eta_{\mathrm{s}}\, \zeta_{\mathrm{c}}}. \tag{7.11}$$

The relaxation time for a single blob can be derived from the expression ,

$$\tau_c = \frac{\xi_c^2}{\mathcal{D}_c} = \frac{\xi_c^2}{k_B\, T/\eta_s\, \xi_c},$$

or,

$$\tau_c = \frac{\eta_s\, \xi_c^3}{k_B\, T}. \tag{7.12}$$

If we define ,

$$\tau_0 = \frac{\eta_s\, b^3}{k_B\, T}, \tag{7.13}$$

as the monomer relaxation time, it follows from Equation 7.8 that,

$$\tau_c = \tau_0 N^{3\nu} \left(\frac{c}{c^*}\right)^{\frac{-3\nu}{3\nu-1}}. \tag{7.14}$$

Since a single chain in a semidilute solution is equivalent to a Rouse chain of correlation blobs in a melt, it follows that the relaxation time of the chain as a whole, τ_{chain} is given by (Rubinstein and Colby, 2003)

$$\tau_{\text{chain}} = \tau_c N_c^2$$

or,

$$\tau_{\text{chain}} = \left(\frac{\eta_s\, \xi_c^3}{k_B\, T}\right) N_c^2. \tag{7.15}$$

These results will prove useful shortly.

Consider a system of chains with N monomers each, in the semidilute concentration regime, undergoing simple shear flow at a shear rate $\dot{\gamma}$ (see Figure 7.18). Under these conditions, it is envisaged that the chain breaks up into a series of 'Pincus' blobs (Pincus, 1976), where the blob size ξ_S sets the length scale at which the stretching energy of the chain segment within the Pincus blob is equal to $k_B\, T$.

Clearly, with the onset of flow, it is the chain of correlation blobs that breaks up into a sequence of Pincus blobs, and one can consider each Pincus blob to consist

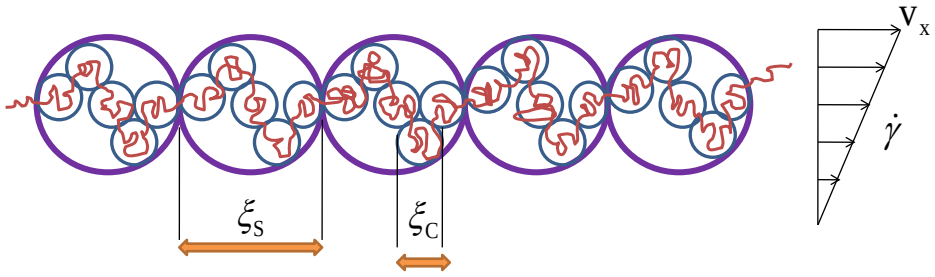

Figure 7.18: Illustration of a linear polymer chain in a semidilute solution as a series of correlation blobs, each of size ξ_c. In shear flow, this chain of smaller correlation blobs breaks up into a sequence of larger Pincus blobs, each with a size ξ_S. See text for explanation.

of m correlation blobs. As a result, random walk statistics dictate that,

$$\xi_S = \xi_c m^{1/2}. \tag{7.16}$$

One can obtain an estimate of m, and its dependence on the shear rate as follows. We know that the stretching energy of chain segment within a Pincus blob is of order $k_B\ T$. As a result,

$$f\xi_S = k_B\ T, \tag{7.17}$$

where, f is the stretching force on the chain. The stretching force arises due to the drag exerted by the flowing solvent on the segment within the Pincus blob. The drag force is equal to the velocity difference across a Pincus blob times the friction coefficient of a Pincus blob, ζ_S. The velocity difference is equal to $(\dot{\gamma}\xi_S)$ and $\zeta_S = m\zeta_c$, since the correlation blobs obey Rouse dynamics. As a result, from Equation 7.10,

$$f = (\dot{\gamma}\xi_S) m\eta_s\ \xi_c. \tag{7.18}$$

Substituting Equation 7.18 into Equation 7.17 leads to,

$$m\xi_S^2\eta_s\ \xi_c\dot{\gamma} = k_B\ T. \tag{7.19}$$

From Equation 7.16, it follows that,

$$m^2 \xi_S^3 \eta_s \, \dot{\gamma} = k_B \, T, \tag{7.20}$$

or

$$m = \left[\left(\frac{k_B \, T}{\eta_s \, \xi_c^3} \right) \frac{1}{\dot{\gamma}} \right]^{\frac{1}{2}}. \tag{7.21}$$

Using the result in Equation 7.12, we get,

$$m = (\tau_c \dot{\gamma})^{\frac{-1}{2}}. \tag{7.22}$$

The number of correlation blobs within a Pincus blob decrease with increasing shear rate, as might be expected, since the size of the Pincus blob decreases with increasing shear rate.

The recognition of the inverse shear rate dependence of the Pincus blob size is responsible for the development of a scaling model to explain shear thinning in polymer melts by Colby and coworkers (Colby et al., 2007). We adopt their arguments (with some important differences) to develop an expression for the shear rate dependence of η_p in semidilute solutions, and by this means, come up with the choice of an appropriate concentration dependent relaxation time.

According to Rouse theory, the shear viscosity in a polymer melt is given by the expression,

$$\eta = k_B \, T \left(\frac{\tilde{c}}{N} \right) \tau_{chain} \sum_{p=1}^{N} \frac{1}{p^2} \tag{7.23}$$

for $(\tau_{chain} \dot{\gamma}) < 1$, where, the sum is carried out over the N normal modes of the chain. It is appropriate to recall here that the 'p'th mode corresponds to a segment of the chain containing (N/p) monomers. Colby and coworkers (Colby et al., 2007) argue that in a shear flow, the chain breaks up into a series of Pincus blobs that are aligned in the flow direction, i.e., the chain forms a 'blob' pole, unlike in the case where the chain ends are separated by a stretching force (which was the original Pincus (1976) scenario), where the chain is a directed random walk of Pincus blobs. Since the stretching energy is less than $k_B \, T$ within the Pincus blob, the

conformation of the chain segment within the blob is unperturbed from its equilibrium configuration. According to Colby and coworkers, the Rouse expression for the viscosity (Equation 7.23) only applies to chain segments within the Pincus blob, since they are the ones contributing to viscous dissipation, while the segments on larger length scales are stretched and store energy elastically. Colby et al. (2007) derive an alternative expression for the viscosity by changing the lower bound of the summation in Equation 7.23 to the mode number corresponding to the length scale of the Pincus blob. They use (R_{eq}/ξ_S) as a measure of this mode number, and by using the shear rate dependence of ξ_S, they obtain a expression for the viscosity that depends on the shear rate.

In the case of semidilute solutions, Equation 7.23 takes the form (using Equation 7.3 for $\tilde{c}/N$),

$$\eta = k_B\, T \left(\frac{1}{N_c \xi_c^3}\right) \tau_{chain} \sum_{p=1}^{N_c} \frac{1}{p^2} \tag{7.24}$$

for $(\tau_{chain}\dot{\gamma}) < 1$ where, τ_{chain} is given by Equation 7.15. For $N_c \gg 1$, this implies,

$$\eta = \frac{k_B\, T}{N_c \xi_c^3} \frac{\eta_s\, \xi_c^3}{k_B\, T} N_c^2$$

or,

$$\frac{\eta}{\eta_s} N_c \sim \left(\frac{c}{c^*}\right)^{\frac{1}{3\nu-1}}, \tag{7.25}$$

in agreement with the expression derived by Jain et al. (2012a) for the zero shear rate viscosity of semidilute solutions.

For strong flows, as argued by Colby et al. (2007), $\tau_p\dot{\gamma} < 1$ only for the modes 'p' that lies within a Pincus blob. Rather than (R_{eq}/ξ_S) we suggest that it is more appropriate to use the number of Pincus blobs in a chain, X, as the lower bound of the sum in Equation 7.24, since the chain is divided in 'X' segments by the action of the flow. For low shear rates, $X \to 1$, since the entire chain is contained in a Pincus blob, while at high shear rates, $X \to N_c$. Note that,

$$X = \frac{N_c}{m}. \tag{7.26}$$

At high shear rates consequently, Equation 7.24 becomes,

$$\eta = k_B\, T \left(\frac{1}{N_c \xi_c^3}\right) \tau_{\text{chain}} \sum_{p=X}^{N_c} \frac{1}{p^2}. \tag{7.27}$$

Converting the sum to an integral, and carrying out the integral in the limit $N_c \gg 1$, we get,

$$\eta = \frac{k_B\, T}{N_c \xi_c^3} \cdot \frac{\eta_s\, \xi_c^3 N_c^2}{k_B\, T} \cdot \frac{1}{X} = \eta_s \cdot N_c \cdot \frac{m}{N_c}$$

or,

$$\frac{\eta}{\eta_s} = m. \tag{7.28}$$

From Equation 7.22, this implies that at high shear rates, for semidilute solutions,

$$\frac{\eta}{\eta_s} = \left[\tau_c \dot{\gamma}\right]^{\frac{-1}{2}}. \tag{7.29}$$

Using the expression for τ_c from Equation 7.14, we get,

$$\frac{\eta}{\eta_s} = \tau_0 N^{3\nu} \left(\frac{c}{c^*}\right)^{\frac{3\nu}{1-3\nu}}. \tag{7.30}$$

We have seen from our experimental observations that the shear thinning exponent is typically less than (1/2). Nevertheless, Equation 7.30 suggests that the dependence of the relaxation time on concentration should be $(c/c^*)^{3\nu/(1-3\nu)}$, rather than the $(c/c^*)^{(2-3\nu)/(3\nu-1)}$ dependence of λ_η.

The scaling analysis here suggests that data collapse may be achieved by using the relaxation time,

$$\lambda = \tau_0 N^{3\nu_{\text{eff}}} \left(\frac{c}{c^*}\right)^{\frac{3\nu_{\text{eff}}}{1-3\nu_{\text{eff}}}}, \tag{7.31}$$

where, ν_{eff} is used to account for differences in solvent quality. This hypothesis is tested in the results presented in the next subsection.

7.2.3 Universal shear thinning of semidilute solutions

The viscosity data discussed earlier, is reinterpreted in terms of the scaling variables suggested by the analysis of the previous subsection, and plotted in Figures 7.19,

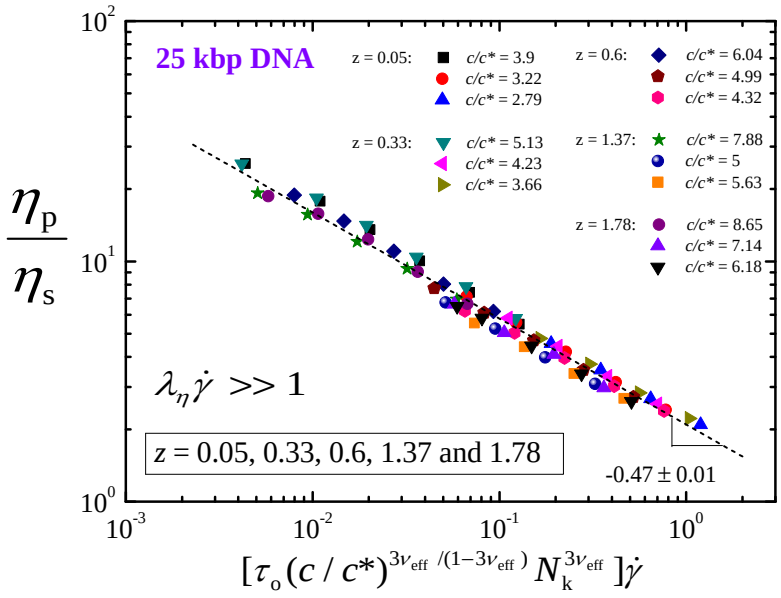

Figure 7.19: Concentration and z collapse for 25 kbp DNA at very high shear rates, when represented in terms of an Wi that depends on a relaxation time based on the Rouse theory, as shown in Equation 7.31. A terminal slope of -0.47 has been obtained by least-squares fitting of the data. The value of the ν_{eff} corresponding to the particular value of z has been used.

7.20 and 7.21 for 25 kbp, λ-DNA and T4 DNA, respectively. It is immediately apparent that in each case, for $\lambda_\eta\dot{\gamma} \gg 1$, the viscosity collapses on to master curves, independent of c/c^* and the solvent quality z. It should be noted that the value of ν_{eff} corresponding to the particular value of z has been used in these plots. The slope of the shear thinning region seems to vary with molecular weight, with the magnitude decreasing as the molecular weight increases. This can be seen more clearly in Figure 7.22, where representative data for all the three DNA molecular weights are plotted side by side. It is possible that the experimental data lies in a crossover region, and that the Weissenberg numbers at which the asymptotic shear thinning with exponent -0.5 is observed, have not been explored. This is in line with the simulation results of Huang et al. (2010) for semidilute solutions, and of Schroeder et al. (2005) and Jendrejack et al. (2002), for dilute solutions. In the latter case, Wi exceeding 10^4 were required to observe the predicted exponent of -2/3.

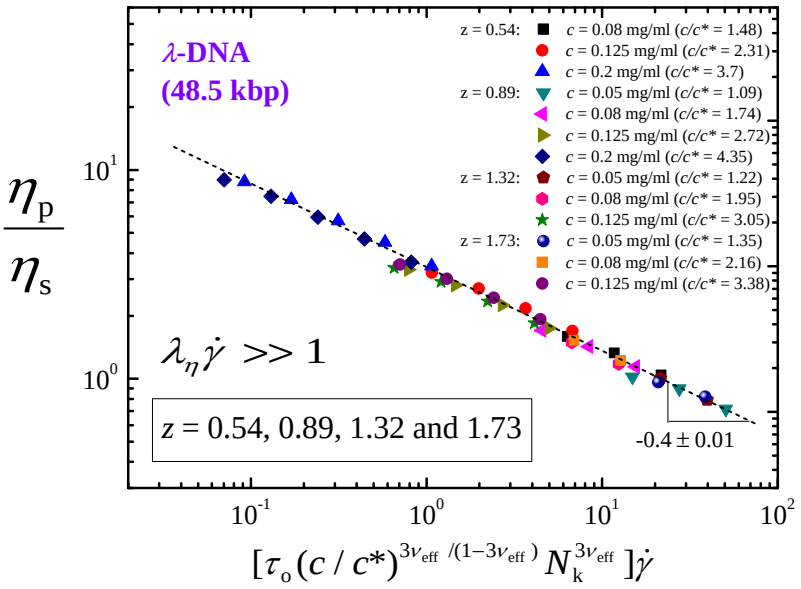

Figure 7.20: Concentration and z collapse for λ-DNA at very high shear rates, when represented in terms of an Wi that depends on a relaxation time based on the Rouse theory, as shown in Equation 7.31. A terminal slope of -0.4 has been obtained by least-squares fitting of the data. The value of the ν_{eff} corresponding to the particular value of z has been used.

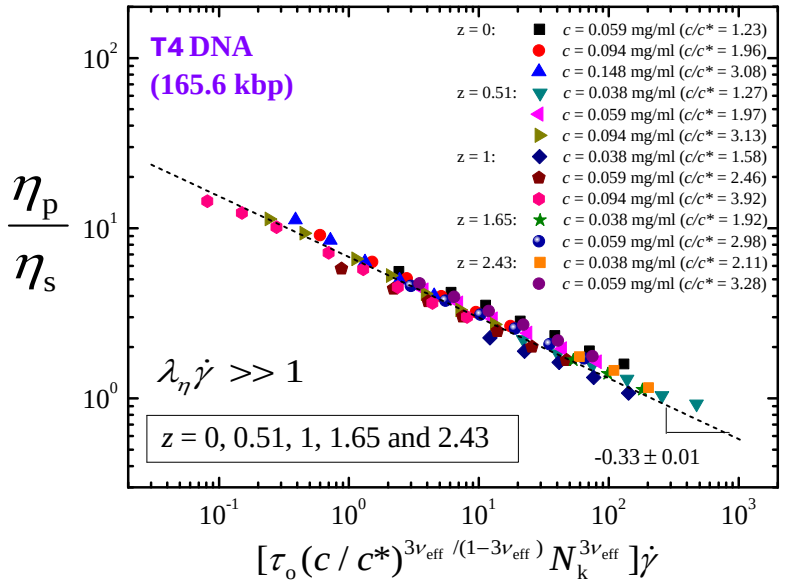

Figure 7.21: Concentration and z collapse for T4 DNA at very high shear rates, when represented in terms of an Wi that depends on a relaxation time based on the Rouse theory, as shown in Equation 7.31. A terminal slope of -0.33 has been obtained by least-squares fitting of the data. The value of the ν_{eff} corresponding to the particular value of z has been used.

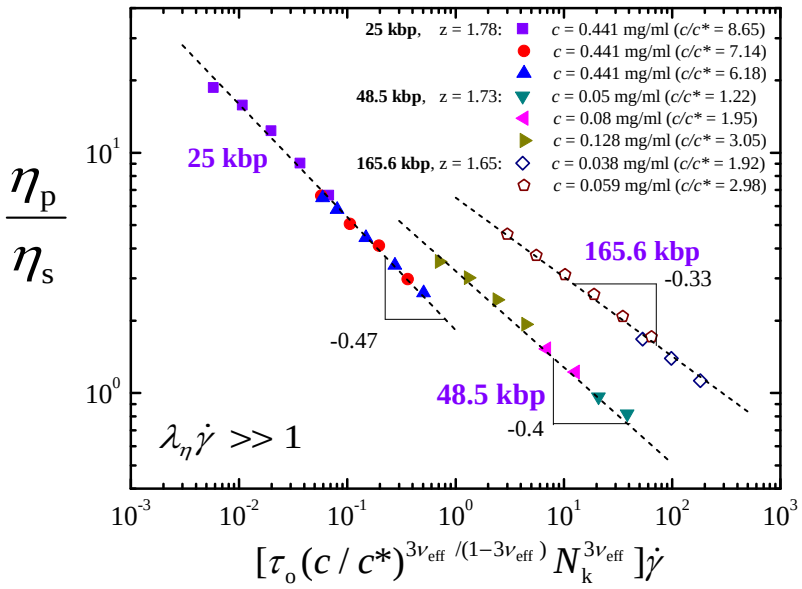

Figure 7.22: Representative data from Figures 7.19–7.21 for all three DNA molecular weights. The terminal slope at very high shear rates seems to decrease with increasing molecular weight.

An attempt to use the relaxation time given by Equation 7.31 to collapse the data for the two polystyrene solutions is shown in Figures 7.23 (a) and (b). Clearly, all the data is in the regime prior to the onset of significant shear thinning, and no conclusions can consequentially be drawn from the lack of data collapse, which is expected only in the power law regime. More data at higher shear rates is necessary to resolve this issue.

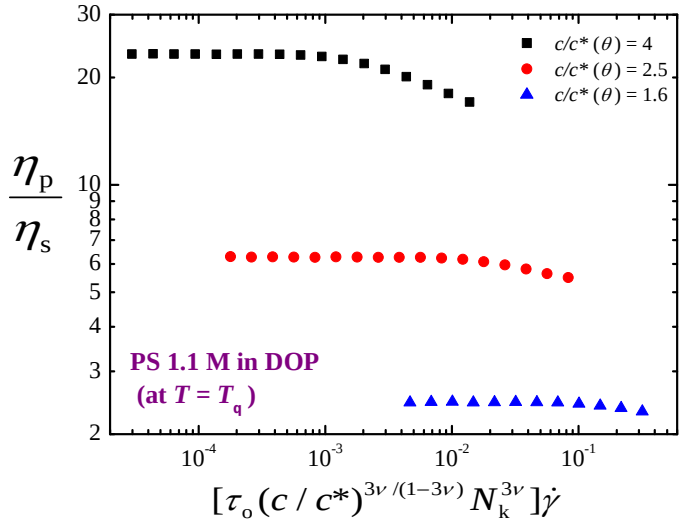

(a)

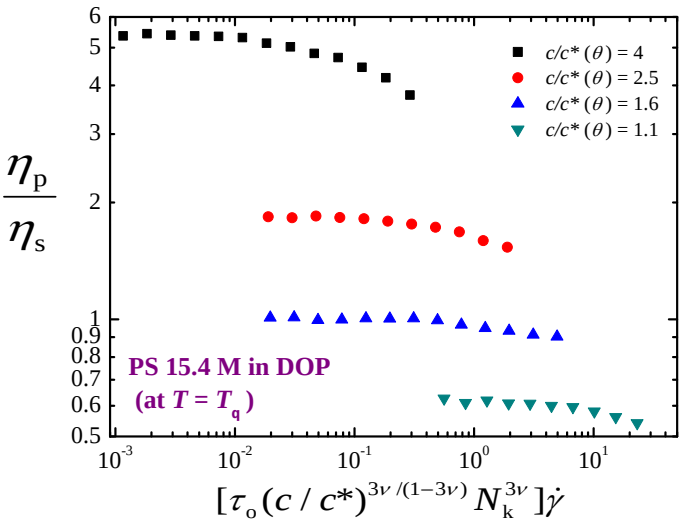

(b)

Figure 7.23: No concentration collapse for linear polystyrene in DOP at T_θ (22°C) for two different M: (a) 1.1 M and (b) 15.4 M, when represented in terms of an Wi that depends on a relaxation time based on the Rouse theory, as shown in Equation 7.31. A ν value of 0.5 has been used (for a θ-solvent) corresponding to the particular value of $z = 0$. In order to see a collapse, we probably need to go to still higher shear rates.

7.2.4 Dilute DNA solutions in shear flow

We have also accumulated data for the three DNA samples at concentrations corresponding to the dilute regime. In this case, it is well established that the appropriate Weissenberg number Wi to use is,

$$\mathrm{Wi} = \lambda_Z \dot{\gamma}$$

where λ_Z is a large scale relaxation time based on the intrinsic viscosity (same as $\lambda_{\eta,z}$), as defined in Equation 6.5. Data for $[\eta]$, for the various conditions considered here, has been tabulated previously in Chapter 5 for 25 kbp and T4 DNA (see Table 5.2). For λ-phage DNA, the intrinsic viscosity at T_θ was determined from the estimated zero shear rate viscosities from the measured viscosity data in dilute regime following the procedure discussed in Chapter 5. The $[\eta]$ values at all other temperatures have been calculated as: $\eta = [\eta]_\theta \alpha_\eta^3$. The values of α_η for λ-DNA at different temperatures (or z) have been obtained analytically using the same expression and fitting parameters as in Table 5.4.

Plots of the scaled viscosity $\eta_\mathrm{p}/\eta_{\mathrm{p}0}$ versus $\lambda_Z\ \dot{\gamma}$, for each of the three DNA samples (25, 48.5 and 165.6 kbp) at a range of solvent qualities and c/c^* in the dilute regime are displayed in Figures 7.24, 7.25 and 7.26, respectively. Both a time-temperature superposition, and a collapse of data across concentrations is observed in all three cases.

When all the three sets of data (25 kbp, λ-phage and T4 DNA) are plotted together in Figure 7.27, we observe that the onset of shear thinning does not occur at the same Wi, and that the slope in the power law regime is different in the three cases. Both these points have been noted previously by Hua and Wu (2006) in their experiments on dilute polystyrene solutions.

Hua and Wu (2006) observed that the value of $\dot{\gamma}$ at which shear thinning was initiated scaled as $M^{1.7\pm0.09}$, while $\lambda_Z \sim M^{1.52\pm0.02}$. This suggests that the onset of shear thinning is related to finite-extensibility effects, and that the relaxation time for capturing shear thinning is more Rouse like at high shear rates, where non-

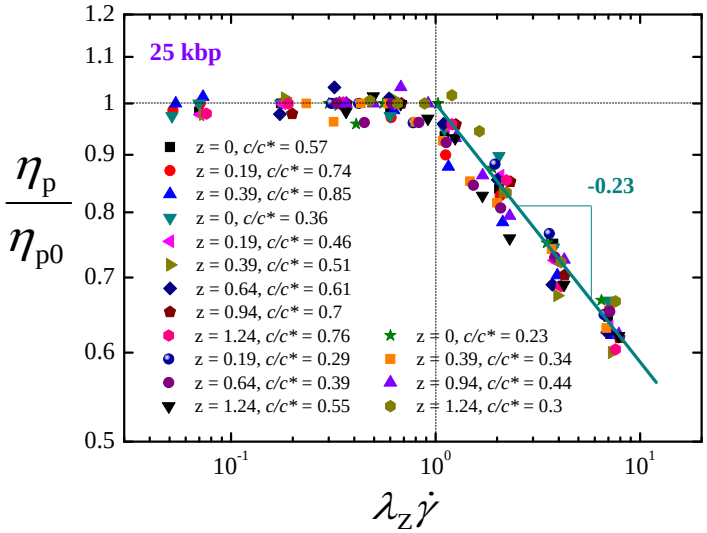

Figure 7.24: Shear dependence of normalized polymer contribution to viscosity for dilute 25 kbp DNA solutions. When represented in terms of an Wi based on a concentration independent relaxation time (λ_Z), data for different concentrations (or c/c^*) and temperatures (or z) can be collapsed for a particular molecular weight in the dilute regime. The z and corresponding c/c^* values have been bracketed against each symbol. The terminal slope was obtained to be -0.23, by a least-squares fitting of the data at very high shear rates.

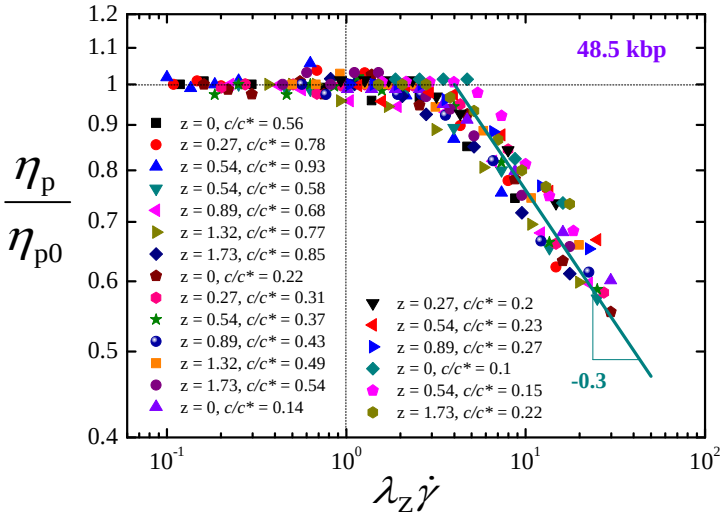

Figure 7.25: Shear dependence of normalized polymer contribution to viscosity for dilute λ-DNA solutions. The z and corresponding c/c^* values have been bracketed against each symbol. The terminal slope was obtained to be -0.3, by a least-squares fitting of the data at very high shear rates.

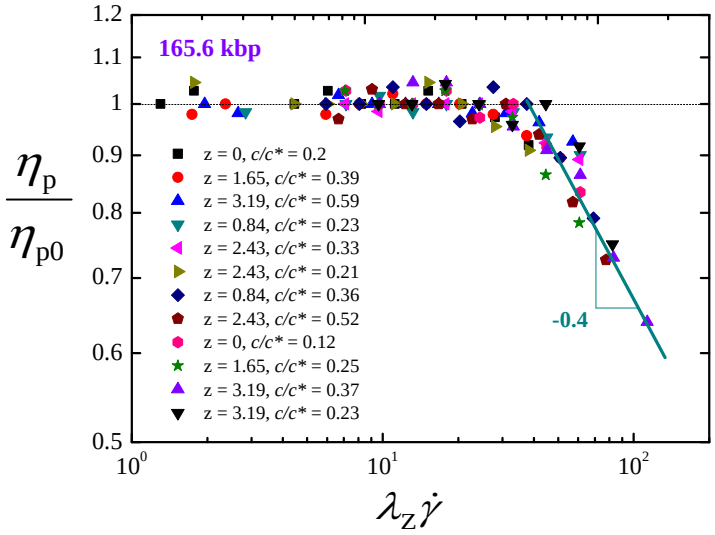

Figure 7.26: Shear dependence of normalized polymer contribution to viscosity for dilute T4 DNA solutions. The z and corresponding c/c^* values have been bracketed against each symbol. The terminal slope was obtained to be -0.4, by a least-squares fitting of the data at very high shear rates.

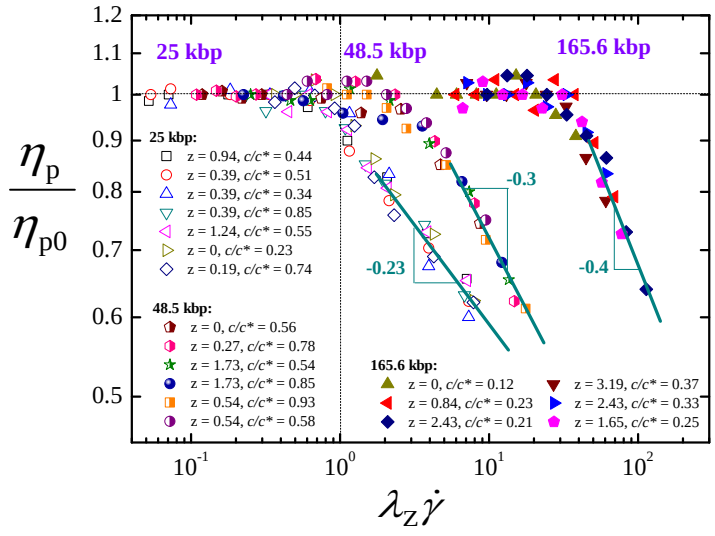

Figure 7.27: Representative data from Figures 7.24–7.26 for dilute DNA solutions in shear flow. The data for 25, λ and T4 DNA are represented by open, half-filled and filled symbols, respectively. The terminal slope at very high shear rates seems to increase with increasing molecular weight. The onset of shear thinning shows a molecular weight dependence.

linear effects such as HI and EV interactions are weak due to chain extension.

The values of the shear thinning exponent that are observed suggest that the data is probably in the crossover region, and much higher shear rates would be required before the asymptotic shear thinning exponent is attained.

7.3 Conclusions

Experimental results on semidilute unentangled DNA solutions far from equilibrium are reported across a range of molecular weights, temperatures and concentrations. Away from equilibrium, in shear flow, the shear behaviour of unentangled DNA molecules in the semidilute regime can be understood in terms of characteristic concentration dependent Weissenberg number Wi. The shear data at different absolute concentrations do not collapse by using either the longest relaxation time (λ_1) or the zero shear rate viscosity dependent relaxation time (λ_η) dependent Wi, though a temperature collapse is observed for all the molecular weights used in the current work. By using an alternative scaling based on Rouse theory and deriving a suitable concentration dependence, the collapse for different absolute concentrations could be achieved at very high shear rates. Also, a master plot with collapse of all the molecular weights at different temperatures (or z) and concentrations (c/c^*) can be achieved by representing the data through this alternate concentration based Wi.

The focus of the current work to characterize semidilute polymer solutions was extended to investigate dilute DNA solutions as well. The dynamics of dilute DNA solutions in shear flow could be well captured based on an Wi that depends on an intrinsic viscosity based relaxation time. Represented this way, we get a collapse of different concentrations and temperatures irrespective of the molecular weight. Also, the shear behaviour of dilute DNA solutions is in agreement with that of dilute polystyrene solutions, as observed by Hua and Wu (2006).

The results obtained in the current work validates the anticipation that in addition to the flow-induced variable Wi, two other scaling variables, the excluded volume parameter z, and the scaled concentration c/c^*, are equally important in

order to aptly characterize the concentration and temperature dependent dynamics of the nonlinear viscoelastic properties of semidilute and dilute polymer solutions. The current work provides benchmark experiential data that can be used for the validation of theoretical studies and predictions.

8

Extensional Flow of Semidilute DNA Solutions

8.1 Introduction

The rheological behaviour of polymer melts and dilute polymer solutions in elongational flow have been extensively examined through experiments, simulation studies and theoretical predictions. This is primarily because we can focus on the single chain dynamics and consequently have a reasonable understanding of the polymer solution behaviour in both these regimes. However, an elaborate experimental study to understand the extensional rheological properties of polymer solutions in the semidilute regime is currently lacking in terms of a systematic examination of the effects of concentration and molecular weight. The semidilute regime of polymer solutions is important because it involves multi-particle effects and many-body interactions, leading to complex behavior requiring systematic rheological characterization. In Chapter 6, we have shown experimentally that a rational theoretical understanding of both static and dynamic properties of polymer chains in a semidilute unentangled solution close to equilibrium can be obtained from scaling theories based on correlation blobs. Our experiments on semidilute solutions

have revealed that a clear understanding of the concentration and temperature dependent dynamics of the nonlinear viscoelastic properties of semidilute and dilute polymer solutions in shear flow can be achieved in terms of Weissenberg number Wi, scaled concentration c/c^*, and the solvent quality parameter z, as shown in Chapter 7. It is anticipated that these effects will be even more pronounced in extensional flows, which play a critical role in a number of industrial contexts, and therefore it is important to study the extensional rheological behaviour of semidilute polymer solutions.

Till date, significant progress has been achieved to measure and analyze the elongational or extensional deformation of polymer solutions (Tirtaatmadja and Sridhar, 1993; Gupta et al., 2000; Bhattacharjee et al., 2003; Sunthar et al., 2005). Several significant industrial processes like fiber spinning, ink-jet printing, extrusion of polymeric materials and applications like coatings, turbulent drag reduction and lubrication highlight the predominant involvement of the extensional mode of deformation (McKinley and Sridhar, 2002). Also, unlike shear flows, which are weak and encounter problems related to vorticity; extensional flows are irrotational and highly proficient at unravelling and orienting flexible macromolecules (McKinley and Sridhar, 2002). Considerable advancement has been made in extensional viscosity measurements for both dilute polymer solutions (Gupta et al., 2000; Sunthar et al., 2005) and polymer melts (McKinley and Hassager, 1999; Bach et al., 2003). Effective uniaxial elongational viscosities of dilute DNA solutions have been determined in cross-slot cells (Smith and Chu, 1998; Schroeder et al., 2004) and the conformational behavior of DNA molecules have been theoretically predicted (Hsieh et al., 2003; Sunthar et al., 2005; Shaqfeh, 2005). It is not easy to measure the true elongational viscosity of a polymer solution and for this; a filament stretching rheometer (FSR) is the best solution (McKinley and Sridhar, 2002). An extensive review of the filament stretching rheometry has been given by McKinley and Sridhar (2002). In our group, FSR has been rigorously used so far to characterize dilute polystyrene solutions at various concentrations and molecular weights (Gupta et al., 2000) and to quantify the elongational stress of dilute solutions of stained

DNA (Sunthar et al., 2005). It is worth noting that very scarce experimental observations have been reported from extensional flow studies on semidilute polymer solutions (Juarez and Arratia, 2011).

In addition to experiments, theoretical predictions of the extensional behaviour of polymer solutions in both dilute and entangled regimes has also been carried out (Yao and McKinley, 1998; Rasmussen and Hassager, 1999; Larson et al., 1999). Of late, Brownian Dynamics simulations have been carried out for DNA and polystyrene systems in extensional flow that are in agreement with experimental observations (Jendrejack et al., 2002; Sunthar et al., 2005; Shaqfeh, 2005). A procedure termed successive fine graining (SFG) has recently been introduced (Prabhakar et al., 2004; Sunthar et al., 2005) by our group by which it is possible to carry out parameter-free predictions. An attempt to predict the extensional flow properties in terms of solvent quality has also been made (Sunthar et al., 2005). Recently Stoltz et al. (2006) have predicted the behaviour of dilute and semidilute solutions of λ-DNA in planar extensional flow. However, this has not been validated by experiments. So, a systematic experimental characterization of semidilute polymer solutions in extensional flow in terms of concentrations and molecular weights is still lacking.

In this work, we have investigated the extensional rheology of linear DNA molecules in a wide range of molecular weights (25 to 289 kbp) and concentrations. The reasons for using DNA as our investigating polymer system has been explained in Chapter 1. The objectives of the current work are two-fold: first, we want to generate a set of benchmark data for semidilute DNA solutions across a range of molecular weights and concentrations in elongational flow and second, we want to find out that if the concentration dependence for the extensional viscosities in the semidilute regime can be interpreted according to some generic principles for the demonstration of universal behaviour, which will help in developing predictive models.

In this chapter, the shear characteristics and the extensional properties are discussed in Section 8.3. In Section 8.4, we summarize the principal conclusions of the present work.

8.2 Methodology

8.2.1 Preparation of DNA solutions

Four linear double stranded DNA samples were used in the current work: 25 kbp DNA, λ-phage DNA, T4 DNA and 289 kbp DNA. Details regarding the procurement of the λ and T4 DNA and procurement, synthesis and purification of the 25 and 289 kbp DNA are mentioned in Section 2.1.

For all the extensional viscosity measurements, the final DNA solutions for 25 kbp and 289 kbp were prepared by adding desired volumes of a viscous solvent (see Table 2.3), which is predominantly sucrose; and evaporating the excess water out, to ensure efficient dissolving of the DNA in this solvent. The same solvent and procedure was used for preparing final solutions for λ-DNA and T4-DNA too, by dissolving the DNA pellet after precipitation and for preparing subsequent dilutions.

For T4 and λ-DNA, company specified values of concentrations were used as maximum concentrations (see Section 2.1). For 25 kbp and 289 kbp linear DNA, the maximum concentrations were determined to be 0.272 mg/ml and 0.012 mg/ml, respectively.

8.2.2 Shear rheometry

As a part of the study, steady state shear viscosities for all the DNA samples were also measured in the viscous solvent at different temperatures (15 to 30°C) and concentrations (0.012 to 0.3 mg/ml). Details about the rheometer used, measuring principle, temperature sensitivity, shear rheometry procedure, precautions taken while measurements, instrument calibration, shear rate range employed and avoidance of shear ramp, sample equilibration time, dependence on rheometer geometry etc., are mentioned in Section 2.4. At each shear rate, a delay of 5 to 15 minutes was employed so that the DNA chains get ample time to relax to their equilibrium state. The shear rate dependence of the measured steady state shear viscosity η of the solutions are shown in Figure 8.1.

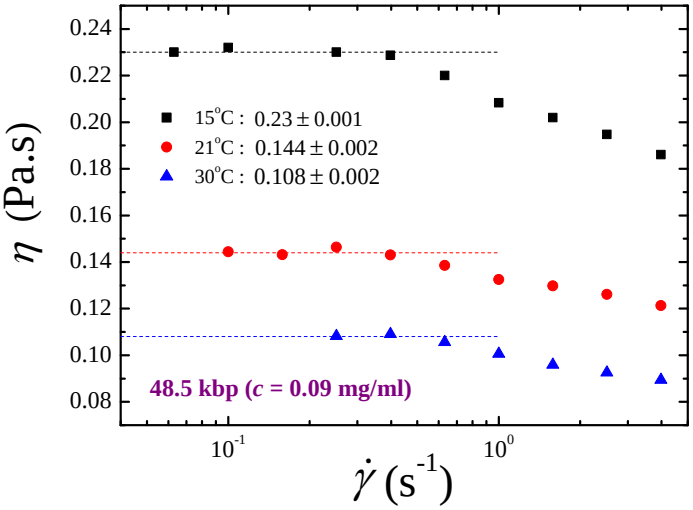

(a)

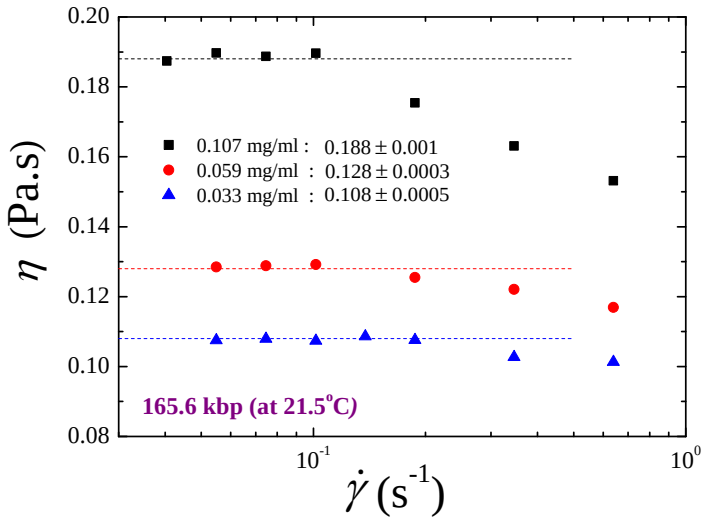

(b)

Figure 8.1: Determination of the zero shear rate solution viscosity η_0. The shear rate dependence of solution viscosity η in the region of low shear rate is extrapolated to zero shear rate (a) for λ-DNA at a fixed concentration, for a range of temperatures and (b) for T4 DNA at a fixed temperature, for a range of concentrations. The extrapolated values in the limit of zero shear rate are indicated in the legends.

8.2.3 Extensional rheometry

The extensional rheometry procedure using a filament stretching rheometer has been discussed in Section 2.5. The steady state uniaxial extensional viscosities for all the DNA samples along with the concentrations are listed in Table 8.1.

8.3 Results and Discussion

8.3.1 Shear characterization

The shear viscosities were measured at different finite shear rates at different temperatures and the estimated zero shear rate viscosities η_0, for all the DNA solutions in the viscous solvent, determined using the same procedure as discussed in Section 5.2, are listed in Table 8.1. The experimental data covers a high range of molecular weights (1.6×10^7 to 1.9×10^8 g/mol) and concentrations (see above section), which is ideal for investigating scaling laws. As predicted by the blob model, the polymer contribution to the zero shear rate viscosity, η_{p0} is highly dependent on polymer concentration c in the semidilute unentangled regime and grows as a power law with c (Rubinstein and Colby, 2003). The concentration range of DNA samples used in this work is characterized in terms of overlap concentration, c^*. The c^* values have been calculated based on analytical R_g^θ values from Table 2.1 in Chapter 2 using Equation 1.8. Close to equilibrium, the absolute concentration dependence of the specific viscosity for different molecular weights at room temperature is shown in Figure 8.2 (a). The substantial difference observed in the concentration dependence for the different molecular weights disappears when the data is reinterpreted in terms of the non-dimensional ratio (c/c^*), and we see a master plot, as shown in Figure 8.2 (b). The determination of these shear parameters will help us in evaluating the response of these DNA solutions to a uniaxial extensional flow field.

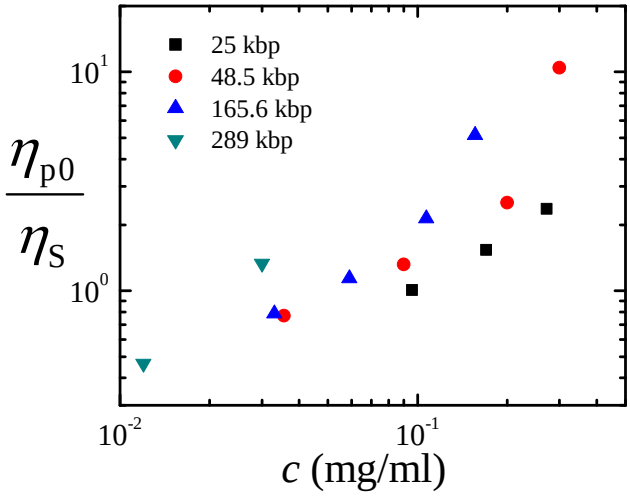

(a)

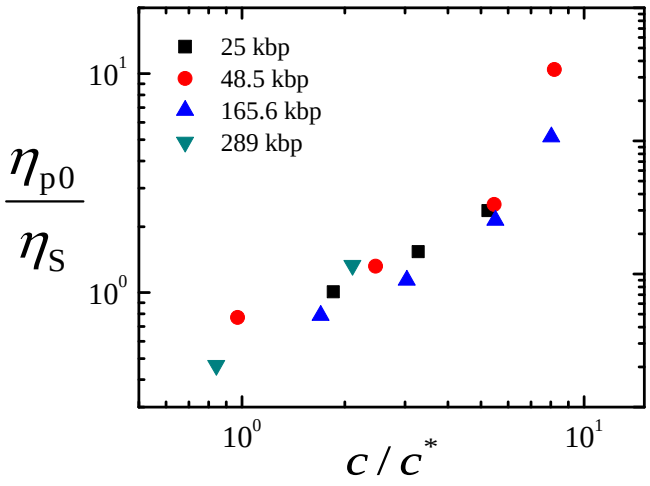

(b)

Figure 8.2: (a) Molecular weight dependence of the specific viscosity η_{sp} (defined in Equation 5.3) when plotted as a function of absolute concentration c. (b) Molecular weight dependence disappears when η_{sp} is plotted as a function of the normalized concentration, c/c^*.

Table 8.1: Steady state zero shear viscosities (η_0), uniaxial extensional viscosities (η_E) , Trouton ratio (Tr) and Weissenberg number (Wi) for all the DNA samples used in this work along with concentrations. All measurements were done at 21 $\pm$ 0.5°C. The c^* values are calculated based on analytical R_g^θ values from Table 2.1 using Equation 1.8. The Trouton ratios Tr are calculated using Equation 8.2. The solvent viscosity η_s at 21°C was measured to be 61$\pm$0.4 mPa.s. An indicative range of Weissenberg numbers (between Wi_{min} and Wi_{max}) is shown for various strain rates used. Here, Wi $= \lambda_\eta\ \dot{\varepsilon}$, where λ_η have been estimated from $\eta_{p0} = \eta_0 - \eta_s$ values in this solvent using Equation 1.9.

Size (kbp)	c (mg/ml)	c^* (mg/ml)	c/c^*	η_0 (Pa.s)	η_E (Pa.s)	Tr	Wi_{min}	Wi_{max}
25	0.096	0.123	0.78	0.1215	54.2	446.4	148	247
	0.17		1.38	0.1535	106.3	692.6	65	180
	0.272		2.21	0.2035	143.1	698.2	37	169
48.5	0.09		1.01	0.144	55.2	393.3	292	629
	0.2		2.25	0.2132	128.8	604.2	246	392
	0.3		3.37	0.6933	508.9	734.1	75	1090
165.6	0.033	0.048	0.69	0.111	56.4	508.3	1280	3850
	0.059		1.23	0.133	114.2	858.6	422	1880
	0.107		2.23	0.195	218.7	1121.4	414	1620
	0.156		3.25	0.382	709.2	1856.5	332	1500
289	0.012	0.036	0.33	0.091	20.2	221.7	12200	14200
	0.03		0.83	0.2334	86.2	369.3	2570	7850

8.3.2 Extensional properties

It is now well-established that a reasonable understanding of polymer solution behavior in uniaxial extensional flow can be obtained by analyzing the data in terms of dimensionless parameters (Gupta et al., 2000). We have analyzed the results of the current study in terms of strain and Trouton ratio as the governing dimensionless parameters. Strain (ε) is expressed as a product of the strain-rate ($\dot{\varepsilon}$) and time (t), and the transient Trouton ratio Tr, is defined as the ratio of the extensional stress growth coefficient to the steady zero shear rate viscosity

$$Tr^+ = \frac{\eta_E^+(\dot{\varepsilon}, t)}{\eta_0}. \tag{8.1}$$

and the steady state ($t \to \infty$) Trouton ratio is given by the corresponding steady state extensional viscosity η_E:

$$Tr = \frac{\eta_E}{\eta_0}. \tag{8.2}$$

The Trouton ratios for all the DNA samples along with the concentrations are listed in Table 8.1. In the current work, a procedure is implemented by which a pre-determined strain-rate can be imposed on the fluid, based on a 'master-plot', as suggested and shown earlier by our group (for an elaborate discussion, see the text by Gupta et al. (2000)). Briefly, for each fluid, there is an exclusive relationship between the filament length (L) and the mid-filament diameter (D) and can be expressed as:

$$\frac{L}{L_0} = f\left(\frac{D}{D_0}\right), \tag{8.3}$$

Here L_0 and D_0 are the initial values of the length and diameter, respectively. It has been shown that for any desired record of strain-rate and the equivalent diameter-time profile, the length-time profile can be obtained using Equation 8.3. The use of these master plots compensate for the non-ideality in the extensional flow due to end effects and makes data analysis considerably simpler (Gupta et al., 2000). Figure 8.3 (a) shows the results of using such a technique and the same is used extensively in the current work. Figure 8.3 (b) shows the time dependence of the transient Tr^+ at different strain rates. Figure 8.3 (c) shows the extensional stress growth data in terms of transient Tr^+, indicating the attaining of steady states at high strains as shown in Figure 8.4.

This strain-hardening and deviation from linear-viscoelastic behavior for the semidilute DNA solutions are observed for all the DNA molecular weights when subjected to uniaxial extensional deformations. The existence of a unique steady state independent of strain rate (see Figure 8.4) also suggests that all the DNA molecules at all the molecular weights are in a state of near full extension and the average conformations of the linear DNA molecules do not change with time. This assumes that there are no other impediments to extension such as knots. The absolute concentration dependence of steady state uniaxial extensional viscosities η_{E}, for semidilute DNA solutions at various concentrations, are shown in Figure 8.5. To our knowledge, this is the first time that steady state uniaxial extensional viscosities have been reported for semidilute DNA solutions. Figure 8.5 suggests that η_{E} is dependent on molecular weight, and has a power law dependence on c.

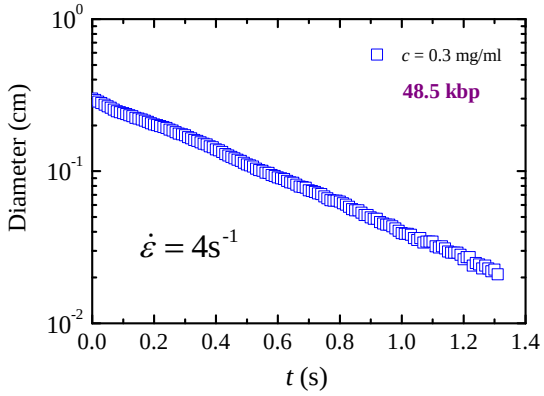

(a)

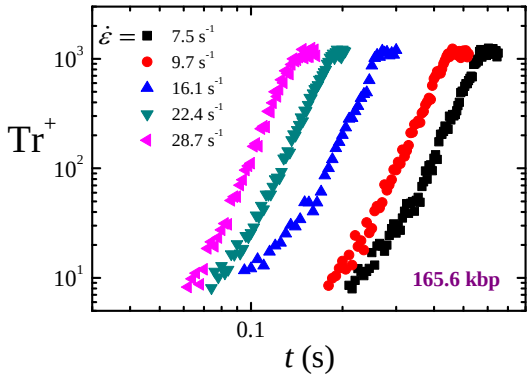

(b)

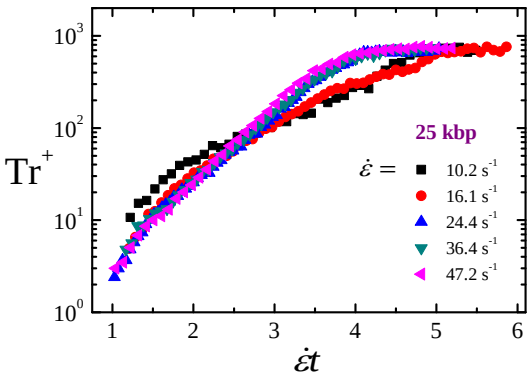

(c)

Figure 8.3: (a) Diameter profile obtained using the master plot for a strain rate of 4 s^{-1} for linear λ-DNA (absolute concentration indicated in the legend)(b) Dimensionless transient Trouton ratio Tr^+ for a semidilute solution of linear T4 DNA at different strain rates (at c = 0.107 mg/ml). The strain rates are indicated in the legend. (c) Asymptotic nature of the experimental normalized elongational stress growth coefficient for a semidilute solution of linear 25 kbp DNA as a function of strain (at c = 0.272 mg/ml). The strain rates are indicated in the legend.

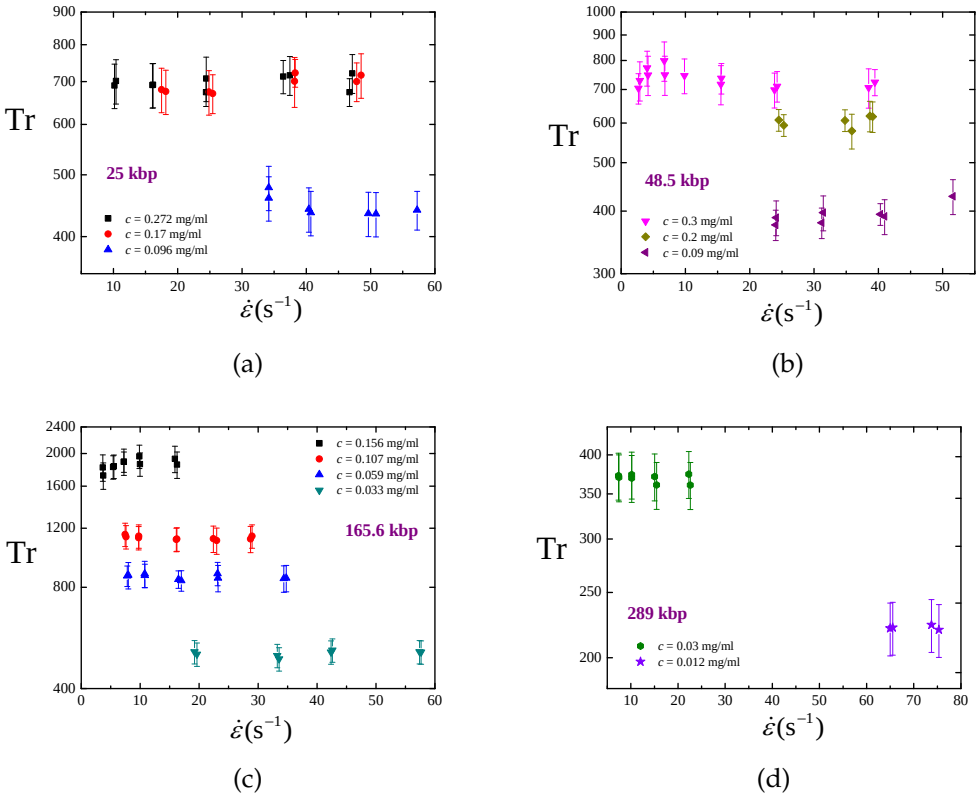

Figure 8.4: Tr as a function of strain rate for different concentrations at 21.5°C for (a) 25 kbp (b) λ-DNA (c) T4 DNA and (d) 289 kbp DNA. The absolute concentrations are indicated in the legends and the percentage errors calculated for each strain rate from the steady state time averaged Tr are indicated on the data.

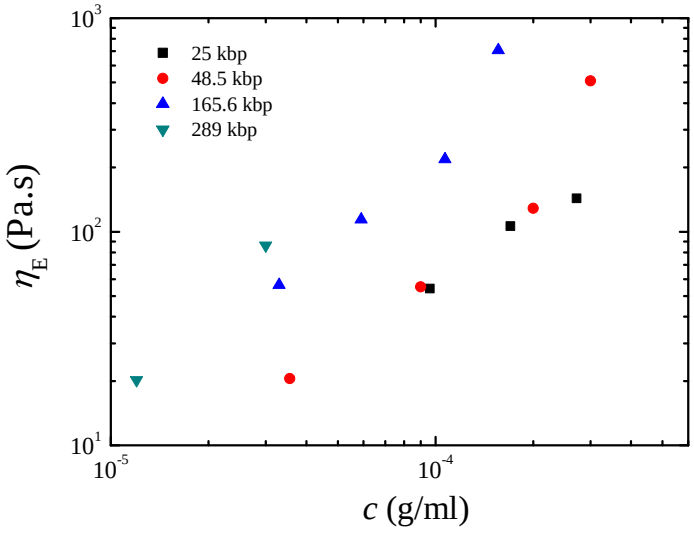

Figure 8.5: Steady state uniaxial extensional viscosity η_E as a function of absolute concentration c for DNA of different molecular weights.

We now attempt to collapse the data shown in Figure 8.5, by choosing appropriate scaling variables. We first note that in a suspension of polymers, which is semidilute at equilibrium, the parameter c/c^* is no longer the relevant scaling variable for the steady state elongational viscosity when it is subjected to strong elongational flows (Wi $\gg 1$). This is because all the polymers are very likely stretched out to a length of the order of the contour length L_0, as seen from the high viscosity in Figure 8.5, and its independence on Wi in Figure 8.4. The parameter c^* reflects more of the coiled state properties through its dependence on the equilibrium gyration radius as $\sim R_g^{-3}$ which is no longer a relevant variable at the fully stretched state (c/c^* may however be an important parameter in the transient Trouton ratio as the coils stretch out, as observed in the BD simulations of Stoltz et al. (2006). Even in these simulations, no explicit dependence on various molecular weights was studied).

Batchelor (1971) has derived an expression for the elongational viscosity for a suspension of non-dilute slender rods. Assuming the stretched out polymers to be slender rods, we can attempt to collapse the data based on this theory. Batchelor (1971) provides expressions for the elongational viscosity in the dilute as well as the concentrated limit. There is also a simple interpolation formula for the intermediate regimes.

For a given number density of the polymer n, each of stretched length L_0, and a cross-sectional radius R_0, the volume fraction is given by

$$\phi = \pi R_0^2 L_0 n.$$

For DNA, the diameter is taken to be $R_0 = 1$ nm, and the contour length of a base pair is taken as $l_0 = 0.34$ nm (Berg et al., 2002). In the non-dilute regime, from Equation 5.2 of Batchelor (1971), a dimensionless elongational viscosity is given by

$$\frac{\eta_E}{3\eta_s}\epsilon^2 = \frac{1}{9}\frac{\phi}{\log \pi/\phi}. \tag{8.4}$$

Here, $\epsilon = R_0/L_0$. This formula is applicable for $\sqrt{\phi} \ll 1$ and $\sqrt{\phi}/\epsilon \gg 1$. For the

DNA molecular weights and concentrations employed in the current work, both these limits are satisfied, suggesting the suspensions are not dilute. From the above argument, a plot of LHS of Equation (8.4) against ϕ should collapse all the data for rods of various lengths and number densities (concentrations), and therefore we may expect a similar behaviour for the non-dilute suspension of DNA.

The attempted collapse by Batchelor's theory is shown in Figure 8.6, where we compare our experimental data for four different molecular weights with the predicted values from Batchelor (1971). The figure shows that apart from λ-DNA (48.5 kbp), which is in close agreement with the theoretical prediction, all the other DNA are widely separated from the expected behaviour of rods. All the data however seem to have the same slope with varied shift factors. We considered for possible errors in the estimation of the ratio $\epsilon = R_0/L_0$—assuming that the DNA molecule could be effectively of a larger diameter owing to counter-ion condensation. But an increase in R_0 to up to 4 nm only marginally shifted the data, because of a weak dependence going as $\sim 1/\log R_0$. More experiments and analysis need to be carried out with DNA and other polymer-solvent systems to investigate data collapse further.

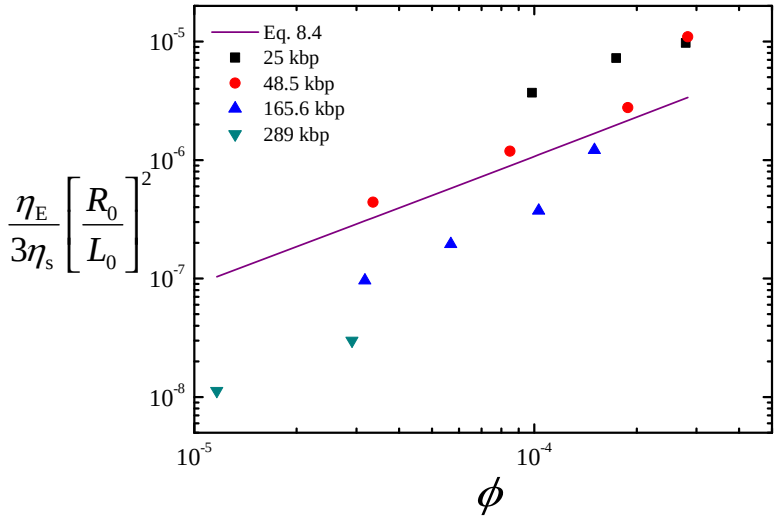

Figure 8.6: Dimensionless extensional viscosity as a function of the volume fraction ϕ. The solid line from Equation (8.4) based on the theory of non-dilute rods given in Batchelor (1971).

8.4 Conclusions

In this work, semidilute unentangled DNA solutions of four different molecular weights were investigated by subjecting them to uniaxial extensional flows for a wide range of concentrations at room temperature, using a filament stretching rheometer in a solvent which is predominantly sucrose. To our knowledge, this is the first time that steady state uniaxial extensional viscosities have been reported for semidilute DNA solutions. The experimental results were compared with the theoretical predictions by Batchelor (1971) for non-dilute suspension of slender rods. While the data showed the expected scaling with the volume fraction of DNA ϕ, the data for various molecular weights and concentrations could not be collapsed as per the slender rod theory. More experimental and numerical investigations are required to confirm this.

9

Conclusions and Future Work

9.1 Equilibrium Characterization

We have found several evidences that support the claim that double stranded DNA (ds-DNA), in the presence of excess salt, can be used as a model neutral polymer. They are:

1. The existence of a θ-temperature and the scaling of the hydrodynamic radius with molecular weight, in Sections 3.4 and 4.3.

2. The scaling of the second virial coefficient, which is static property at equilibrium, in Section 3.4.

3. The solvent quality scaling of the swelling of the hydrodynamic radius α_{H}, in Section 4.3.

4. The solvent quality scaling of the swelling of the viscosity radius α_{η}, in Section 5.3.

5. The scaling of the viscosity with concentration in semidilute solutions, in Section 6.3.

Thus it can be concluded that ds-DNA can be used as a model polymer for rheological studies. In the process of establishing the above scalings, we have determined:

1. The θ-temperature of DNA in Tris-EDTA buffer to be $T_\theta = 14.7 \pm 0.5°\text{C}$.

2. The chemistry dependent constant k in Equation (1.1) to be $k = 0.0047 \pm 0.0003$ $\text{g/mol}^{-1/2}$.

The solvent quality z for any DNA molecular weight at any temperature is therefore known for the Tris-EDTA buffer solution, and can be used to estimate other equilibrium static and dynamic properties (using the universal scaling functions) both in the dilute and semidilute unentangled concentration regimes.

9.2 Non-equilibrium characterization

1. In shear flow, the shear rate dependence of the semidilute viscosity data at different temperatures collapses onto master curves when interpreted in terms of a concentration dependent Weissenberg number Wi (based on zero shear rate viscosity dependent relaxation time, λ_η). Notably, the concentration data collapse only occurs when Wi is defined based on the relaxation time of a 'concentration blob' (see Section 7.2), and not λ_η. For dilute DNA solutions, both temperature and concentration data collapses when Wi is based on a large scale relaxation time from the intrinsic viscosity (see Section 7.2).

2. In extensional flow, it is found that the steady state uniaxial extensional viscosity of semidilute polymer solutions, in the limit of high extensional rates broadly scales with the volume fraction of the polymers as expected from the theory of Batchelor (1971), however only one of the experimental data closely matches with the exact prediction (see Section 8.3).

9.3 Future scope

Some directions in which the current work can be taken further are listed below.

1. The experimental results reported here will provide benchmark data for validations of theoretical predictions of polymeric behavior in general and DNA behavior in particular. It will lead to a better understanding of polymeric behaviour in the semidilute unentangled regime which has significant industrial applications including extensive polymer processing.

2. One important static equilibrium property we could not establish in this work is the temperature crossover of the gyration radius, R_g. It is important to confirm the scaling agrees with that of the neutral polymers using the same z obtained from the dynamic light scattering measurements of R_H.

3. Visualization studies with stained DNA (with YOYO1 dye) can be designed in a fluorescence microscopy to investigate the diffusivity of unentangled DNA molecules in the semidilute regime. It will be interesting to find out whether the concentration dependence of the diffusivity of unentangled DNA molecules in semidilute solutions, across a range of molecular weights, obey the power law scaling predicted by blob theory at the θ-temperature. Also, in the crossover region between the θ-temperature and very good solvents, whether this concentration dependence also obeys universal scaling behaviour which can be described by the blob scaling law and in terms of solvent quality, just as has been shown in the current work with zero shear rate viscosity.

4. The insights gained by identifying ds-DNA (in excess salt) as a neutral polymer and characterising its solvent quality, can be used to design microdevices for flow manipulation of DNA. This may lead to significant possibilities for Biotechnological applications. It is anticipated that in the future, flow induced nucleic acid analysis will provide an economical and faster alternative to other methods, and serve as a viable technique for diagnostic bio-medical devices.

A

Thermal Blobs and Measurements in Poor Solvents

A.1 Size of a thermal blob and polymer, and the excluded volume parameter

The focus of the experimental measurements in the dilute limit reported in Sections 2.2 and 2.3 is twofold: (i) determining the θ-temperature, and (ii) describing the θ to good solvent crossover behaviour of a solution of double-stranded DNA. The analysis of properties under poor solvent conditions has been carried out essentially only in order to locate the θ-temperature. As is well known, the experimental observation of single chains in poor solvents is extremely difficult because of the problem of aggregation due to interchain attraction. Nevertheless, in this section we show that a careful analysis of the dynamic light scattering data, in the light of the blob picture, enables us to discuss the reliability of the measurements that have been carried out here under poor solvent conditions.

According to the blob picture of dilute polymer solutions, a polymer chain in a good or poor solvent can be considered to be a sequence of thermal blobs, where the thermal blob denotes the length scale at which excluded volume interactions become of order $k_{\mathrm{B}}T$ (Rubinstein and Colby, 2003). Under good solvent conditions,

the blobs obey self-avoiding-walk statistics, while they are space filling in poor solvents. As a result, the mean size R of a polymer chain (assumed here to be the magnitude of the end-to-end vector) is given by (Rubinstein and Colby, 2003),

$$R = R_{\mathrm{blob}}(T) \left(\frac{N_k}{N_{\mathrm{blob}}(T)} \right)^{\nu}, \tag{A.1}$$

where, N_{blob} is the number of Kuhn-steps in a thermal blob, and R_{blob} is the mean size of a thermal blob. The Flory exponent $\nu \approx 0.59$ in a good solvent, and $1/3$ in a poor solvent. The size of the thermal blob is a function of temperature. For instance, under athermal solvent conditions, the entire chain obeys self avoiding walk statistics, so the blob size is equal to the size of a single Kuhn-step. On the other hand, for temperatures approaching the θ-temperature, the blob size grows to engulf the entire chain.

It is convenient to define the following dimensionless scaling variable :

$$\Pi_{\mathrm{H}} \equiv \frac{R_{\mathrm{H}}}{a\sqrt{M}}, \tag{A.2}$$

where, a is a constant with dimensions of length, which we have set equal to 1 nm. In general, Π_{H} should increase with molecular weight for good solvents, remain constant for theta solvents, and decrease for poor solvents. However, Equation A.1 suggests that on length scales smaller than the blob length scale Π_{H} must remain constant, while on length scales large compared to the blob length scale, Π_{H} must scale as $M^{0.09}$ in good solvents, and $M^{-1/6}$ in poor solvents. Figure A.1 is a plot of $\log \Pi_{\mathrm{H}}$ versus $\log M$, obtained from the measurements carried out in this study, in the light of these arguments. It is clear that after an initial regime of constant values, there is a crossover to the expected scaling laws in both the good and poor solvent regimes. The crossover from one scaling regime to the next begins approximately at the blob length scale, an estimate of which can be made as follows.

The requirement that the energy of excluded volume interactions within a thermal blob are of order $k_{\mathrm{B}}T$ leads to the following expressions for N_{blob} and R_{blob} (Ru-

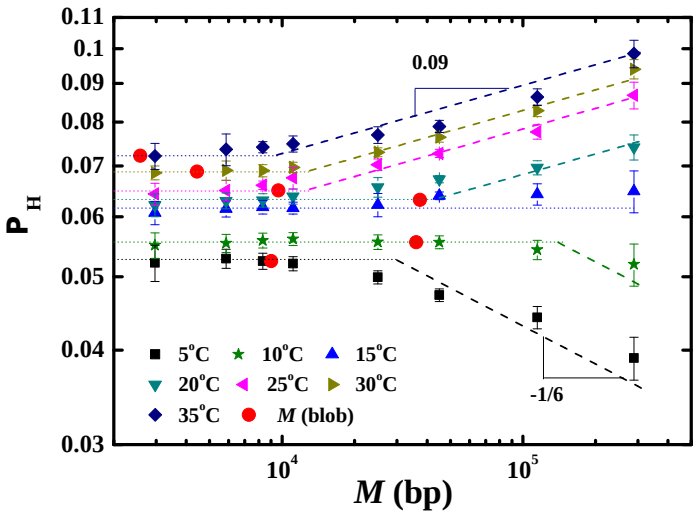

Figure A.1: Different scaling regimes for the scaled variable Π_H as a function of molecular weight M. The filled red circles correspond to the molecular weight M_{blob} of the chain segment within a thermal blob.

binstein and Colby, 2003),

$$N_{blob}(T) = \frac{b_k^6}{v(T)^2} \tag{A.3}$$

$$R_{blob}(T) = \frac{b_k^4}{|v(T)|} \tag{A.4}$$

where, $v(T)$ is the excluded volume at temperature T. The excluded volume can be shown to be related to the temperature through the relation,

$$v(T) = \begin{cases} v_0 \left(1 - \dfrac{T_\theta}{T}\right) & \text{for good solvents,} \\ \\ -v_0 \left(1 - \dfrac{T}{T_\theta}\right) & \text{for poor solvents.} \end{cases} \tag{A.5}$$

where, v_0 is a chemistry dependent constant. These expressions are consistent with the expectation that $v \to v_0$ in an athermal solvent ($T \to \infty$), and $v \to -v_0$ in a non-solvent ($T \to 0$) (Rubinstein and Colby, 2003). Since measurements of

the mean size (via R_H) have been carried out here at various temperatures, and we have estimated both T_θ and b_k, it is possible to calculate v_0 using Equations A.1–A.4. As a result the size of a thermal blob as a function of temperature can also be estimated.

The equations that govern the dimensionless excluded volume parameter v_0/b_k^3 and the molecular weight M_{blob} of a chain segment within a thermal blob, in good and poor solvents, are tabulated in Table A.1, when the hydrodynamic radius R_H is used as a measure of chain size. Here, m_k is the molar mass of a Kuhn-step, and the universal amplitude ratio U_R has been used to relate the magnitude of the end to end vector R to R_g ($R = U_R\, R_g$), while the universal ratio U_{RD} relates R_g to R_H ($R_g = U_{RD}\, R_H$). The values of these ratios are known analytically for the case of Gaussian chains and Zimm hydrodynamics under θ-conditions (Doi and Edwards, 1986), and numerically in the case of good solvents (Kumar and Prakash, 2003), and when fluctuating hydrodynamic interactions are taken into account (Sunthar and Prakash, 2006).

Using the known values of $a, \Pi_H, b_k, m_k, U_{RD}, U_R$ in the appropriate equations in Table A.1, we find that for sufficiently high molecular weights, $v_0/b_k^3 \approx 5.4 \pm 0.2$ in *both* good and poor solvents. This is significant since an inaccurate measurement of mean size in a poor solvent (as a consequence of, for instance, chain aggregation), would result in different values of v_0/b_k^3 in good and poor solvents. Further evidence regarding the reliability of poor solvent measurements can be obtained by calculating $M_{blob}(T)$ in good and poor solvents.

Figure A.2 displays the variation of M_{blob} with respect to the temperature difference $T - T_\theta$, calculated using the equations given in Table A.1. The figure graphically demonstrates the temperature dependence of the blob size, and confirms that essentially the blob size is the same in either a good or poor solvent when the temperature is equidistant from the θ-temperature. The symbols in Figure A.2 denote values of M_{blob}, evaluated at the temperatures at which experimental measurements have been made. These values have been represented by the filled red circles in Figure A.1. As can be seen from Figure A.1, the magnitude of M_{blob} is roughly

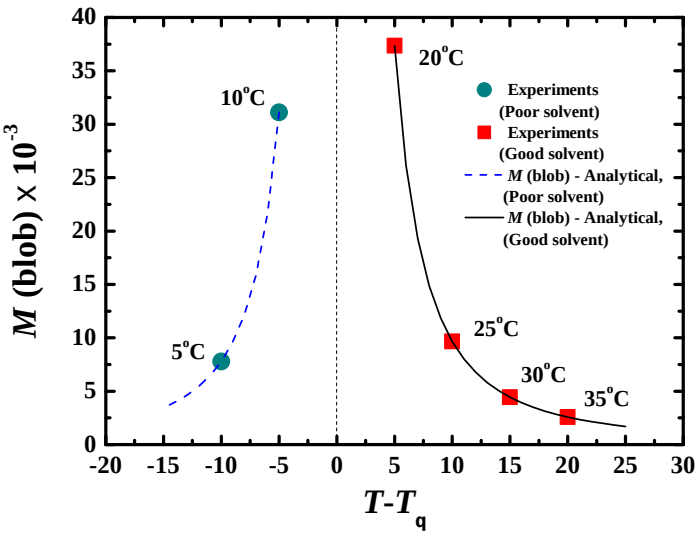

Figure A.2: Variation of the molecular weight of the chain segment within a thermal blob with respect to temperature, on either side of the θ-temperature (see Table A.1 for the equations governing $M_{\rm blob}$). The symbols denote values at temperatures at which experimental measurements have been made.

consistent with the location of the crossover from the scaling regime within a blob, to the scaling regime that holds at length scales larger than the blob, in both good and poor solvents. The two scaling regimes, in good and poor solvents, are illustrated explicitly in Figure A.3.

Table A.1: Equations for the dimensionless excluded volume parameter v_0/b_k^3, and the molecular weight of the chain segment within a thermal blob M_{blob}, in good and poor solvents. Here, m_k is the molar mass of a Kuhn-step, and U_R and U_{RD} are universal amplitude ratios, such that $R = U_R R_g$, and $R_g = U_{RD} R_H$. In all the calculations here, we assume $U_R = \sqrt{6}$, and $U_{RD} = 1.46$.

solvent quality	good	poor
$\frac{v_0}{b_k^3}$ (for $M > M_{blob}$)	$\left[\frac{a\,\Pi_H\,(U_R U_{RD})\,m_k^\nu}{b_k}\right]^{\frac{1}{2\nu-1}} \frac{1}{M^{\frac{1}{2}}\left(1-\frac{T_\theta}{T}\right)}$	$\left[\frac{a\,\Pi_H\,(U_R U_{RD})}{b_k}\right]^{-3} \frac{1}{m_k\,M^{\frac{1}{2}}\left(1-\frac{T}{T_\theta}\right)}$
$M_{blob}(T)$	$\frac{m_k\,b_k^6}{v_0^2\left(1-\frac{T_\theta}{T}\right)^2}$	$\frac{m_k\,b_k^6}{v_0^2\left(1-\frac{T}{T_\theta}\right)^2}$

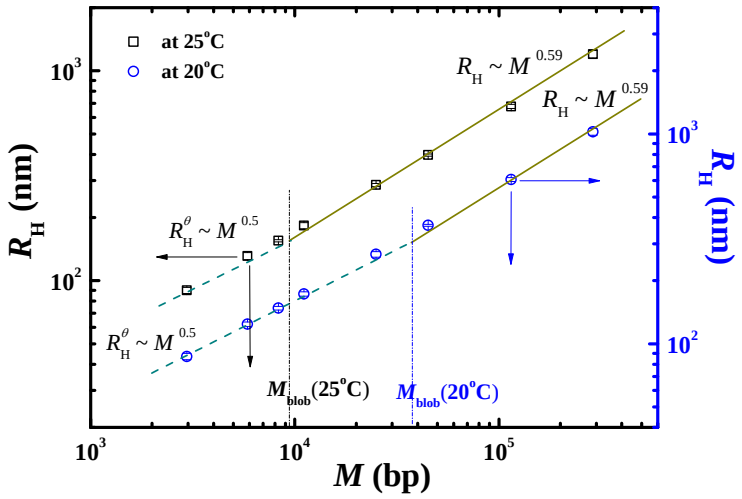

(a)

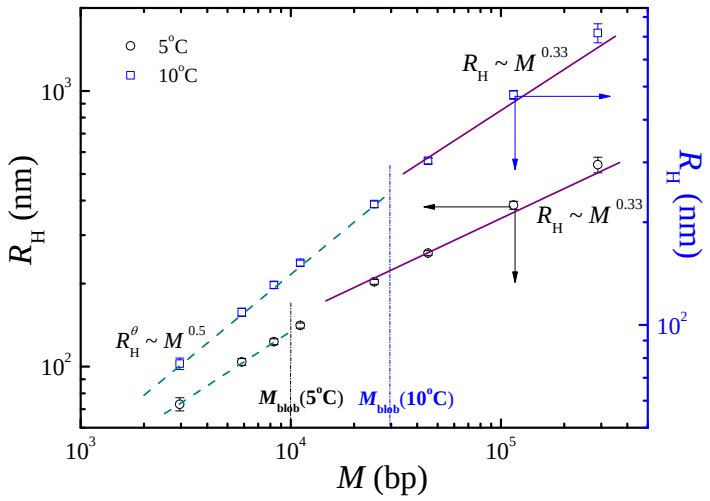

(b)

Figure A.3: The variation of hydrodynamic radius (R_H) with molecular weight (in bp) in (a) good solvents at 20°C and 25°C and (b) poor solvents at 5°C and 10°C. The scaling of R_H with M appears to obey Gaussian statistics within the thermal blob and self-avoiding walk statistics for $M > M_{blob}$ in good solvents, and collapsed globule statistics for $M > M_{blob}$ in poor solvents.

A.2 Flory-Huggins χ parameter and the phase diagram

The possibility of phase separation under poor solvent conditions, as polymer-solvent interactions become less favourable, is the primary reason for the difficulty of accurately measuring the size scaling of single chains. An approximate estimate of the thermodynamic driving force for phase separation can be obtained with the help of Flory-Huggins mean field theory. Since the Flory-Huggins χ parameter is related to the excluded volume parameter through the relation (Rubinstein and Colby, 2003) $\chi = \frac{1}{2}\left[1 - \frac{v(T)}{b_{\mathrm{k}}^3}\right]$, and we have estimated the value of $v(T)$ in both solvents, the phase diagram predicted by Flory-Huggins theory for dilute DNA solutions considered here can be obtained. It is appropriate to note that we are not interested in accurately mapping out the phase diagram for DNA solutions with the help of Flory-Huggins theory. This has already been studied in great detail, using sophisticated versions of mean-field theory, starting with the pioneering work of Post and Zimm (1982), and the problem of DNA condensation is an active field of research (Yoshikawa et al., 1996, 2011; Teif and Bohinc, 2011). Our primary interest is to obtain an approximate estimate of the location of the current experimental measurements relative to the unstable two-phase region (whose boundary is determined by the spinodal curve), since phase separation can occur spontaneously within this region. Figure A.4 displays the spinodal curves for the 25 to 289 kbp molecular weight samples, predicted by Flory-Huggins theory. Details of how these curves can be obtained are given, for instance, in Rubinstein and Colby (2003). Also indicated on each curve are the critical concentration and temperature. It is clear by considering the location of the symbols denoting the concentration-temperature coordinates of the poor solvent experiments, that for each molecular weight, they are located outside the unstable two-phase region, lending some justification to the reliability of the present poor solvent measurements. It is appropriate to note here that mean-field theories do not accurately predict the shape of the binodal curve, and in general concentration fluctuations tend to make the curve wider close to the critical point (Rubinstein and Colby, 2003). Interestingly, even for the 289 kbp sample, that has a very large molecular weight ($\approx 1.9 \times 10^8$ g/mol), there is

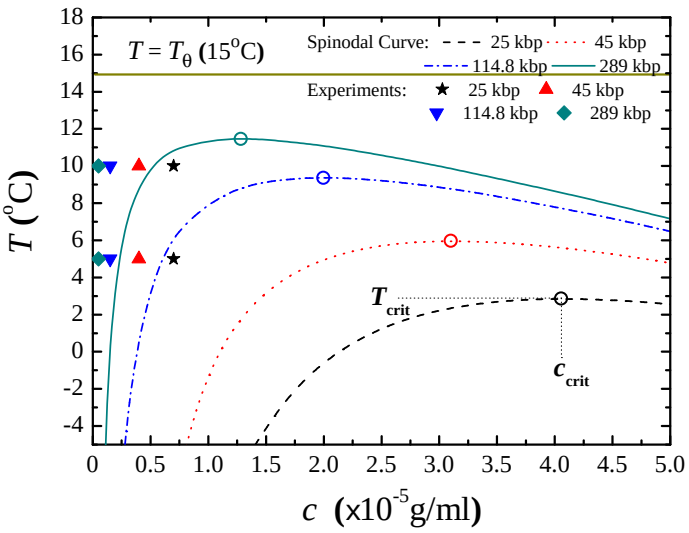

Figure A.4: Spinodal curves and critical temperatures and concentrations (filled circles) predicted by Flory-Huggins mean-field theory for a range of molecular weights. Values of concentrations and temperatures at which the poor solvent experiments have been conducted are also indicated.

still a considerable gap between the critical and θ-temperatures ($\approx 4^{\circ}$C). The reason for this is because the stiffness of double-stranded DNA leads to a relatively small number of Kuhn-steps (983) even at this large value of molecular weight, and the value of the critical temperature predicted by Flory-Huggins theory depends on the number of Kuhn-steps in a chain rather than the molecular weight.

B

The Viscosity Radius in Dilute Polymer Solutions: BD Simulations

Here we describe the methodology employed in Ahirwal (2009) and explained in Pan et al. (2014). The simulations have not been carried out as part of this thesis, but the results have been used to compare with the experimental data in Chapter 5. The methodology is described here for convenience of reference.

B.1 Brownian dynamics simulations

The dilute polymer solution is modelled as an ensemble of non-interacting bead-spring chains, each of which has N beads connected by massless springs. The evolution of the position vector $\mathbf{r}_\mu(t)$ of bead μ as a function of time t is described by the non-dimensional stochastic differential equation (Öttinger, 1996)

$$\mathrm{d}\mathbf{r}_\mu = \frac{1}{4}\sum_\nu \mathbf{D}_{\mu\nu}\cdot\mathbf{F}^\circ\,\mathrm{d}t + \frac{1}{\sqrt{2}}\sum_\nu \mathbf{B}_{\mu\nu}\cdot\mathrm{d}\mathbf{W}_\nu \tag{B.1}$$

The length scale $l_H = \sqrt{k_BT/H}$ and time scale $\lambda_H = \zeta/4H$ have been used for the purpose of non-dimensionalization, where k_B is Boltzmann's constant, T is the temperature, H is the spring constant and ζ is the hydrodynamic friction coefficient associated with a bead. The dimensionless diffusion tensor $\mathbf{D}_{\mu\nu}$ is a 3×3 matrix

for a fixed pair of beads μ and ν. It is related to the hydrodynamic interaction tensor, as discussed further subsequently. The sum of all the non-hydrodynamic forces on bead ν due to all the other beads is represented by $\mathbf{F}_\nu$, $\mathbf{W}_\nu$ is a Wiener process, and the quantity $\mathbf{B}_{\mu\nu}$ is a non-dimensional tensor whose presence leads to multiplicative noise (Öttinger, 1996). Its evaluation requires the decomposition of the diffusion tensor. Defining the matrices $\boldsymbol{\mathcal{D}}$ and $\boldsymbol{\mathcal{B}}$ as block matrices consisting of $N \times N$ blocks each having dimensions of 3×3, with the (μ, ν)-th block of $\boldsymbol{\mathcal{D}}$ containing the components of the diffusion tensor $\mathbf{D}_{\mu\nu}$, and the corresponding block of $\boldsymbol{\mathcal{B}}$ being equal to $\mathbf{B}_{\mu\nu}$, the decomposition rule for obtaining $\boldsymbol{\mathcal{B}}$ can be expressed as

$$\boldsymbol{\mathcal{B}} \cdot \boldsymbol{\mathcal{B}}^{\mathrm{T}} = \boldsymbol{\mathcal{D}} \tag{B.2}$$

The non-hydrodynamic forces on a bead μ are comprised of the non-dimensional spring forces $\mathbf{F}_\mu^{\mathrm{spr}}$ and non-dimensional excluded-volume interaction forces $\mathbf{F}_\mu^{\mathrm{exv}}$, i.e., $\mathbf{F}_\mu = \mathbf{F}_\mu^{\mathrm{spr}} + \mathbf{F}_\mu^{\mathrm{exv}}$. The entropic spring force on bead μ due to adjacent beads can be expressed as $\mathbf{F}_\mu^{\mathrm{spr}} = \mathbf{F}^c(\mathbf{Q}_\mu) - \mathbf{F}^c(\mathbf{Q}_{\mu-1})$ where $\mathbf{F}^c(\mathbf{Q}_{\mu-1})$ is the force between the beads $\mu - 1$ and μ, acting in the direction of the connector vector between the two beads $\mathbf{Q}_{\mu-1} = \mathbf{r}_\mu - \mathbf{r}_{\mu-1}$. Since simulations are carried out at equilibrium, a linear Hookean spring force is used for modelling the spring forces, $\mathbf{F}^c(\mathbf{Q}_\mu) = \mathbf{Q}_\mu$. The vector $\mathbf{F}_\mu^{\mathrm{exv}}$ is given in terms of the excluded volume potential $E\left(\mathbf{r}_\mu - \mathbf{r}_\nu\right)$ between the beads μ and ν of the chain, by the expression,

$$\mathbf{F}_\mu^{\mathrm{exv}} = -\sum_{\substack{\nu=1 \\ \nu\neq\mu}}^{N} \frac{\partial}{\partial \mathbf{r}_\mu} E\left(\mathbf{r}_\mu - \mathbf{r}_\nu\right) \tag{B.3}$$

A narrow Gaussian excluded volume potential is used, with $E\left(\mathbf{r}_\mu - \mathbf{r}_\nu\right)$ given by,

$$E\left(\mathbf{r}_\mu - \mathbf{r}_\nu\right) = \left(\frac{z^*}{d^{*3}}\right) \exp\left[-\frac{\mathbf{r}_{\mu\nu}^2}{d^{*2}}\right] \tag{B.4}$$

where, $\mathbf{r}_{\mu\nu} = \mathbf{r}_\mu - \mathbf{r}_\nu$, is the vector between beads ν and μ, and the parameters z^* and d^* are nondimensional quantities which characterize the narrow Gaussian potential: z^* measures the strength of the excluded volume interaction, while d^*

is a measure of the range of excluded volume interaction. The narrow Gaussian potential is a means of regularizing the Dirac delta potential since it reduces to a δ-function potential in the limit of d^* tending to zero.

The non-dimensional diffusion tensor $\mathbf{D}_{\nu\mu}$ is related to the non-dimensional hydrodynamic interaction tensor $\boldsymbol{\Omega}$ through

$$\mathbf{D}_{\mu\nu} = \delta_{\mu\nu}\,\boldsymbol{\delta} + (1 - \delta_{\mu\nu})\,\boldsymbol{\Omega}(\boldsymbol{r}_\nu - \boldsymbol{r}_\mu) \tag{B.5}$$

where $\boldsymbol{\delta}$ and $\delta_{\mu\nu}$ represent a unit tensor and a Kronecker delta, respectively, while $\boldsymbol{\Omega}$ represents the effect of the motion of a bead μ on another bead ν through the disturbances carried by the surrounding fluid. The hydrodynamic interaction tensor $\boldsymbol{\Omega}$ is assumed to be given by the Rotne-Prager-Yamakawa (RPY) regularisation of the Oseen function

$$\boldsymbol{\Omega}(\mathbf{r}) = \Omega_1\,\boldsymbol{\delta} + \Omega_2 \frac{\mathbf{rr}}{r^2} \tag{B.6}$$

where for $r \equiv |\mathbf{r}| \geq 2\sqrt{\pi}h^*$,

$$\Omega_1 = \frac{3\sqrt{\pi}}{4}\,\frac{h^*}{r}\left(1 + \frac{2\pi}{3}\,\frac{h^{*2}}{r^2}\right) \quad \text{and} \quad \Omega_2 = \frac{3\sqrt{\pi}}{4}\,\frac{h^*}{r}\left(1 - 2\pi\,\frac{h^{*2}}{r^2}\right) \tag{B.7}$$

while for $0 < r \leq 2\sqrt{\pi}h^*$,

$$\Omega_1 = 1 - \frac{9}{32}\,\frac{r}{h^*\sqrt{\pi}} \quad \text{and} \quad \Omega_2 = \frac{3}{32}\,\frac{r}{h^*\sqrt{\pi}} \tag{B.8}$$

Here, h^* is the familiar hydrodynamic interaction parameter defined as

$$h^* = a\sqrt{H/(\pi k_{\mathrm{B}}\,T)}, \tag{B.9}$$

where a is the dimensional bead radius. In the presence of fluctuating HI, the problem of the computational intensity of calculating the Brownian term is reduced by the use of a Chebyshev polynomial representation for the Brownian term (Fixman, 1986; Jendrejack et al., 2000); the details of the exact algorithm are given in Prabhakar and Prakash (2004).

Universal predictions, independent of details of the coarse-grained model used to represent a polymer, are obtained in the limit of long chains, since the self-similar character of real polymer molecules is captured in this limit. It is common to obtain predictions in the long chain limit by accumulating data for finite chain lengths and extrapolating to the limit $N \to \infty$. This procedure has been used successfully to calculate universal properties of dilute polymer solutions predicted by a variety of approaches to treating hydrodynamic and excluded volume interactions, including approximate closure approximations (Öttinger, 1987; Öttinger, 1989; Prakash and Öttinger, 1997; Prakash, 2002), and exact Brownian dynamics simulations (Kröger et al., 2000; Kumar and Prakash, 2003, 2004; Sunthar et al., 2005; Sunthar and Prakash, 2006; Bosko and Prakash, 2011). In particular, Sunthar and Prakash (2006) showed that universal predictions in the non-draining limit ($h^* \sqrt{N} \to \infty$), and at any fixed value of the solvent quality parameter $z = z^* \sqrt{N}$, could be obtained by simultaneously keeping h^* and z constant, while taking the limit $N \to \infty$. Clearly, the parameter $z^* \to 0$ in this limit. Further, $d^* \to 0$, since d^* is set equal to $K\,(z^*)^{1/5}$ in order to use larger step sizes in the numerical integration scheme (Kumar and Prakash, 2003). As a result, the long chain limit of the model corresponds to the Edwards continuous chain model with a delta function excluded volume potential (Doi and Edwards, 1986). As mentioned in the introduction to the Chapter 5, by accounting for fluctuating hydrodynamic and excluded volume interactions in this manner, Sunthar and Prakash (2006) were able to obtain quantitatively accurate parameter free prediction of α_{H} as a function of z. Here, we show that this approach can also be used to successfully predict universal properties related to the zero shear rate viscosity of dilute polymer solutions.

B.2 Universal properties derived from the viscosity radius

We focus our attention on two properties that are defined in terms of the viscosity radius (Equation (5.1)) which have been shown to be universal in the sense that they are independent of the chemistry of the particular polymer-solvent sys-

tem for sufficiently long polymers. The first of these is the universal viscosity ratio, $U_{\eta R}$ (defined in Equation (5.2)), and the second is the swelling ratio α_η (defined in Equation (1.6)). We discuss the evaluation of these properties by Brownian dynamics simulations in turn below.

In terms of dimensionless variables, $U_{\eta R}$ can be shown to be given by

$$U_{\eta R} = \frac{9}{8}\sqrt{\pi}h^* \frac{\eta^*_{\mathrm{p}0}}{R^{*3}_{\mathrm{g}}} \tag{B.10}$$

where, R^*_{g} is the dimensionless radius of gyration and $\eta^*_{\mathrm{p}0} = \eta_{\mathrm{p}0}/(n_{\mathrm{p}}\lambda_{\mathrm{H}}k_{\mathrm{B}}\,T)$ is the dimensionless zero-shear rate viscosity. Here, n_{p} is the number of chains per unit volume. Kröger et al. (2000) have estimated $\eta^*_{\mathrm{p}0}$ by carrying out non-equilibrium BD simulations at finite shear rates, and extrapolating the data to the limit of zero shear rate. An alternative method is used which is based on a Green-Kubo relation (Fixman, 1981) which gives the viscosity as an integral of the equilibrium-averaged stress-stress auto-correlation function

$$\eta^*_{\mathrm{p}0} = \int_0^\infty \mathrm{d}t\ \langle C_{\mathrm{S}}(\mathbf{r}_1, \mathbf{r}_2, \ldots, \mathbf{r}_N, t)\rangle_{\mathrm{eq}} \tag{B.11}$$

where,

$$C_{\mathrm{S}}(\mathbf{r}_1, \mathbf{r}_2, \ldots, \mathbf{r}_N, t) = S_{xy}(t)S_{xy}(0) \tag{B.12}$$

The quantity S_{xy} is the xy-component of the stress tensor given by Kramers expression $S_{xy} = \sum_\mu F_{\mu x}(r_{\mu y} - r_{cy})$, where $F_{\mu x}$ is the x-component of $\mathbf{F}_\mu$, $r_{\mu y}$ is the y-component of $\mathbf{r}_\mu$, and r_{cy} is the y-component of the position vector of the center-of-mass of the bead-spring chain, $\mathbf{r}_c = (1/N)\sum_\mu \mathbf{r}_\mu$. The use of the Green-Kubo method mitigates the problem of the large error bars associated with estimating polymer solution properties at low shear rates. The noise in measured properties can be significantly reduced by evaluating the integral in Equation (B.11) with the help of equilibrium simulations of a large ensemble of trajectories. Additionally, for some simulations, a variance reduction technique has been employed, as explained in Section B.3 below.

Rather than evaluating the swelling of the viscosity radius directly from its definition in Equation (1.6), it is advantageous to use the expression defined in Equation 5.13 which gives α_η in terms of $U_{\eta R}$ and α_g, since the $N \to \infty$ extrapolations of $U^\theta_{\eta R}$ and $U_{\eta R}$ (at various values of z) are more accurate than the extrapolations for α_η. The swelling of the radius of gyration α_g for different values of z is calculated from Equation 5.15, with values of the fitting parameters, a, b, c, and m as given in Table 5.4 in Chapter 5. Equation (5.15) has been shown by Kumar and Prakash (2003) to be an excellent fit to the asymptotic predictions of α_g by Brownian dynamics simulations of Equation (B.1), in the absence of hydrodynamic interactions. This corresponds to the pure excluded volume problem, which is adequate for determining α_g, since it is a static property unaffected by hydrodynamic interactions.

B.3 Variance reduced simulations

The statistical error in the estimation of the equilibrium-averaged stress-stress auto-correlation function $\langle C_S(t)\rangle_{eq}$ can be significantly reduced if the fluctuations in $C_S(\mathbf{r}_1, \mathbf{r}_2, \ldots, \mathbf{r}_N, t)$ can be made to be small. A variance reduction technique (Öttinger, 1996), based on the use of control variates (Melchior and Öttinger, 1996) has been used, as described below.

In general, the fluctuations $f_{C_S} = C_S(\mathbf{r}_1, \mathbf{r}_2, \ldots, \mathbf{r}_N, t) - \langle C_S(t)\rangle_{eq}$, cannot be estimated a priori. However, if an approximate estimate of the fluctuations, $\hat{f}_{C_S} = \hat{C}_S(\hat{\mathbf{r}}_1, \hat{\mathbf{r}}_2, \ldots, \hat{\mathbf{r}}_N, t) - \langle \hat{C}_S(t)\rangle_{eq}$, can be obtained for a stochastic process $\hat{\mathbf{r}}_\nu$, for which the equilibrium-averaged stress-stress auto-correlation $\langle \hat{C}_S(t)\rangle_{eq}$ is known analytically, then the control variate

$$\hat{E}_{C_S} = C_S(\mathbf{r}_1, \mathbf{r}_2, \ldots, \mathbf{r}_N, t) - \hat{f}_{C_S} \tag{B.13}$$

can be used to estimate the stress-stress auto-correlation function with reduced statistical error, since $\langle \hat{E}_{C_S}\rangle_{eq} = \langle C_S(t)\rangle_{eq}$. The extent of the reduction in statistical error depends on the extent to which C_S and $\hat{C}_S$ are correlated, as can be seen from

the expression for the variance of $\hat{E}_{C_S}$,

$$\left\langle \left[\hat{E}_{C_S} - \langle E_{C_S}\rangle_{eq}\right]^2 \right\rangle_{eq} = \left\langle \left[C_S - \langle C_S\rangle_{eq}\right]^2 \right\rangle_{eq} + \left\langle \left[\hat{C}_S - \langle \hat{C}_S\rangle_{eq}\right]^2 \right\rangle_{eq} - 2\left[\langle C_S\,\hat{C}_S\rangle_{eq} - \langle C_S\rangle_{eq}\langle \hat{C}_S\rangle_{eq}\right] \tag{B.14}$$

The stochastic process $\hat{\mathbf{r}}_\nu$, governed by the stochastic differential equation,

$$d\hat{\mathbf{r}}_\mu = \frac{1}{4}\sum_\nu H_{\mu\nu}\,\mathbf{F}^\circ\,dt + \frac{1}{\sqrt{2}}\sum_\nu S_{\mu\nu}\,d\mathbf{W}_\nu \tag{B.15}$$

is used as a trajectory-wise approximation to $\mathbf{r}_\nu$, where,

$$H_{\mu\nu}\,\boldsymbol{\delta} = \left\langle \mathbf{D}_{\mu\nu}\right\rangle_{eq} = \left[\delta_{\mu\nu} + (1-\delta_{\mu\nu})\,\bar{H}_{\mu\nu}\right]\boldsymbol{\delta} \tag{B.16}$$

and,

$$\sum_\alpha S_{\mu\alpha}\,S_{\nu\alpha} = \bar{H}_{\mu\nu}\,, \quad \text{for} \quad \mu \neq \nu \tag{B.17}$$

Note that, $\bar{H}_{\mu\mu} = S_{\mu\mu} = 1$. The equilibrium average of $\mathbf{D}_{\mu\nu}$ in Equation B.16 is carried out with the equilibrium distribution function in the absence of excluded volume interactions, since an analytical solution for the distribution function is only known under θ-solvent conditions. Fixman (Fixman, 1983, 1981) has previously calculated $\bar{H}_{\mu\nu}$ and $\langle \hat{C}_S(t)\rangle_{eq}$ analytically for the RPY tensor, as discussed shortly. By simulating Equation B.15 simultaneously with Equation B.1, using the same Weiner process $\mathbf{W}_\nu$, the fluctuations $\hat{f}_{C_S}$ can be estimated, and consequently the mean value of the control variate, $\left\langle \hat{E}_{C_S}\right\rangle_{eq}$.

Fixman's expressions for $\bar{H}_{\mu\nu}$ and $\langle \hat{C}_S(t)\rangle_{eq}$ has been rewritten with the non-dimensionalization scheme and notation used here. Fixman (Fixman, 1983) has shown that the equilibrium averaged hydrodynamic interaction tensor is given by

$$\bar{H}_{\mu\nu} = \mathrm{erf}(x_{\mu\nu}) - \frac{1}{\sqrt{\pi}}\frac{1-\exp(-x_{\mu\nu}^2)}{x_{\mu\nu}} \tag{B.18}$$

where,

$$x_{\mu\nu} \equiv \sqrt{\frac{2\,\pi\,h^{*2}}{|\mu-\nu|}} \quad \text{for } \mu \neq \nu \tag{B.19}$$

By defining the components of the $(N-1)\times(N-1)$ matrix $\widetilde{\boldsymbol{A}}$, with the expression,

$$\widetilde{A}_{jk} = \sum_{\mu,\nu} \overline{B}_{j\mu}\, H_{\mu\nu}\, \overline{B}_{k\nu} \tag{B.20}$$

where, $\overline{B}_{k\nu} = \delta_{k+1,\nu} - \delta_{k\nu}$, for $1 \le k \le (N-1)$; $1 \le \nu \le N$, Fixman (Fixman, 1981) has derived the following analytical expression for the stress-stress auto-correlation function of the stochastic process $\hat{\mathbf{r}}_\nu$,

$$\langle \hat{C}_S(t) \rangle_{eq} = \mathrm{tr}\left(\exp\left[-\frac{1}{2}\, \widetilde{\boldsymbol{A}}\, t \right] \right) \tag{B.21}$$

Clearly, if the RPY tensor is replaced with the Oseen tensor in the definition of $\mathbf{D}_{\mu\nu}$, then $\widetilde{A}_{jk}$ is nothing but the modified Kramers matrix (Bird et al., 1987).

The efficacy of the variance reduction procedure used here is demonstrated in Figure B.1, where the various auto-correlation functions obtained from the simulation of a bead-spring chain under θ-conditions, with $N = 18$, and $h^* = 0.25$, are displayed. The positive correlation between the two functions C_S and $\hat{C}_S$, and the reduction in the variance in $\hat{E}_{C_S}$ can be clearly observed.

Variance reduction was used here only for simulations with $z = 0$ (θ-solvent), $z = 0.01$, and $z = 0.1$. For higher z, the correlation between the two stochastic processes was lost and there was no benefit in using $\hat{E}_{C_S}$ in place of C_S. This is not unexpected since the equilibrium averaging of $\mathbf{D}_{\mu\nu}$ in Equation B.16 is carried out with the equilibrium distribution function in the absence of excluded volume interactions.

B.4 Integration of the correlation functions

The stress-stress auto-correlation function must be integrated to obtain the intrinsic viscosity, as can be seen from Equation B.11, where, when appropriate, the control variate $\hat{E}_{C_S}(t)$ is used instead of $C_S(t)$. In spite of the reduced variance, the numerical integration of this function is subject to errors. Consequently, a non-linear least square fit of the auto-correlation function is used instead, and the integral of the

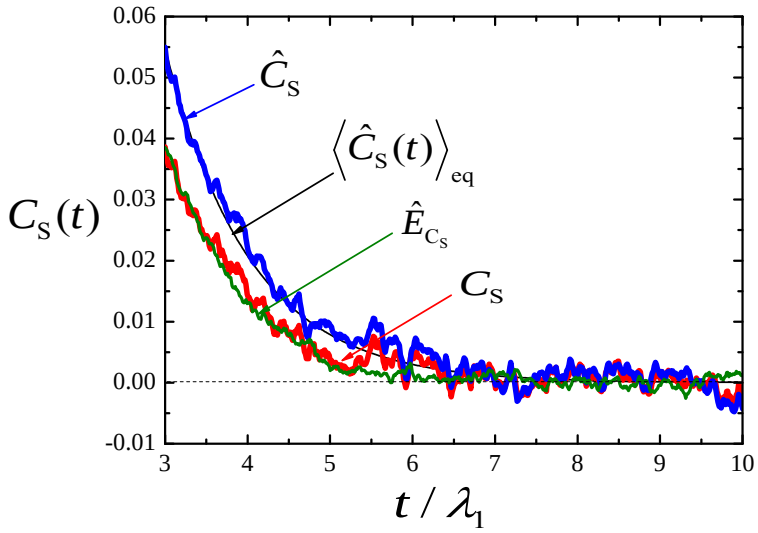

Figure B.1: Reduction in the variance of the stress auto-correlation function. The two auto-correlation functions, C_S (red curve) calculated with fluctuating hydrodynamic interactions, and $\hat{C}_S$ (blue curve) calculated with pre-averaged hydrodynamic interactions, can be seen visually to be positively correlated. The control variate $\hat{E}_{C_S}$ (green curve), on the other hand, has significantly lower fluctuations. The analytical function $\langle \hat{C}_S(t) \rangle_{eq}$ (black curve) is obtained from Equation B.21. The range of the axes have been chosen to magnify the noise at small values of C_S. In this simulation $\lambda_1 = 38.2$, is the longest relaxation time, estimated from Thurston's correlation (Thurston, 1974) for $N = 18$, and $h^* = 0.25$. The averages have been obtained over roughly 57000 independent trajectories.

fitting function has been evaluated from that. The time correlation function $\hat{C}_S(t)$ is expected to decay as a sum of exponentials (Fixman, 1981),

$$\hat{C}_S(t) = \sum_k a_k e^{-t/\tau_k} \tag{B.22}$$

so that,

$$\int_0^\infty dt\ \hat{C}_S(t) = \sum_k a_k\ \tau_k \tag{B.23}$$

Similar behaviour is expected for $C_S(t)$, although the relaxation spectrum need not be discrete. It was found sufficient to use a small number of discrete modes (typically three to six in number) to fit the data with an acceptable error (determined by a χ^2 test of fit). A Levenberg-Marquardt least square regression algorithm provided as part of GNU-octave package (version 3+) was used to carry out the fitting. Initial guesses for the relaxation times τ_k have been obtained from estimates of the relaxation spectrum using the Thurston correlation (Thurston, 1974).

References

Ahirwal, D., Shear Viscosity of Dilute Polymer Solutions, Master's thesis, Indian Institute of Technology Bombay, Department of Chemical Engineering (2009).

Anna, S. L., G. H. McKinley, D. A. Nguyen, T. Sridhar, S. J. Muller, J. Huang, and D. F. James, "An inter-laboratory comparison of measurements from filament stretching rheometers using common test fluids.," *J. Rheol.*, **45**(1), 83–114 (2001).

Arai, T., F. Abe, T. Yoshizaki, Y. Einaga, and H. Yamakawa, "Excluded-Volume Effects on the Hydrodynamic Radius of Oligo- and Polystyrenes in Dilute Solution," *Macromolecules*, **28**(10), 3609–3616 (1995).

Aust, C., M. Kröger, and S. Hess, "Structure and dynamics of dilute polymer solutions under shear flow via nonequilibrium molecular dynamics," *Macromolecules*, **32**(17), 5660–5672 (1999).

Babcock, H. P., R. E. Teixeira, J. S. Hur, E. S. G. Shaqfeh, and S. Chu, "Visualization of molecular fluctuations near the critical point of the coil-stretch transition in polymer elongation," *Macromolecules*, **36**(12), 4544–4548 (2003).

Bach, A., H. K. Rasmussen, and O. Hassager, "Extensional viscosity for polymer melts measured in the filament stretching rheometer," *J. Rheol.*, **47**(2), 429–441 (2003).

Barrat, J.-L. and J.-F. Joanny, "Theory of polyelectrolyte solutions," *Adv. Chem. Phys.*, **94 (XCIV)**, 1–66 (1996).

Barrett, A. J., "Intrinsic viscosity and friction coefficients for an excluded volume polymer in the Kirkwood approximations," *Macromolecules*, **17**(8), 1566–1572 (1984).

Barrett, A. J., M. Mansfield, and B. C. Benesch, "Numerical study of self-avoiding walks on lattices and in the continuum," *Macromolecules*, **24**(7), 1615–1621 (1991).

Batchelor, G. K., "The stress generated in a non-dilute suspension of elongated particles by pure straining motion," *J. Fluid Mech.*, **46**(4), 813–829 (1971).

Berg, J. M., J. L. Tymoczko, and L. Stryer, *Biochemistry, Fifth Edition*. W. H. Freeman, USA (2002).

Berry, G. C., "Thermodynamic and Conformational Properties of Polystyrene. I. Light-Scattering Studies on Dilute Solutions of Linear Polystyrenes," *J. Chem. Phys.*, **44**, 4550 (1966).

Berry, G. C., "Crossover behaviour in the viscosity of semiflexible polymers: Intermolecular interactions as a function of concentration and molecular weight," *J. Rheol.*, **40**, 1129–1154 (1996).

Bhattacharjee, P. K., D. A. Nguyen, G. H. McKinley, and T. Sridhar, "Extensional stress growth and stress relaxation in entangled polymer solutions," *J. Rheol.*, **47**(1), 269–290 (2003).

Bird, R. B., C. F. Curtiss, R. C. Armstrong, and O. Hassager, *Dynamics of Polymeric Liquids - Volume 2: Kinetic Theory*. John Wiley, New York, 2nd edition (1987).

Bosko, J. T. and J. R. Prakash, "Universal Behavior of Dendrimer Solutions," *Macromolecules*, **44**(3), 660–670 (2011).

Brandrup, J., E. H. Immergut, and E. A. Grulke, editors, *Polymer Handbook*. John Wiley and Sons, New York, fourth edition (1999).

Burchard, W., Light Scattering from Polysaccharides as Soft Materials, In Borsali, R. and R. Pecora, editors, *Soft Matter Characterization*, pages 463–603. Springer Netherlands, Dordrecht (2008).

Colby, R. H., D. C. Boris, W. E. Krause, and S. Dou, "Shear thinning of unentangled flexible polymer liquids," *Rheol. Acta*, **46**(5), 569–575 (2007).

Colby, R. H. and M. Rubinstein, "Two-parameter scaling for polymers in Theta solvents," *Macromolecules*, **23**(10), 2753–2757 (1990).

de Gennes, P.-G., *Scaling Concepts in Polymer Physics*. Cornell University Press, Ithaca (1979).

Doi, M. and S. F. Edwards, *The Theory of Polymer Dynamics*. Clarendon Press, Oxford, New York (1986).

Domb, C. and A. J. Barrett, "Universality approach to the expansion factor of a polymer chain," *Polymer*, **17**(3), 179–184 (1976).

Doty, P., B. B. McGill, and S. A. Rice, "The properties of sonic fragments of Deoxyribose Nucleic Acid," *Proc. Natl. Acad. Sci. U. S. A.*, **44**(5), 432–438 (1958).

Doyle, P. S., E. S. G. Shaqfeh, and A. P. Gast, "Dynamic simulation of freely draining flexible polymers in steady linear flows," *J. Fluid Mech.*, **334**, 251–291 (1997).

Encyclopaedia Britannica, I., Genetic engineering: recombinant DNA, `http://www.britannica.com/EBchecked/topic/493667/recombinant-DNA-technology` (2012). Accessed May 19, 2014.

Fishman, D. M. and G. D. Patterson, "Light scattering studies of supercoiled and nicked DNA," *Biopolymers*, **38**, 535–552 (1996).

Fixman, M., "Inclusion of hydrodynamic interaction in polymer dynamical simulations," *Macromolecules*, **14**(6), 1710–1717 (1981).

Fixman, M., "Effects of fluctuating hydrodynamic interaction," *J. Chem. Phys*, **78**, 1594–1599 (1983).

Fixman, M., "Construction of Langevin forces in the simulation of hydrodynamic interaction," *Macromolecules*, **19**(64), 1204–1207 (1986).

Fujimoto, B. S., J. M. Miller, N. S. Ribeiro, and J. M. Schurr, "Effects of different cations on the hydrodynamic radius of DNA," *Biophys. J.*, **67**(1), 304–308 (1994).

Graessley, W. W., "Polymer chain dimensions and the dependence of viscoelastic properties on concentration, molecular weight and solvent power," *Polymer*, **21**(3), 258–262 (1980).

Grosberg, A. Y. and A. R. Khokhlov, *Statistical physics of macromolecules*. AIP Press, New York (1994).

Gupta, R. K., D. A. Nguyen, and T. Sridhar, "Extensional viscosity of dilute polystyrene solutions: Effect of concentration and molecular weight," *Phys. Fluids*, **12**(6), 1296–1318 (2000).

Harding, S. E., Classical Light Scattering for the Deterrnination of Absolute Molecular Weights and Gross Conforrnation of Biological Macromolecules, In Jones, C., B. Mulloy, and A. H. Thomas, editors, *Methods in Molecular Biology, Vol.22: Microscopy, Optical Spectrcscopy, and Macrcscopic Technique*, pages 85–95. Humana Press Inc., Totowa, NJ (1994).

Hayward, R. C. and W. W. Graessley, "Excluded volume effects in polymer solutions. 1. Dilute solution properties of linear chains in good and theta solvents," *Macromolecules*, **32**(10), 3502–3509 (1999).

Heo, Y. and R. G. Larson, "The scaling of zero-shear viscosities of semidilute polymer solutions with concentration," *J. Rheol.*, **49**(5), 1117–1128 (2005).

Hodnett, J. L., R. J. Legerski, and H. B. Gray Jr., "Dependence upon temperature of corrected sedimentation coefficients measured in a Beckman analytical ultracentrifuge," *Anal. Biochem.*, **75**(2), 522–537 (1976).

Hsieh, C.-C., L. Li, and R. G. Larson, "Modeling hydrodynamic interaction in Brownian dynamics: Simulations of extensional flows of dilute solutions of DNA and polystyrene," *J. Non-Newton. Fluid Mech.*, **113**(2-3), 147–191 (2003).

Hua, C. C. and M. S. Wu, "Viscometric properties of dilute polystyrene/dioctyl phthalate solutions," *J. Polym. Sci. Part B Polym. Phys*, **44**(5), 787–794 (2006).

Huang, C.-C., R. G. Winkler, G. Sutmann, and G. Gompper, "Semidilute polymer solutions at equilibrium and under shear flow," *Macromolecules*, **43**(23), 10107–10116 (2010).

Hur, J. S., E. S. G. Shaqfeh, H. P. Babcock, D. E. Smith, and S. Chu, "Dynamics of dilute and semidilute DNA solutions in the start-up of shear flow," *J. Rheol.*, **45**(2), 421–450 (2001).

Jain, A., B. Dünweg, and J. R. Prakash, "Dynamic Crossover Scaling in Polymer Solutions," *Phys. Rev. Lett.*, **109**, 088302 (2012a).

Jain, A., P. Sunthar, B. Dünweg, and J. R. Prakash, "Optimization of a Brownian-dynamics algorithm for semidilute polymer solutions," *Phys. Rev. E*, **85**, 066703 (2012b).

Jamieson, A. M. and R. Simha, NEWTONIAN VISCOSITY OF DILUTE, SEMIDILUTE, AND CONCENTRATED POLYMER SOLUTIONS, In Utracki, L. A. and A. M. Jamieson, editors, *Polymer Physics: From Suspensions to Nanocomposites and Beyond*, pages 15–87. John Wiley & Sons, Inc. (2010).

Jendrejack, R. M., J. J. De Pablo, and M. D. Graham, "Stochastic simulations of DNA in flow: Dynamics and the effects of hydrodynamic interactions," *J. Chem. Phys.*, **116**(17), 7752–7759 (2002).

Jendrejack, R. M., M. D. Graham, and J. J. de Pablo, "Hydrodynamic interactions in long chain polymers: Application of the Chebyshev polynomial approximation in stochastic simulations," *J. Chem. Phys.*, **113**(7), 2894–2900 (2000).

Juarez, G. and P. E. Arratia, "Extensional rheology of DNA suspensions in microfluidic devices," *Soft Matter*, **7**(19), 9444–9452 (2011).

Kröger, M., A. Alba-Pérez, M. Laso, and H. C. Öttinger, "Variance reduced Brownian simulation of a bead-spring chain under steady shear flow considering hydrodynamic interaction effects," *J. Chem. Phys.*, **113**(11), 4767–4773 (2000).

Kumar, K. S. and J. R. Prakash, "Equilibrium swelling and universal ratios in dilute polymer solutions: Exact Brownian dynamics simulations for a Delta function excluded volume potential," *Macromolecules*, **36**(20), 7842–7856 (2003).

Kumar, K. S. and J. R. Prakash, "Universal consequences of the presence of excluded volume interactions in dilute polymer solutions undergoing shear flow," *J. Chem. Phys.*, **121**(8), 3886–3897 (2004).

Laib, S., R. M. Robertson, and D. E. Smith, "Preparation and characterization of a set of linear DNA molecules for polymer physics and rheology studies," *Macromolecules*, **39**(12), 4115–4119 (2006).

Langowski, J., "Salt effects on internal motions of superhelical and linear pUC8 DNA. Dynamic light scattering studies," *Biophys. Chem.*, **27**(3), 263–271 (1987).

Larson, R. G., H. Hu, D. E. Smith, and S. Chu, "Brownian dynamics simulations of a DNA molecule in an extensional flow field," *J. Rheol.*, **43**(2), 267–304 (1999).

Latinwo, F. and C. M. Schroeder, "Model systems for single molecule polymer dynamics," *Soft Matter*, **7**(18), 7907–7913 (2011).

Lee, J. S., E. S. G. Shaqfeh, and S. J. Muller, "Dynamics of DNA tumbling in shear to rotational mixed flows: Pathways and periods," *Phys. Rev. E*, **75**(4) (2007).

Leighton, S. B. and I. Rubenstein, "Calibration of molecular weight scales for DNA," *J. Mol. Biol.*, **46**(2), 313–328 (1969).

Lewis, R. J., J. H. Huang, and R. Pecora, "Rotational and translational motion of supercoiled plasmids in solution," *Macromolecules*, **18**(5), 944–948 (1985).

Li, L., R. G. Larson, and T. Sridhar, "Brownian dynamics simulations of dilute polystyrene solutions," *J. Rheol.*, **44**(2), 291–322 (2000).

Liu, H., J. Gapinski, L. Skibinska, A. Patkowski, and R. Pecora, "Effect of electrostatic interactions on the dynamics of semiflexible monodisperse DNA fragments," *J. Chem. Phys.*, **113**(14), 6001–6010 (2000).

Liu, T. W., "Flexible polymer chain dynamics and rheological properties in steady flows," *J. Chem. Phys.*, **90**(10), 5826–5842 (1989).

Liu, Y., Y. Jun, and V. Steinberg, "Concentration dependence of the longest relaxation times of dilute and semi-dilute polymer solutions," *J. Rheol.*, **53**(5), 1069–1085 (2009).

Lueth, C. A. and E. S. G. Shaqfeh, "Experimental and numerical studies of tethered DNA shear dynamics in the flow-gradient plane," *Macromolecules*, **42**(22), 9170–9182 (2009).

Marathias, V. M., B. Jerkovic, H. Arthanari, and P. H. Bolton, "Flexibility and curvature of duplex DNA containing mismatched sites as a function of temperature," *Biochemistry*, **39**(1), 153–160 (2000).

Marko, J. F. and E. D. Siggia, "Stretching DNA," *Macromolecules*, **28**(26), 8759–8770 (1995).

McKinley, G. H. and O. Hassager, "The Considère condition and rapid stretching of linear and branched polymer melts," *J. Rheol.*, **43**(5), 1195–1212 (1999).

McKinley, G. H. and T. Sridhar, "Filament-stretching rheometry of complex fluids," *Annu. Rev. Fluid Mech.*, **34**, 375–415 (2002).

Melchior, M. and H. C. Öttinger, "Variance reduced simulations of polymer dynamics," *J. Chem. Phys.*, **105**(8), 3316–3331 (1996).

Miyaki, Y., Y. Einaga, H. Fujita, and M. Fukuda, "Flory's Viscosity Factor for the System Polystyrene + Cyclohexane at 34.5C," *Macromolecules*, **13**(3), 588–592 (1980).

Miyaki, Y. and H. Fujita, "Excuded-volume effects in dilute polymer solutions. 11. Tests of the two-parameter theory for radius of gyration and intrinsic viscosity," *Macromolecules*, **14**(3), 742–746 (1981).

Nayvelt, I., T. Thomas, and T. J. Thomas, "Mechanistic differences in DNA nanoparticle formation in the presence of oligolysines and poly-L-lysine," *Biomacromolecules*, **8**(2), 477–484 (2007).

Nicolai, T. and M. Mandel, "Dynamic light scattering by aqueous solutions of low-molar-mass DNA fragments in the presence of sodium chloride," *Macromolecules*, **22**(5), 2348–2356 (1989).

Ostrander, D. A. and H. B. Gray Jr, "Sedimentation and intrinsic viscosity behavior of PM2 bacteriophage DNA in alkaline solution," *Biopolymers*, **12**(6), 1387–1419 (1973).

Öttinger, H. C., "Generalized Zimm model for dilute polymer solutions under theta conditions," *J. Chem. Phys.*, **86**(6), 3731–3749 (1987).

Öttinger, H. C., "Gaussian approximation for Rouse chains with hydrodynamic interaction," *J. Chem. Phys.*, **90**, 463 (1989).

Öttinger, H. C., *Stochastic Processes in Polymeric Fluids*. Springer, Berlin (1996).

Pamies, R., J. G. Hernández Cifre, M. del Carmen López Martínez, and J. García de la Torre, "Determination of intrinsic viscosities of macromolecules and nanoparticles. Comparison of single-point and dilution procedures," *Colloid Polym Sci.*, **286**(11), 1223–1231 (2008).

Pan, S., D. Ahirwal, D. A. Nguyen, P. Sunthar, T. Sridhar, and J. Ravi Prakash, The viscosity radius in dilute polymer solutions: Universal behaviour from DNA rheology and Brownian dynamics simulations (2014). arXiv:1405.4056v1.

Pecora, R., "DNA: A model compound for solution studies of macromolecules," *Science*, **251**(4996), 893–898 (1991).

Pincus, P., "Excluded volume effects and stretched polymer chains," *Macromolecules*, **9**(3), 386–388 (1976).

Post, C. B. and B. H. Zimm, "Theory of DNA condensation: Collapse versus aggregation," *Biopolymers*, **21**(11), 2123–2137 (1982).

Prabhakar, R. and J. R. Prakash, "Multiplicative separation of the influences of excluded volume, hydrodynamic interactions and finite extensibility on the rheological properties of dilute polymer solutions," *J. Non-newtonian Fluid Mech.*, **116**, 163–182 (2004).

Prabhakar, R., J. R. Prakash, and T. Sridhar, "A successive fine-graining scheme for predicting the rheological properties of dilute polymer solutions," *J. Rheol.*, **48**(6), 1251–1278 (2004).

Prakash, J. R., "Rouse chains with excluded volume interactions in steady simple shear flow," *J. Rheol.*, **46**(6), 1353–1380 (2002).

Prakash, J. R. and H. C. Öttinger, "Universal viscometric functions for dilute polymer solutions," *J. Non-Newtonian Fluid Mech.*, **71**, 245–272 (1997).

Rasmussen, H. K. and O. Hassager, "Three-dimensional simulations of viscoelastic instability in polymeric filaments," *J. Non-Newton. Fluid Mech.*, **82**(2-3), 189–202 (1999).

Robertson, R. M., S. Laib, and D. E. Smith, "Diffusion of isolated DNA molecules: Dependence on length and topology," *Proc. Natl. Acad. Sci. U. S. A.*, **103**(19), 7310–7314 (2006).

Ross, P. D. and R. L. Scruggs, "Viscosity study of DNA. II. The effect of simple salt concentration on the viscosity of high molecular weight DNA and application of viscometry to the study of DNA isolated from T4 and T5 bacteriophage mutants.," *Biopolymers - Peptide Science Section*, **6**(8), 1005–1018 (1968).

Rubinstein, M. and R. H. Colby, *Polymer Physics*. Oxford University Press (2003).

Rushing, T. S. and R. D. Hester, "Intrinsic viscosity dependence on polymer molecular weight and fluid temperature," *J. Appl. Polym. Sci.*, **89**(10), 2831–2835 (2003).

Sambrook, J. and D. W. Russell, *Molecular Cloning: A Laboratory Manual (3rd edition*. Cold Spring Harbor Laboratory Press, USA (2001).

Schäfer, L., *Excluded Volume Effects in Polymer Solutions*. Springer-Verlag, Berlin (1999).

Schroeder, C. M., H. P. Babcock, E. S. G. Shaqfeh, and S. Chu, "Observation of polymer conformation hysteresis in extensional flow," *Science*, **301**(5639), 1515–1519 (2003).

Schroeder, C. M., E. S. G. Shaqfeh, and S. Chu, "Effect of hydrodynamic interactions on DNA dynamics in extensional flow: Simulation and single molecule experiment," *Macromolecules*, **37**(24), 9242–9256 (2004).

Schroeder, C. M., R. E. Teixeira, E. S. G. Shaqfeh, and S. Chu, "Dynamics of DNA in the flow-gradient plane of steady shear flow: Observations and simulations," *Macromolecules*, **38**(5), 1967–1978 (2005).

Selis, J. and R. Pecora, "Dynamics of a 2311 base pair superhelical DNA in dilute and semidilute solutions," *Macromolecules*, **28**(3), 661–673 (1995).

Shaqfeh, E. S. G., "The dynamics of single-molecule DNA in flow," *J. Non-Newton. Fluid Mech.*, **130**(1), 1–28 (2005).

Sibileva, M. A., A. N. Veselkov, S. V. Shilov, and E. V. Frisman, "Effect of temperature on the conformation of native DNA in aqueous solutions of various electrolytes [Vliianie temperatury na konformatsiiu molekuly nativno DNK v vodnykh rastvorakh razlichnykh lektrolitov.]," *Molekulyarnaya Biologiya*, **21**(3), 647–653 (1987).

Smith, D. E. and S. Chu, "Response of flexible polymers to a sudden elongational flow," *Science*, **281**(5381), 1335–1340 (1998).

Smith, D. E., T. T. Perkins, and S. Chu, "Dynamical Scaling of DNA Diffusion Coefficients," *Macromolecules*, **29**(4), 1372–1373 (1996).

Soda, K. and A. Wada, "Dynamic light-scattering studies on thermal motions of native DNAs in solution," *Biophys. Chem.*, **20**(3), 185–200 (1984).

Solomon, O. F. and I. Z. Ciută, "Détermination de la viscosité intrinsèque de solutions de polymères par une simple détermination de la viscosité.," *J. Appl. Polym. Sci.*, **6**(24), 683–686 (1962).

Somani, S., E. S. G. Shaqfeh, and J. R. Prakash, "Effect of Solvent Quality on the Coil-Stretch Transition," *Macromolecules*, **43**(24), 10679–10691 (2010).

Sorlie, S. S. and R. Pecora, "A dynamic light scattering study of four DNA restriction fragments," *Macromolecules*, **23**(2), 487–497 (1990).

Sridhar, T., V. Tirtaatmadja, D. A. Nguyen, and R. K. Gupta, "Measurement of extensional viscosity of polymer solutions," *J. Non-Newton. Fluid Mech.*, **40**(3), 271–280 (1991).

Stockmayer, W. H. and M. Fixman, "On the estimation of unperturbed dimensions from intrinsic viscosities," *J. polym. sci., C Polym. symp.*, **1**(1), 137–141 (1963).

Stoltz, C., J. J. De Pablo, and M. D. Graham, "Concentration dependence of shear and extensional rheology of polymer solutions: Brownian dynamics simulations," *J. Rheol.*, **50**(2), 137–167 (2006).

Sunthar, P., D. A. Nguyen, R. Dubbelboer, J. R. Prakash, and T. Sridhar, "Measurement and prediction of the elongational stress growth in a dilute solution of DNA molecules," *Macromolecules*, **38**(24), 10200–10209 (2005).

Sunthar, P. and J. R. Prakash, "Parameter Free Prediction of DNA Conformations in Elongational Flow by Successive Fine Graining," *Macromolecules*, **38**(2), 617–640 (2005).

Sunthar, P. and J. R. Prakash, "Dynamic scaling in dilute polymer solutions: The importance of dynamic correlations," *Europhys. Lett.*, **75**, 77–83 (2006).

Teif, V. B. and K. Bohinc, "Condensed DNA: Condensing the concepts," *Prog. Biophys. Mol. Biol.*, **105**(3), 208–222 (2011).

Thurston, G. B., "Exact and approximate eigenvalues and intrinsic functions for the Gaussian chain theory," *Polymer*, **15**(9), 569–572 (1974).

Tirtaatmadja, V. and T. Sridhar, "A filament stretching device for measurement of extensional viscosity," *J. Rheol.*, **37**(6), 1081–1102 (1993).

Tominaga, Y., I. Suda, M. Osa, T. Yoshizaki, and H. Yamakawa, "Viscosity and hydrodynamic-radius expansion factors of oligo- and poly(a-methylstyrene)s in dilute solution," *Macromolecules*, **35**(4), 1381–1388 (2002).

Tree, D. R., A. Muralidhar, P. S. Doyle, and K. D. Dorfman, "Is DNA a good model polymer?," *Macromolecules*, **46**(20), 8369–8382 (2013).

Utiyama, H., "Rayleigh Scattering by Linear Flexible Macromolecules," *J. Chem. Phys.*, **55**(7), 3133–3145 (1971).

Valle, F., M. Favre, P. De Los Rios, A. Rosa, and G. Dietler, "Scaling exponents and probability distributions of DNA end-to-end distance," *Phys. Rev. Lett.*, **95**(15), 1–4 (2005).

Winkler, R. G., "Semiflexible polymers in shear flow," *Phys. Rev. Lett.*, **97**(12) (2006).

Winkler, R. G., "Conformational and rheological properties of semiflexible polymers in shear flow," *J. Chem. Phys.*, **133**(16) (2010).

Yamakawa, H., *Helical Wormlike Chains in Polymer Solutions*. Springer, Berlin Heidelberg (1997).

Yamakawa, H., *Modern Theory of Polymer Solutions*. Kyoto University (formerly by Harper and Row), Kyoto, electronic edition (2001).

Yamakawa, H. and T. Yoshizaki, "Effects of Fluctuating Hydrodynamic Interaction on the Hydrodynamic-Radius Expansion Factor of Polymer Chains," *Macromolecules*, **28**(10), 3604–3608 (1995).

Yao, M. and G. H. McKinley, "Numerical simulation of extensional deformations of viscoelastic liquid bridges in filament stretching devices," *J. Non-Newton. Fluid Mech.*, **74**(1-3), 47–88 (1998).

Yoshikawa, K., M. Takahashi, V. Vasilevskaya, and A. Khokhlov, "Large Discrete Transition in a Single DNA Molecule Appears Continuous in the Ensemble," *Phys. Rev. Lett.*, **76**(16), 3029–3031 (1996).

Yoshikawa, Y., Y. Suzuki, K. Yamada, W. Fukuda, K. Yoshikawa, T. K., and T. Imanaka, "Critical behavior of megabase-size DNA toward the transition into a compact state," *J. Chem. Phys.*, **135**(22), 225101 (2011).

Zimm, B. H., "Dynamics of polymer molecules in dilute solution: Viscoelasticity, flow birefringence and dielectric loss," *J. Chem. Phys.*, **24**(2), 269–281 (1956).

List of Publications

Papers in Refereed Journals

1. **Sharadwata Pan**, Duc At Nguyen, P. Sunthar, T. Sridhar and J. Ravi Prakash (2014), "Universal solvent quality crossover of the zero shear rate viscosity of semidilute DNA solutions," *Journal of Rheology*, vol. 58 (2), pp. 339–368. DOI:10.1122/1.4861072. [2012 Impact Factor: 2.795; Journal Citation Reports (Thomson Reuters)]

Papers in Refereed Journals (Under review)

1. **Sharadwata Pan**, D. Ahirwal, Duc At Nguyen, P. Sunthar, T. Sridhar and J. Ravi Prakash (2014), "The viscosity radius in dilute polymer solutions: Universal behaviour from DNA rheology and Brownian dynamics simulations," (Under review in *Macromolecules*.) [2012 Impact Factor: 5.521; Journal Citation Reports (Thomson Reuters)]

Papers in Refereed Journals (manuscripts under preparation)

1. **Sharadwata Pan**, Duc At Nguyen, P. Sunthar, T. Sridhar and J. Ravi Prakash, "Semidilute and dilute DNA solutions in shear flow," manuscript under preparation.

2. Duc At Nguyen, **Sharadwata Pan**, P. Sunthar, T. Sridhar and J. Ravi Prakash, "Semidilute DNA solutions in extensional flow," manuscript under preparation.

3. **Sharadwata Pan**, P. Sunthar, T. Sridhar and J. Ravi Prakash, "The role of DNA as a model polymer in polymer physics and rheology," manuscript under preparation.

Peer-reviewed Conference Proceedings

1. **Pan, Sharadwata**; Nguyen, Duc At; Sunthar, P; Sridhar, Tamarapu; and Prakash, J Ravi (2013). "Temperature-superposition of shear-thinning of Semi-dilute DNA solutions". In: Proceedings of the Asia Australia Regional Meeting of the Polymer Processing Society (PPS) – 2013. At Ramada Powai Hotel and Convention Center, Mumbai, India. 04–07 December, 2013.

2. Nguyen, Duc At; **Pan, Sharadwata**; Sunthar, P; Sridhar, T and Prakash, J Ravi (2013). "The extensional rheology of semidilute DNA solutions [online]". In: Chemeca 2013 (41st: 2013: Brisbane, Qld.). Chemeca 2013: Challenging Tomorrow. 23–26 September 2013, Brisbane, Australia. Barton, ACT: Engineers Australia, 2013: 52-57. ISBN: 9781922107077.

3. **Pan, Sharadwata**; Sunthar, P; Sridhar, T and Prakash, J Ravi (2012). "Universal crossover of static and dynamic properties of dilute DNA solutions [online]". In: Chemeca 2012: Quality of life through chemical engineering: 23–26 September 2012, Wellington, New Zealand. Barton, A.C.T.: Engineers Australia, 2012: [339]–[348]. EISBN: 9781922107596.

4. **Pan, Sharadwata**; At Nguyen, Duc; Sunthar, P; Sridhar, T and Prakash, J Ravi (2011). "The shear rheology of semi-dilute DNA solutions [online]". In: Chemeca 2011: Engineering a Better World: Sydney Hilton Hotel, NSW, Australia, 18–21 September 2011. Barton, A.C.T.: Engineers Australia, 2011: [725]–[733]. ISBN: 9780858259676.

Contributed Conference Abstracts / Conference Presentations

1. **Sharadwata Pan**, Duc At Nguyen, P. Sunthar, T. Sridhar, and J. Ravi Prakash (2014); "Unravelling the dynamics of Semi-dilute Polymer Solutions using DNA Rheology," 9th Annual European Rheology Conference (AERC 2014) of the European Society of Rheology at Karlsruhe (Germany), from April 08–11th, 2014.

2. **Sharadwata Pan**, Duc At Nguyen, P. Sunthar, T. Sridhar, and J. Ravi Prakash (2013); "Shear rheology of semi-dilute DNA solutions: Close-to and Far from equilibrium," 3rd FAPS Polymer Congress and MACRO – 2013. (By the Federation of the Asian Polymer Societies and the Society of Polymer Science India). From May 15–18th, 2013, at Indian Institute of Science, Bangalore, India.

3. **Sharadwata Pan**, Aashish Jain, Duc At Nguyen, P. Sunthar, T. Sridhar, B. Dünweg and J. Ravi Prakash (2012); "Concentration Dependent Dynamics of

Semi-Dilute DNA solutions," The XVIth International Congress on Rheology at Lisbon (Portugal). From 5–10 August, 2012.

4. **Sharadwata Pan**, Duc At Nguyen, P. Sunthar, T. Sridhar, and J. Ravi Prakash (2012); "Shear Rheology of Semi-dilute DNA solutions," COMPFLU 2012 (SERC School and Sixth National Symposium on 'Rheology of Complex Fluids'). From January 6–7, 2012, at Indian Institute of Technology Guwahati, Assam, India.

5. **Sharadwata Pan**, Duc At Nguyen, P. Sunthar, T. Sridhar and J. Ravi Prakash (2011); "The shear rheology of semi-dilute DNA solutions," 83rd Annual Meeting of US Society of Rheology at Cleveland, Ohio (USA), from 9–13 October, 2011.

6. **Sharadwata Pan**, Aashish Jain, Duc At Nguyen, P. Sunthar, T. Sridhar, B. Dünweg and J. Ravi Prakash (2011); "Concentration Dependent Dynamics of Semi-Dilute DNA solutions," The Korean-Australian Rheology Conference 2011. From September 25–27, 2011 at Daejeon, Korea.

7. **Sharadwata Pan**, P. Sunthar, T. Sridhar, and J. Ravi Prakash (2010); "Effects of Solvent Quality on Static and Dynamic Properties of dilute DNA solutions," COMPFLU 2010 (SERC School and Fifth National Symposium on 'Rheology of Complex Fluids'). From January 8–9, 2010, at Indian Institute of Technology Madras, Chennai, India.